AN ASSESSMENT OF SATELLITE DERIVED TOTAL EVAPORATION DATA AS A DATA SOURCE TO THE ACRU HYDROLOGICAL MODEL

S Gokool

Submitted in fulfillment of the requirements for the degree of MSc Hydrology

Centre for Water Resources Research
School of Agriculture, Earth and Environmental Sciences
University of KwaZulu-Natal
Pietermaritzburg
18th November 2014

Supervisor: Miss KT Chetty
Co-Supervisor: Professor GPW Jewitt

DEDICATED TO:

MY GRANDMOTHER MISS PARBATHI SINGH

AND

MY PARENTS PRAVEEN GOKOOL AND NISHA CASSIM

ABSTRACT

Hydrological models and tools are often used as decision support systems to inform water resources management. The successful application of these systems is largely dependent on the quality of data being incorporated into them. Accurate information with regards to total evaporation is of paramount importance to water resources managers, as it is a key indicator in determining if water resources are being used for their specific purposes. Due to the inherent spatial limitations associated with conventional techniques to estimate total evaporation, the application of satellite earth observation as a tool to estimate total evaporation is being advocated more frequently. The focus of this Dissertation was to develop an approach which would allow for the incorporation of total evaporation estimates from an existing evaporation model that incorporates satellite earth observation data i.e. the SEBS model, into a hydrological simulation model i.e. ACRU, to simulate streamflow.

The SEBS model was first validated in the Komatipoort study site against the surface renewal system. The results of this investigation indicated that the SEBS model over-estimated total evaporation by approximately 47% and produced R^2 and RMSE values of 0.33 and 2.19, respectively, when compared to total evaporation estimates obtained from the surface renewal system. Once, the model had been validated, it was then applied to estimate total evaporation for quarternary catchment X23_A for the period 01st December 2011 to 25th November 2012. These estimates were used to create a continuous total evaporation time series, which was used as an input to ACRU to model streamflow.

The EVTR3 approach was derived to allow for the incorporation of the aforementioned SEBS total evaporation estimates in ACRU and to estimate streamflow amongst other hydrological parameters. The simulated streamflow for this technique was under-estimated by approximately 10% and produced R^2 and RMSE values of 0.41 and 1.05, respectively, when compared to observed streamflow. Although these results appear to be satisfactory at best, similar results were obtained when using the conventional evaporation routine in ACRU to estimate streamflow. This occurrence circuitously highlights the potential of utilizing satellite earth observation data as a data source for a hydrological model.

DECLARATION 1 - PLAGIARISM

I, Shaeden Gokool declare that

(i) The research reported in this dissertation, except where otherwise indicated, is my original work.

(ii) This dissertation has not been submitted for any degree or examination at any other university.

(iii) This dissertation does not contain other persons' data, pictures, graphs or other information, unless specifically acknowledged as being sourced from other persons.

(iv) This dissertation does not contain other persons' writing, unless specifically acknowledged as being sourced from other researchers. Where other written sources have been quoted, then:

(a) their words have been re-written but the general information attributed to them has been referenced;

(b) where their exact words have been used, their writing has been placed inside quotation marks, and referenced.

(v) Where I have reproduced a publication of which I am an author, co-author or editor, I have indicated in detail which part of the publication was actually written by myself alone and have fully referenced such publications.

(vi) This dissertation does not contain text, graphics or tables copied and pasted from the Internet, unless specifically acknowledged, and the source being detailed in the Dissertation and in the References sections.

Signed: ……..

Shaeden Gokool

Supervisor: ……..

Miss KT Chetty

Co-supervisor: ……

Prof. Graham PW Jewitt

PREFACE

The work described in this dissertation was carried out in the Centre for Water Resources Research, School of Agriculture, Earth and Environmental Sciences, University of KwaZulu-Natal, Pietermaritzburg under the supervision of Miss Tinisha Chetty and Professor Graham Jewitt.

The research represents original work by the author and has not otherwise been submitted in any form for any degree or diploma to any tertiary institution. Where use has been made of the work of others it is duly acknowledged in the text

ACKNOWLEDGEMENTS

This Masters Research Project titled "An Assessment of Satellite Derived Total Evaporation Data as a Data Source to the ACRU Hydrological Model" has been funded by the Centre for Water Resources Research (CWRR), the National Research Foundation (NRF) and the Risk-based Operational Water Management (RISKOMAN) Project. I wish to thank the aforementioned institutions for funding this research, as well as the Almighty for the opportunity to further my studies and for the guidance and blessing which I received throughout the duration of this project. I would also like to acknowledge the following people and institutions:

- Miss KT Chetty, my Supervisor. Thank you for the day-to-day support and guidance you extended towards me throughout the duration of this study. The amount of time and effort you expended was invaluable, to the successful completion of this research. The knowledge you have imparted to me will form a strong foundation for any future ventures that I undertake.
- Mr D Clark. I would like to extend my gratitude to you for your resolute effort in assisting me with the modification of the ACRU Model code, as well, as the endless supply of priceless advice. I have truly learned a lot from you.
- Mr S Thornton-Dibb. I would like to express my gratitude to you for the special support you provided me with during the configuration of the ACRU Model.
- Dr M Mengistu. I would like to thank you for the assistance you provided during the application of the SEBS model.
- Dr HH Bulcock and Mrs L Bulcock. Thank you for the support and advice you shared with me during this study; it was greatly appreciated.
- Dr C Jarmain. Thank you for your sound advice and for the provision of validation and meteorological data required in this study.
- The Agricultural Research Council – Institute for Soil, Climate and Water, with special mention going to Maureen Fritz and Chris Kaempffer, for the provision of meteorological data.
- Ms RB Solomon. I am truly grateful for the role you have played for the duration of this study. Your support and words of motivation were really invaluable.
- Mr R Ramasis, for sparking my interest in the field of science and providing me with the foundations to further my scientific knowledge.

- Mrs S Rees. Thank you for assisting me with the editing of this dissertation. I really appreciate the time and effort you expended.
- Colleagues and staff at the Centre for Water Resources Research. Thank you for the assistance and support that you all provided; it is deeply appreciated.
- Thank you to all my family and friends for the support, encouragement and advice which I received throughout the duration of this research project.

TABLE OF CONTENTS

LIST OF TABLES

Page

LIST OF FIGURES

Page

LIST OF SYMBOLS

A_{swe} = Actual soil water evaporation (mm/day)

A_{trans} = Actual transpiration (mm/day)

C_d = Drag coefficient of foliage elements (0.2)

CO_2 = Carbon Dioxide

C_p = Heat capacity of dry air ($J.kg^{-1}$)

C_t = Heat transfer coefficient of the leaf ($0.005N \leq C_t \leq 0.075N$) (dimensionless)

C_t^* = Heat transfer coefficient of the soil (dimensionless)

d_o = Displacement height (m)

e_a = Actual vapour pressure (hPa)

E_{daily} = Daily total evaporation (mm/day)

EptA = Potential transpiration of the A-Horizon (mm/day)

E_r = A-pan equivalent reference potential evaporation (mm)

e_s = Saturated vapour pressure (hPa)

E_s = Stage two soil water evaporation (mm/day)

ET_1 = The first known daily total evaporation value (mm/day)

ET_2 = The unknown daily total evaporation value (mm/day)

ET_3 = The next known daily total evaporation value

E_{tA} = Actual transpiration of the A-Horizon (mm/day)

E_w = Enhanced wet canopy evaporation (mm)

f_c = Fractional canopy coverage (dimensionless)

f_s = Complement to the fractional vegetation cover (dimensionless)

f_s = Fraction of PAW

F_t = The fraction of total available transpiration (dimensionless)

g = Acceleration due to gravity ($m.s^{-2}$)

G_o = Soil heat flux energy ($W.m^{-2}$)

H = Sensible heat flux energy ($W.m^{-2}$)

H_{dry} = Sensible heat flux at the dry limit ($W.m^{-2}$)

h_s = The roughness height of the soil (m)

H_{wet} = Sensible heat flux at the wet limit ($W.m^{-2}$)

Il = Interception loss (mm/day)

k = von Karman's constant (0.4)

KB^{-1} = Inverse Stanton number (dimensionless)

KB_s^{-1} = Inverse Stanton number for bare soils

K_c = Crop coefficient (dimensionless)

L = Obhukov length (m)

LAI = Leaf area index (dimensionless)

N = Number of sides of the leaf which is involved in the heat transfer process

N_{ec} = Within-canopy wind profile extinction coefficient (dimensionless)

PAW_A = Plant available water (PAW) for the A-Horizon (mm)

P_g = Gross daily rainfall (mm/day)

Pr = The Prandtl number

P_{SWE} = Potential soil water evaporation (mm)

r_e = Aerodynamic resistance ($s.m^{-1}$)

R_{e*} = The roughness Reynolds number

r_i = The bulk surface internal resistance ($s.m^{-1}$)

RL_{wd} = Incoming long wave radiation ($W.m^{-2}$)

Rn = Net radiation ($W.m^{-2}$)

Rn_{24} = The daily net radiation ($W.m^{-2}$)

RS_{wd} = Incoming solar radiation ($W.m^{-2}$)

T_c = The brightness temperature from a central wavelength

t_d = Time (days)

T_o = Surface temperature (K)

u = Wind speed ($m.s^{-1}$)

u(h) = Horizontal wind speed at the top of the canopy ($m.s^{-1}$)

u^* = Friction velocity ($m.s^{-1}$)

U_1 = Stage 1 upper limit of SWC (mm)

v = The kinematic viscosity of the air (dimensionless)

z = Reference meteorological height (m)

z_{oh} = Scalar roughness height for heat (m)

z_{om} = Roughness height for momentum(m)

α = Land surface albedo (dimensionless)

α_s = Soil water transmission parameter

γ = The psychometric constant(hPa.K^{-1})

Δ = Rate of change of saturated vapour pressure with temperature (hPa.K^{-1})

ε = Surface emissivity (dimensionless)

θ_A = SWC of the A-Horizon (mm)

θ_a = Air temperature at height z (K)

θ_{DULA} = SWC of the A-Horizon at the drained upper limit (mm)

θ_o = Potential surface temperature (K)

θ_{POA} = SWC of the A-Horizon at saturation (mm)

θ_{PWPA} = SWC of the A-Horizon at permanent wilting point (mm)

θ_v = Virtual temperature near the surface (K)

λ = The latent heat of vaporization (J.kg^{-1})

λ_c = The sensors central wavelength

λE = The latent heat at the dry limit (W.m^{-2})

λET = Latent heat flux energy (W.m^{-2})

λE_{wet} = The latent heat at the wet limit (W.m^{-2})

Λ_o^{24} = The daily evaporative fraction (dimensionless)

Λr = The relative evaporation (dimensionless)

ρ = Density of air (kg.m^{-3})

ρ_w = Density of water (kg.m-^{3})

σ = Stefan Boltzman constant (5.67x10^{-8} W.m^{-}2.K^{-4})

ψ_h = Stability correction factors for sensible heat transfer

ψ_m = Stability correction factors for momentum

Γ_c = Ratio of soil heat flux to net radiation for a fully vegetated canopy (0.05)

Γ_s = Ratio of soil heat flux to net radiation for a bare soil surface (0.315)

LIST OF ABBREVIATIONS

AATSR	=	Advanced Along-Track Scanning Radiometer
ACRU	=	Agricultural Catchments Research Unit model
AET	=	Total evaporation (mm/day)
ARC-ISCW	=	Agricultural Research Council Institute for Soil, Climate and Water
DEM	=	Digital Elevation Model (m)
DHI	=	Danish Hydrological Institute
DWAF	=	Department of Water Affairs
ENVISAT	=	Environmental Satellite
ET_0	=	Reference evaporation (mm)
EVTR1	=	Evapotranspiration routine one in ACRU
EVTR2	=	Evapotranspiration routine two in ACRU
EVTR3	=	Evapotranspiration routine three in ACRU
GAET	=	Total evaporation which is output by ACRU
HRU	=	Hydrological Response Unit
ILWIS	=	Integrated Land and Water Information System
Kc_{act}	=	Actual Kc
MAP	=	Mean annual precipitation (mm.year-1)
MERIS	=	MEdium Resolution Imaging Spectrometer
METRIC	=	Mapping Evapotranspiration at High Resolution with Internalized Calibration
MODIS	=	Moderate Resolution Imaging Spectroradiometer
NDVI	=	Normalized difference vegetation index
PT	=	Potential transpiration (mm/day)
r1	=	Visible channel Band1
R^2	=	Coefficient of determination
r2	=	Visible channel Band2
r3	=	Visible channel Band3
r4	=	Visible channel Band4
r5	=	Visible channel Band5
r7	=	Visible channel Band7
RF-AVG	=	Average A-Horizon root fraction
RFL	=	Rainfall (mm)

RF-MAX = Maximum A-Horizon root fraction

RF-MIN = Minimum A-Horizon root fraction

RISKOMAN = Risk-based Operational Water Management Project

RMSE = Root Mean Square Error

RVE = Relative volume error

SEBAL = Surface Energy Balance Algorithm for Land

SEBI = Surface Energy Balance Index

SEBS = Surface Energy Balance System

SEBS = Surface Energy Balance System model

SMAC = A Simplified Method for the Atmospheric Correction of Satellite Measurements

SWC = Soil water content (mm)

URFLOW = Runoff (mm)

WRC = Water Research Commission

X_1 = Julian day for ET_1

X_2 = Julian day for ET_2

X_3 = Julian day for ET_3

Δ DELSTS = Delayed stormflow store (mm)

Δ RUNCO = Difference between the initial and final baseflow storage (mm)

Δ STO2 = Difference between the initial and final B-Horizon storage (mm)

1. INTRODUCTION

1.1 Background and Significance

Semi-arid environments, such as South Africa, are predominantly water-scarce (Jarmain *et al.,* 2009). There is a diverse community of water resources consumers in South Africa, all competing for a share of a limited resource (Jarmain *et al.*, 2009). Subsequently, the need to accurately estimate and understand the temporal and spatial variations of total evaporation takes on added significance in these environments (Jarmain *et al.*, 2009). Approximately 91% of the mean annual precipitation which southern Africa receives is returned to the atmosphere through total evaporation (Whitmore, 1971).

The loss of water to total evaporation is quite substantial, as daily water requirements usually surpass the amount of available rainfall and therefore the demands for water resources have to be supplemented by dams, water transfer schemes and irrigation systems, which utilize additional surface water and ground water resources (Kongo and Jewitt, 2006; Gowda *et al.*, 2007; Jarmain *et al.,* 2009). Consequently, total evaporation has become one of the key factors in water resources management, since accurate estimates of total evaporation assist in making well-informed decisions for various activities such as the design and management of irrigation schemes, regulating water laws and providing greater insight to hydrological studies (Bastiaansen, 2000; Bastiaansen *et al*., 2012).

Obtaining accurate estimates of total evaporation will enable water resources managers and practitioners to account for the loss of water from the land surface and to assist in the prevention of wastage which could have occurred previously (Bastiaansen, 2000). Therefore, it is of utmost importance to possess techniques which acquire accurate information with regards to total evaporation (Allen *et al.*, 1998; Bastiaansen, 2000). Conventional techniques which are commonly used to estimate total evaporation, both locally and internationally, are confined to the field scale, providing point-based estimates (Bastiaansen, 2000; Su, 2002; Jin *et al.*, 2005; Jarmain *et al.*, 2009; Li *et al.*, 2011; Bastiaansen *et al.*, 2012).

These techniques have been extremely useful in acquiring total evaporation data, however they are only representative at the field scale and generally cannot be used to estimate total evaporation over large geographic scales (Bastiaansen, 2000; Twine *et al.*, 2000; Su, 2002; Jin *et al.*, 2005; Jarmain *et al.*, 2009; Bastiaansen *et al.*, 2012; Teixera and Batsiaansen, 2012). This is largely due to the heterogeneity of land surfaces, which becomes more pronounced over larger geographical scales, as well as the changing nature of heat transfer processes at greater spatial scales (Bastiaansen, 2000; Su, 2002; Li *et al.*, 2011; Bastiaansen *et al.*, 2012). In addition to this, the use of conventional techniques to estimate total evaporation over large geographic scales would prove to be impractical and somewhat costly (Elhaddad and Garcia, 2008; Badola, 2009; Bastiaansen *et al.*, 2012).

Advancements in satellite earth observation systems over the past four decades have provided a suitable alternative to capturing hydro-meteorological data. Satellite earth observation has shown a great deal of potential in providing information at large geographic scales, capturing information which is not easily accessible through the use of conventional techniques and providing time series data of variables fairly easily, due to the periodic updating of information (Sandholt *et al.*, 1999; Bastiaansen, 2000; Su, 2002; Bastiaansen and Harshadeep, 2005; Jarmain *et al.*, 2009; Jovanovic and Israel, 2012; Li *et al.*, 2009; van Dijk and Renzullo, 2011; Bastiaansen *et al.*, 2012; Ershadi *et al.*, 2011; Fern´andez-Prieto *et al.*, 2012; Ma *et al.*, 2012; Muhammed, 2012; Wu *et al.*, 2012).

1.2 Research Problem

Numerous hydrological models and tools are used as decision support systems to inform water resources management. However, the success of these systems is not dependent on the type of model or tool used, but rather by the data being incorporated into them (van Dijk and Renzullo, 2011; Mengistu *et al.*, 2014). Effective and efficient water resources management is therefore dependent on data being available, for the representative spatial and temporal scales (van Dijk and Renzullo, 2011). The use of satellite earth observation data alone is not seen as a solution to the current challenges of data acquisition, however it is a useful alternative in providing crucial data when conventional measures prove to be inadequate or unavailable (Jarmain *et al.*, 2009).

Previous research indicates that satellite earth observation is potentially a very useful information source with regards to environmental variables such as precipitation, total evaporation and soil moisture amongst others (Kite and Pietroniro, 1996; Sandholt *et al.*, 1999; van Dijk and Renzullo, 2011; Fern´andez-Prieto *et al.*, 2012; Xu *et al*., 2014). Satellite earth observation is able to provide information at large geographic scales, capture information which is not easily accessible through the use of conventional techniques and to provide time series data of variables fairly easily, due to the periodic updating of information (Sandholt *et al.*, 1999; Bastiaansen, 2000, Su, 2002; Bastiaansen and Harshadeep, 2005; Jarmain *et al.*, 2009; Li *et al*., 2009; Ershadi *et al.*, 2011; Fern´andez-Prieto *et al.*, 2012; Jovanovic and Israel, 2012).

The ability of satellite earth observation to provide spatially representative observations has created improved prospects for the advancement and application of fully distributed hydrological models (Peck *et al*., 1981; Kuttinen, 1985; Engman and Gurney, 1991; Schultz, 1993; Engman, 1995; Kite and Pietroniro, 1996; Sandholt *et al.*, 1999; van Dijk and Renzullo, 2011; Fern´andez-Prieto *et al.*, 2012; Mengistu, 2014; Xu *et al*., 2014). There has been intensive research conducted on a global scale, to integrate satellite earth observation and hydrological modelling over the past few decades, with noteworthy advancements being made in the land/hydrologic satellite earth observation data integration (Kite and Pietroniro, 1996; Sandholt *et al.*, 1999; Bulcock and Jewitt, 2010; Xu *et al*., 2014).

However, there still remains a number of major challenges in this field that need to be overcome (Xu *et al*., 2014). This is largely due to the lack of appropriate technology required to handle and process satellite earth observation data and the lack of knowledge regarding the application of these techniques (Schultz and Engman, 2000: Bulcock and Jewitt, 2010; van Dijk and Renzullo, 2011).

The nature of currently available hydrological models has also proved to be a major stumbling block to the integration of satellite earth observation data and hydrological models. These hydrological models, whether lumped or distributed, require some form of modification to incorporate satellite-derived data (Sandholt *et al.*, 1999; Wagener *et al*., 2009; Xu *et al*., 2014). A great deal of time, expertise and effort is required to successfully modify these models and as a result, there has been reluctance to move away from traditional and reputable methods (Bulcock and Jewitt, 2010; van Dijk and Renzullo, 2011; Xu *et al*., 2014).

Satellite earth observation data possess a variety of benefits that can be used to assist water resources management. In order to truly understand the potential benefits associated with the integration of satellite earth observation data in hydrological models, the aforementioned challenges need to be overcome (Fern´andez-Prieto *et al.*, 2012). The only means of achieving this is to focus future research on adapting current hydrologic models, to utilize satellite earth observation data, to develop new hydrologic models specifically created to utilize satellite earth observation data, to improve current data collection techniques and to develop new techniques (Sandholt *et al.*, 1999; Wagener *et al.*, 2010; van Dijk and Renzullo, 2011; Fern´andez-Prieto *et al.*, 2012; Xu *et al.*, 2014).

1.3 Research Aims and Objectives

The aim of this study was to develop an approach to allow for the integration of satellite-derived total evaporation data into the Agricultural Conservation Research Unit (ACRU) Model, which can then be used to assist the water resources management decision-making process and to develop an understanding of the hydrological characteristics within a catchment, through improved hydrological modelling. The general objective of this study was to apply the output of an existing evaporation model i.e. the SEBS Model, which incorporates satellite earth observation data into the ACRU Model to simulate streamflow.

1.4 Specific Objectives

- Review current techniques which utilize satellite earth observation data to estimate total evaporation.
- Apply and validate estimates of total evaporation extending from the SEBS model against *in situ* total evaporation estimates obtained from a conventional technique.
- Generate a time series of the satellite-derived SEBS total evaporation which can be used as an input to the ACRU Model.
- Apply and validate an infilling technique which can be used to patch any missing values in the satellite-derived SEBS total evaporation time series.
- Develop and test an approach describing how to incorporate the satellite-derived SEBS total evaporation estimates into the ACRU hydrological model.
- Compare the simulated streamflow obtained from using the satellite-derived SEBS total evaporation estimates against observed streamflow.

1.5 Research Questions

i. How do the satellite-derived SEBS daily total evaporation estimates compare against *in situ* measurements obtained from a conventional technique?
ii. How can the satellite-derived SEBS total evaporation estimates be incorporated into the ACRU hydrological model?
iii. How will simulated streamflow modelled, using the satellite-derived SEBS total evaporation estimates, compare against observed stream flow?

1.6 Research Hypotheses

- Ho: Modelled streamflow volumes obtained using the satellite-derived SEBS total evaporation estimates, as a data source to ACRU, will compare favourably with observed streamflow volumes.
- Ha: Modelled streamflow volumes obtained using the satellite-derived SEBS total evaporation estimates, as a data source to ACRU, will not compare favourably with observed streamflow volumes.

1.7 Organization of Dissertation

This dissertation is divided into seven chapters, starting with an introduction and ending with conclusions and recommendations. The broad overview of the dissertation is presented as follows:

The second chapter briefly explains the current techniques used to estimate total evaporation, using satellite earth observation data and provides an in-depth description of one of these techniques. Chapter three provides a description of the study area. Chapter four provides a detailed description of the satellite data, validation data and meteorological data used in the study, a description of the processing techniques used to estimate total evaporation, a description of the infilling techniques used and a description of the ACRU Model, as well as, the hydrological simulations undertaken. Chapters five and six details the results of the infilling techniques investigation and the total evaporation modelling, as well as the results for the streamflow modelling component of the study, respectively. The conclusions, limitations and recommendations of the study are discussed in chapter seven.

2. LITERATURE REVIEW

2.1 A Brief Review of Current Techniques to estimate Total Evaporation based on Satellite Earth Observation Data

The use of satellite earth observation data to estimate total evaporation began approximately four decades ago in the late 1970's. The type of evaporation models incorporating satellite earth observation data to estimate total evaporation gradually evolved over time, becoming more complex in nature in comparison to their predecessors (Jarmain *et al.*, 2009).

According to Courault *et al.* (2005), there are four broad classes of techniques, which are based on satellite earth observation used to estimate total evaporation. These include; (i) empirical direct methods, (ii) deterministic methods, (iii) the vegetation index approach and (iv) techniques based on the parameterisation of the energy balance.

i. Empirical direct methods of estimating total evaporation incorporate satellite earth observation data directly into semi-empirical models. (Courault *et al*, 2005). This technique is based on the assumption that the daily total evaporation can be directly related to the instantaneous difference between the air and surface temperature. The surface temperature can be estimated, using thermal infrared measurements from satellite earth observation data for the regional scale (Courault *et al*, 2005). This technique has been widely used to map total evaporation over large geographic areas based on surface temperature measurements (Lagouarde and Brunet, 1991; Courault *et al*, 1994).
ii. Deterministic methods are generally based on complex models such as the Soil-Vegetation-Atmospheric Transfer models which are used to determine the different components of the energy budget (Courault *et al*, 2005). Satellite earth observation data is used in this technique, either as an input parameter to describe various surfaces, or in an assimilation procedure, which aims to attain the necessary parameters required for the total evaporation computation (Courault *et al*, 2005).
iii. Vegetation index methods also known as inference methods utilize satellite earth observation data to compute a reduction factor such as the crop coefficient or the Priestley-Taylor alpha parameters (Courault *et al*, 2005). This is then used in conjunction with the reference evaporation which can be obtained from field measurements, to estimate the total evaporation (Courault *et al*, 2005).

iv. Techniques based on parameterisation of the energy balance combine some empirical relationships with physical modules to determine the total evaporation. Satellite earth observation data as well as meteorological data is used directly in these models to estimate the input parameters, which are required for the total evaporation computation (Courault *et al*, 2005).

The advantages and disadvantages of each of the aforementioned techniques are listed in Table 2.1 and have been discussed in Courault *et al* (2005), Jarmain *et al* (2009) and Timmermans (2014). Taking into consideration the relative strengths and weaknesses associated with each technique, the technique based on, utilizing the parameterisation of the energy balance, to estimate total evaporation was chosen, to be applied in this study, as it can be applied operationally, involves little to no cost and possesses minimal data requirements.

Table 2.1 A summary of advantages and disadvantages of the different approaches used to estimate total evaporation from remote sensing data

Summary of advantages and disadvantages of the different approaches used to estimate total evaporation from remote sensing data		
Technique	**Advantages**	**Disadvantages**
Empirical	Operational from local to regional scale	Spatial variations of coefficients
Deterministic	Very detailed in their descriptions	Large number of input parameters, long computation times
Vegetation Index Methods	Simple parameterisation of processes	Only valid for specific conditions, does not account for all surface flux components needed in land surface and climate models
Parameterisation of the energy balance	Operational, low cost, minimal data requirements	Some empirical relationships, dry and wetland requirements to estimate the sensible heat flux

The estimation of total evaporation as a parameterisation of the shortened energy balance is a commonly applied technique for both operational and scientific research purposes (Mu *et al.*, 2007; Senay *et al.*, 2007; Jarmain *et al.*, 2009; Long and Singh, 2012). There are a vast number of total evaporation models which are based on the aforementioned technique. Some of the commonly applied techniques include the Surface Energy Balance Index (SEBI), the Surface Energy Balance Algorithm for Land (SEBAL), the Surface Energy Balance System (SEBS) and Mapping Evapotranspiration at High Resolution with Internalized Calibration (METRIC). A brief description of these models is given below.

SEBI which was proposed by Menenti and Choudary (1993) is a single sourced energy balance model (Li *et al.*, 2009). SEBI is based on the distinction between the wet and dry limits and uses this relationship to derive pixel-by-pixel total evaporation from the relative evaporative fraction, when it is combined with surface parameters obtained from satellite earth observation data and field-based measurements (Li *et al.*, 2009).

The dry limit is characterized by maximum surface temperatures with minimal or no total evaporation occurring, whilst the wet limit is characterized by minimum surface temperatures with high or maximum total evaporation (Li *et al.*, 2009). SEBAL and SEBS have been formulated applying the basic SEBI concept, with the main distinctions between these evaporation models being, the calculation of the sensible heat flux, defining wet and dry limits and interpolating between defined upper and lower limits, to determine the sensible heat flux for specific boundary layer conditions (Li *et al.*, 2009).

SEBAL utilizes visible, near-infra-red and thermal infrared input data obtained from satellite imagery, empirical relationships and other physical modules, to determine the instantaneous fluxes of the shortened energy balance equation (Bastiaansen *et al*., 1998a; 2000; Jarmain *et al.*, 2009; Li *et al.*, 2009; Jovanovic and Israel, 2012). The algorithm computes key hydro-meteorological fluxes, which are used in conjunction with field data to determine the instantaneous terms of the shortened energy balance (Jarmain *et al.*, 2009). The latent heat flux, which is the energy required for total evaporation to occur is calculated, as a residual of the shortened energy balance. Once, the instantaneous latent heat flux has been determined the daily total evaporation can be determined by assuming the evaporative fraction remains constant throughout the day (Bastiaansen *et al*., 1998a; 2000; Jarmain *et al.*, 2009; Li *et al.*, 2009; Jovanovic and Israel, 2012).

The METRIC Model described by Allen *et al*. (2007) is based on the same principles used in SEBAL. The model was derived to overcome the limitations of SEBAL in mapping the regional total evaporation over complex terrain (Li *et al.*, 2009). The main distinction between SEBAL and METRIC is the determination of the cold pixel value. The alfalfa reference evaporation is used to determine the energy balance conditions of the cold pixel (Allen *et al.*, 2007; Jarmain *et al.*, 2009; Li *et al.*, 2009). The cold pixels in METRIC are selected for an agricultural setting in which the biophysical characteristics are similar to that of the alfalfa reference crop (Allen *et al.*, 2007; Li *et al.*, 2009). The daily total evaporation is calculated, based on the ratio of the instantaneous total evaporation and the reference crop evaporation obtained from field-based measurements at the time of satellite overpass (Allen *et al.*, 2007).

The SEBS model, developed by Su (2002), is a single-sourced surface energy balance model which can be utilized to estimate turbulent fluxes within the atmosphere or to determine the evaporative fraction through the use of remote sensing and meteorological data for both local and regional scales (Su, 2002; Jin *et al*., 2005; Badola, 2009; Jarmain *et al.* 2009; Li *et al.*, 2009; van de Kwaast, 2009; Gibson *et al.*, 2011; Ma *et al*., 2011; 2012; Muhammed, 2012; Ershadi *et al.*, 2014; Ma *et al*., 2014 Mengistu *et al.*, 2014; Pardo *et al.*, 2014). The model consists of a suite of tools used to determine roughness length of heat transfer, land surface physical parameters and the evaporative fraction (Su, 2002). Similar to SEBAL, the daily total evaporation is calculated by assuming that the evaporative fraction remains constant throughout the day (Su, 2002).

The advantages and disadvantages of each of the aforementioned techniques are listed in Table 2.2 and have been discussed in Allen *et al*. (2007), Bastiaansen *et al*. (1998a); (2000), Su (2002), Jarmain *et al.* (2009), Li *et al.*, (2009) and Jovanovic and Israel, (2012). Taking into consideration the relative strengths and weaknesses associated with each technique, the SEBS Model was chosen to be applied in this study as it is open source software which can easily be obtained and utilized. The SEBS model is discussed in detail in the following sub-section.

Table 2.2 A limited list of techniques which are based on the parameterisation of the energy balance to estimate total evaporation through the incorporation of satellite earth observation data

Technique	Advantages	Disadvantages
SEBI	Directly relates the effects of temperature and aerodynamic resistance to the latent energy	Requires a lot of field-based measurements, evaporative fraction is assumed to be constant in order to estimate daily total evaporation
SEBAL	Minimal data requirements, physical concept, land use not required, multi-sensor approach	User defined hot and cold pixels, only applicable to flat terrain, evaporative fraction is assumed to be constant in order to estimate daily total evaporation, not open source
METRIC	Similar to SEBAL but surface slope and aspect can be considered	Uncertainty in the determination of hot and cold pixels, up-scaling of instantaneous total evaporation to daily total evaporation based on the ratio of the instantaneous total evaporation and the reference crop evaporation at the time of satellite overpass .
SEBS	No *apriori* knowledge of actual turbulent fluxes needed, computes roughness height of heat transfer instead of using fixed values, open source software available in ILWIS, application of the model is fairly user-friendly, Less assumptions are made then in other techniques and the energy balance is solved with more physical parameterizations in the SEBS formulation.	Dry and wetland requirement to determine the sensible heat flux, combined with Penman-Monteith equation, too many parameters are required, solution to determine turbulent heat flux is fairly complex, evaporative fraction is assumed to be constant in order to estimate daily total evaporation.

2.2 The SEBS Model

The SEBS Model is one of the commonly applied satellite-based techniques utilized to estimate total evaporation and has been applied in a vast array of studies in area of different climate, topography and land uses, including but not limited to; Su (2002), Jin *et al*. (2005), Jarmain *et al.* (2009), Li *et al.* (2009) van de Kwaast (2009), van de Kwaast et al. (2009), Gibson *et al.* (2011), Ma *et al*. (2011); (2012), Muhammed, (2012), Timmermans *et al*. (2013), Ershadi *et al.* (2014), Ma *et al*. (2014), Matinfar and Soorghali (2014), Mengistu *et al*. (2014), Pardo *et al.* (2014). The SEBS Model is easily accessible open source software, which is available in the Integrated Land and Water Information System (ILWIS).

The SEBS Model, developed by Su (2002), is a single-sourced surface energy balance model which can be utilized to estimate turbulent fluxes within the atmosphere or to determine the evaporative fraction through the use of remote sensing and meteorological data at both local and regional scales (Su, 2002). The SEBS model permits the use of data obtained from a variety of satellite sensors, which is available at varying spatial, temporal and spectral resolutions.

A number of tools are presented within the Model, which integrate meteorological data and satellite earth observation data to estimate daily total evaporation (Su, 2002). Su (2002) states that there are three primary sets of data required by SEBS to estimate the daily total evaporation for any region. This data is obtained from two sources i.e. through satellite earth observation systems measuring spectral reflectances and radiances of the land surface and meteorological stations. Satellite earth observation data is used to provide information for a number of land surface parameters required by SEBS, including the land surface albedo, land surface temperature, emissivity, fractional vegetation cover, leaf area index, vegetation roughness height and the normalized difference vegetation index (NDVI) (Su *et al.*, 2001; Su 2002).

Climatic data such as wind speed, air temperature, air pressure at a reference height, humidity and sunshine hours, are obtained from the meteorological stations. Radiation data i.e. the downward short-wave radiation, is also required by SEBS; however, this can be obtained from various sources and is not restricted to one particular source of the two previously described sources (Su *et al.*, 2001; Su, 2002).

The various input data required by SEBS is incorporated into three sub-models, to determine the components of the energy balance, stability factors and the roughness length of heat transfer (Su *et al.*, 2001; Su, 2002). The three sub-models are then used to estimate the evaporative fraction at limiting cases. The evaporative fraction in SEBS is assumed to be constant for the entire day and the daily total evaporation can then be determined from the available latent heat energy (Su *et al.*, 2001; Su, 2002).

The use of remote sensing data within SEBS improves the spatial representation of the estimates, whilst simultaneously accounting for the heterogeneity of the land surface over increasing geographic scales (Su, 2002). In addition to the various SEBS pre-processing functions available in ILWIS, SEBS possesses the added advantage of determining land surface physical parameters such as albedo, fractional vegetation cover and NDVI, amongst others (Su, 2002). The open-source nature of SEBS as well as the previously described advantages make it a promising tool which can be used as a decision support system for water resources research, planning and management.

2.3 Determination of Total Evaporation within SEBS

A number of equations are used to determine the daily total evaporation within SEBS. Satellite data derived from spectral reflectances and radiances of the land surface as well as meteorological data are used to determine the various variables outlined in these equations (Su, 2002). The following equations are used to determine the daily total evaporation in SEBS:

2.3.1 The simplified surface energy balance

The simplified surface energy balance equation is given as (Su, 2002):

$$Rn - G_o - H - \lambda ET = 0 \qquad (2.1)$$

Where Rn is net radiation ($W.m^{-2}$); H is sensible heat flux energy ($W.m^{-2}$); G_o is soil heat flux energy ($W.m^{-2}$) and λET is latent heat flux energy ($W.m^{-2}$).

2.3.2 The net radiation

The net radiation equation is given as (Su, 2002):

$$Rn = (1 - \alpha)\, RS_{wd} + \varepsilon . RL_{wd} - \varepsilon . \sigma . T_o^4 \quad (2.2)$$

Where α is land surface albedo; RS_{wd} is incoming solar radiation ($W.m^{-2}$); ε is surface emissivity; is RL_{wd} is incoming long wave radiation ($W.m^{-2}$); σ is Stefan Boltzman constant ($5.67x10^{-8}$ $W.m^{-}2.K^{-4}$) and T_o is the surface temperature (K).

2.3.3 The soil heat flux

Soil heat flux is one of the components of the energy balance equation. This energy flux enters the land surface during the day and exits the land surface at night. Generally, the soil heat flux is assumed to be zero over a 24-hour period (Muhammed, 2012). The soil heat flux equation is given as (Su, 2002):

$$G_o = Rn.[\Gamma_c + (1 - f_c).(\Gamma_s - \Gamma_c)] \quad (2.3)$$

Where Γ_c is the ratio of soil heat flux to net radiation which is assumed to be equal to 0.05 for a fully vegetated canopy (Monteith, 1973) and Γ_s is the ratio of soil heat flux to net radiation which is assumed to be equal to 0.315 for a bare soil surface (Kustas and Daughtry, 1989). The fractional canopy coverage (f_c), which is derived from satellite earth observation, is then used to perform an interpolation between the two limiting cases described above (Su, 2002).

2.3.4 The sensible heat flux

The sensible heat flux is determined by applying the similarity theory and the Monin-Obukhov stability correction procedure (Su, 2002).The equations used to determine wind and temperature profiles in the vertical direction are given in Equations 2.4 and 2.5 as:

$$u = (u^*/k) \times [\ln((z-d_o)/z_{om}) - \psi_m \times ((z-d_o)/L) + \psi_m \times (z_{om}/L)] \quad (2.4)$$

$$\theta_o - \theta_a = (H/ku^*\rho C_p) \times [\ln((z-d_o)/z_{oh}) - \psi_h \times ((z-d_o)/L) + \psi_h \times (z_{oh}/L)] \quad (2.5)$$

In Equations 2.4 and 2.5; u and u^* are wind and the friction velocity ($m.s^{-1}$) respectively, z and d_o are reference meteorological height (m) and displacement height respectively (m), ρ is the density of air ($kg.m^{-3}$), C_p is the heat capacity of dry air (Jkg^{-1}), k is von Karman's constant (0.4), z_{om} and z_{oh} are the roughness height for momentum and scalar roughness height for heat transfer respectively (m), θ_o and θ_a are the potential surface temperature and air temperature respectively at height z (K), ψ_m and ψ_h are stability correction factors for momentum and sensible heat transfer respectively and L is the Obhukov length (m) which is calculated as:

$$L = -(\rho C_p u^{*3} \theta_v / kgH) \quad (2.6)$$

Where θv is the virtual temperature near the surface (K) and g is the acceleration due to gravity (ms^{-2}).

In order to estimate the sensible heat flux the roughness length for momentum (z_{om}) and scalar roughness height for heat transfer are required (z_{oh}). The scalar roughness heigh for heat transfer is estimated as:

$$z_{oh} = z_{om}/\exp(KB^{-1}) \quad (2.7)$$

Where KB^{-1} is the inverse Stanton number which is a dimensionless heat transfer coefficient. In order to estimate the KB^{-1} value an extended model of Su *et al*. (2001) is proposed as:

$$KB^{-1} = [(kC_d/(4C_t) \times (u^*/(u(h))) \times (1-e^{Nec/2}) \times f_c^2] + [(2 f_c f_s) \times ((k \times (u^*/(u(h))) \times (z_{om}/h)/ C_t^*)) + (KB^{-1} \times f_s^2)] \quad (2.8)$$

Where C_d is the drag coefficient of foliage elements assumed to have a value of 0.2, N_{ec} is the within-canopy wind profile extinction coefficient, u(h) is the horizontal wind speed at the top of the canopy, f_c is the fractional vegetation cover and f_s is its complement, C_t is the heat transfer coefficient of the leaf which for most canopies and environmental conditions is bounded between $0.005N \leq C_t \leq 0.075N$ (N is the number of sides of the leaf which is involved in the heat transfer process).

C_t^* is the heat transfer coefficient of the soil given as $C_t^* = Pr^{-2/3} \times R_{e*}^{-1/2}$, where Pr is the Prandtl number and R_{e*} is the roughness Reynolds number which is estimated as $R_{e*} = h_s u_*/v$, where $h_s$is the roughness height of the soil and v is the kinematic viscosity of the air ($v = 1.327x10^{-5} \times (p_o/p) \times (T/T_o)^{1.81}$ where p and T are the ambient pressure and temeperature p_o = 101.3 Kpa and T_o = 273.5 K. For bare soils the KB^{-1} value can be estimated as:

$$KB_s^{-1} = 2.46(R_{e*})^{1/4} - \ln(7.4) \quad (2.9)$$

According to Su (2002) "the actual sensible heat flux is constrained in the range set by the sensible heat flux at the wet limit (H_{wet}) and the sensible heat flux at the dry limit (H_{dry})".

At, the dry limit, the latent heat is zero and the sensible heat flux possesses its maximum value due to, the limitation of soil moisture. The sensible heat flux under the dry limit is given as (Su, 2002):

$$H_{dry} = Rn - G_o \quad (2.10)$$

At, the wet limit, the sensible heat flux possesses its minimum value as evaporation can take place at near potential rates. The sensible heat flux at the wet limit is given as (Su, 2002):

$$H_{wet} = Rn - G_o - \lambda E_{wet} \quad (2.11)$$

2.3.5 The relative evaporation

The relative evaporation is given as (Su, 2002):

$$\Lambda r = \lambda E/\lambda E_{wet}$$

$$= 1 - (\lambda E_{wet} - \lambda E/ \lambda E_{wet}) \quad (2.12)$$

Where Λr is the relative evaporation; λE is the latent heat at the dry limit and λE_{wet} is the latent heat at the wet limit

Su (2002) then incorporates Equations 2.1, 2.10, and 2.11 into Equation 2.6 to represent the relative evaporation as:

$$\Lambda r = 1 - [(H - H_{wet})/ (H_{dry} - H_{wet}) \quad (2.13)$$

2.3.6 The evaporative fraction

In order to, determine the evaporative fraction; Su (2002) combined Equation 2.11 and a combination equation similar to the Penman combination equation. According to Menenti, (1984) when the resistance terms are grouped into internal and external bulk surface resistances, the combination equation to determine the latent heat energy can be given as follows:

$$\lambda E = [\Delta \times r_e \times (Rn - G_o) + pc_p(e_s - e_a)] / [r_e(\gamma + \Delta) + \gamma \times r_i] \quad (2.14)$$

Where Δ is the rate of change of saturated vapour pressure with temperature ($hPaK^{-1}$); r_e is aerodynamic resistance ($s.m^{-1}$); e_s is saturated vapour pressure (hPa); e_a is actual vapour pressure (hPa); γ is the psychometric constant($hPa.K^{-1}$) and r_i is the bulk surface internal resistance ($s.m^{-1}$).

In Equation 2.14, it is assumed that the roughness length for heat transfer and vapor transfer are equal (Brutsaert, 1982). The Penman-Monteith equation only holds true for a vegetated canopy, however Equation 2.8 is valid for both a vegetated canopy and a soil surface with defined bulk surface internal resistance (Su, 2002).

The use of Equation 2.14 to determine the latent heat energy can be seen as problematic due to the difficulty in determining the bulk surface internal resistance, as this is regulated by the availability of soil moisture (Su, 2002).

Su (2002) proposes a solution to this problem by circumventing the use of the bulk surface internal resistance in the estimation of the latent heat energy. According to definition, the internal bulk surface resistance at the wet limit is equal to zero. Incorporating this value into Equation 2.14 and altering the variables to reflect wet limit conditions, the sensible heat flux is given as (Su, 2002):

$$H_{wet} = [(Rn - Go) - (pc_p/r_{ew})((e_s - e_a)/\gamma)] / ((1 + \Delta)/\gamma) \quad (2.15)$$

The external resistance (r_{ew}) is a function of the Obukhov length, which sequentially is a function of the sensible heat flux and the friction velocity (Su, 2002) Equations 2.4 - 2.6. The friction velocity and the Obukhov length which have been determined previously can then be used to estimate the external resistance from Equation 2.5.

$$r_e = (1/ku^*) \times [\ln((z-d_o)/z_{oh}) - \psi_h \times ((z-d_o)/L) + \psi_h \times (z_{oh}/L)] \quad (2.16)$$

Similarly the external resistance at the wet limit can be determined as:

$$r_{ew} = (1/ku^*) \times [\ln((z-d_o)/z_{oh}) - \psi_h \times ((z-d_o)/L_w) + \psi_h \times (z_{oh}/L_w)] \quad (2.17)$$

The stability length at the wet limit can be determined as:

$$L_w = \rho u^{*3}/(k \times g \times 0.61 \times (Rn - G_o)/ \lambda)$$

The evaporative fraction can then be determined and is given as follows (Su, 2002):

$$\Lambda = \lambda E/(Rn - G)$$

$$= \Lambda r.\lambda E_{wet}/(Rn - G) \quad (2.18)$$

2.3.7 Daily total evaporation

If the evaporative fraction is assumed to be constant throughout the day, the daily actual ET can then be estimated as (Su, 2002):

$$E_{daily} = 8.64x10^7 \times \Lambda_o^{24} \times ((Rn_{24} - G_o)/ \lambda\rho_w) \quad (2.19)$$

Where E_{daily} is daily total evaporation (mm/day); Λ_o^{24} is the daily evaporative fraction; Rn_{24} is the daily net radiation which is measured *in situ* ($W.m^{-2}$); ρ_w is density of water ($kg.m-^3$) and λ is the latent heat of vaporization $(2.501-0.00237x\ T_{air})x10^{\wedge 6}$ ($J.kg^{-1}$).

2.4 Limitations Associated with the use of the Pre-Packaged Version of SEBS and Satellite Earth Observation in The Estimation of Total Evaporation

The benefits of employing satellite-based evaporation estimation techniques can be invaluable to improve water resources management; however, it is important to note that these techniques do possess limitations, some of which are shared by all satellite earth observation techniques, whilst some limitations are technique specific. It is often difficult to obtain continuous total evaporation data series using satellite earth observation techniques due to the effects of cloud cover as well as the revisit and repeat cycle of any given satellite (Jarmain *et al*., 2009; Mertz, 2010). Cloud coverage has a strong influence on the amount of reflected radiation, which can be measured from the earth's surface for both the optical and thermal wavelengths (Jarmain *et al*., 2009; Timmermans, 2012).

The amount of images which can be processed is therefore dependent on the amount of cloud free images available. The availability of an image for a particular region is also influenced by the satellite revisit and repeat cycle. The revisit and repeat cycles vary, depending on the satellite sensor which is being used.

In addition to the aforementioned limitations, the resolution of the satellite sensor influences the accuracy of the daily total evaporation estimate which is obtained. An image obtained using a coarse resolution sensor will not be able to accurately account for the spatial heterogeneity of the land surface which is being captured (McCabe and Wood, 2006; Li *et al.*, 2008; Jarmain, 2009).

With regards to SEBS, the model is highly sensitive to the following four parameters i.e. the gradient between the land surface temperature and air temperature (Su, 2002), the fractional vegetation cover formula (Lin, 2006; Badola, 2009; van de Kwast *et al.*, 2009), the displacement height and the height of wind speed measurements (Timmermans *et al.*, 2005; van de Kwast *et al.*, 2009) and the spatial heterogeneity of the study area (McCabe, and Wood, 2006; Li *et al.*, 2008). A detailed description of the aforementioned sensitive parameters is presented in Gibson *et al.* (2011).

Within the SEBS Model, instantaneous total evaporation values are extrapolated to daily total evaporation values by assuming that the evaporative fraction remains constant throughout the day (Su, 2002). Research undertaken by Stewart (1996); Lhomme and Elguerro (1998); Gentine *et al.* (2007); (2011) and Mkhwanazi and Chavez (2013), indicate that assuming the evaporative fraction to be constant throughout the day may lead to the generation of erroneous daily total evaporation estimates, especially during advective conditions (Gentine *et al.*, 2007; Mkhwanazi and Chavez, 2013).

2.5 Case studies: Application of the SEBS Model

A vast array of studies exist which utilize the SEBS Model to estimate total evaporation, however, only a few select case studies will be discussed in this section. A brief description of these studies is presented below. The key findings for each of these studies are presented in Tables 2.3 and 2.4.

Su (2002), proposed SEBS to estimate turbulent fluxes and the evaporative fraction, using satellite earth observation data. Three field data sets obtained from flux stations and one remote sensing data set obtained from the Thematic Mapper Simulator were used as inputs for the SEBS model. Four experimental data sets were then used to test the reliability of SEBS in this study.

Jarmain *et al*. (2009) conducted a study, to review techniques available to determine total evaporation utilizing satellite earth observation data and to recommend a technique that could be potentially applied in South Africa, in order to assist total evaporation estimation and water resources management. The SEBS model was one of the numerous techniques which were reviewed and applied. The SEBS model was applied to three study sites in South Africa i.e. Seven Oaks, St Lucia and Kirkwood. The simulated results were compared with a Kipp and Zonen Large Aperture Scintillometer, Surface Renewal and Eddy Covariance for each of the study sites, respectively.

Yang *et al*. (2010) applied the SEBS Model, to determine the water consumption of maize/wheat in the Northern China Plain. MODIS Level 1_B images from the period 2006 to 2008 and meteorological data obtained from a field-based flux tower were used as inputs to the SEBS model. The simulated total evaporation estimates were validated against the field-based measurements of the energy fluxes and total evaporation estimates obtained from an eddy covariance system.

Elhag *et al*. (2011) applied the SEBS model over the Nile delta, to estimate daily total evaporation. AATSR and MERIS Level 1_B data were used as inputs to SEBS, in conjunction with meteorological data obtained from six *in situ* meteorological stations. The simulated daily total evaporation estimates were compared against actual ground truth data taken from ninety-two points uniformly distributed over the study area.

Gibson *et al.* (2011) conducted a study in the Piketberg region in the Western Cape Province of South Africa, to investigate the uncertainties associated with the application of the pre-packaged version of SEBS in ILWIS. MODIS Level1_B, Advanced Spaceborne Thermal Emmision and Reflection Radiometer (ASTER) Level 1_B and ASTER Level 2 data, as well as meteorological data obtained from an automatic weather station located in the study area were used in this study.

Rwasoka *et al.* (2011) applied the SEBS model, to determine the total evaporation of the Upper Manyame Catchment in Zimbabwe. Nine clear sky MODIS Level 1_B images and field-based meteorological data were used as inputs to SEBS to generate total evaporation estimates, which corresponded to the time of the satellite overpass. Two study sites were selected i.e. the Harare Kutsage Station and the Grasslands Station. The simulated total evaporation estimates were evaluated for physical/logical consistency, by comparing total evaporation estimates against reference evaporation, spatial variation of total evaporation and understanding the total evaporation of different land types.

Muhammed (2012) conducted a study to investigate the use of satellite earth observation data in a hydrological model. The SEBS Model was used to estimate daily total evaporation, which was one of the inputs required by the TOP model to simulate streamflow for the Upper Gilgal Abbay Basin. Streamflow volume estimates obtained, using SEBS estimates of total evaporation were compared against the streamflow volume estimates which were obtained by using the TOP Model total evaporation estimates.

Ma *et al*. (2014) applied the SEBS model, to determine the regional distribution of total evaporation over the NamCo region in the Tibetan Plateau, situated in the northwest of China. Two scenes of ASTER data for the 11th June 2006 and 25th February 2008 were used as inputs, to the SEBS Model, to estimate total evaporation. The simulated total evaporation estimates were validated against the field-based measurements of the energy fluxes and total evaporation estimates obtained from an eddy covariance system

Mengistu *et al*. (2014) applied the SEBS Model, to derive spatially representative total evaporation for the Baynesfield Estate in KwaZulu Natal South Africa, which would be used to assist in the calibration of hydro-meteorological models. MODIS Terra images and Landsat 7 EM+ were used as inputs to the SEBS Model for the estimation of total evaporation. The SEBS daily total evaporation estimates obtained using the MODIS Terra images and the Landsat 7 EM+ images were compared with Eddy covariance daily total evaporation measurements.

Table 2.3 Summary of key findings for limited list of case studies

STUDY	MAIN OBJECTIVE	SUMMARY OF KEY FINDINGS
Su, 2002	Assess the reliability of SEBS to estimate total evaporation	• SEBS can provide reliable estimates of H. • Errors in the estimation of H due to uncertainties in roughness height for heat transfer equations. • Stability corrections available at the time were inadequate.
Jarmain *et al.*, 2009	Review satellite based total evaporation techniques	• For two of the three sites SEBS estimates of R_n compared favourably with field observations. • SEBS failed to accurately simulate G for all three study sites it was applied to. • SEBS estimates of the sensible heat flux and the evaporative fraction were in good agreement with field observations for two of the three study sites.
Yang *et al.*, 2010	Determine the water consumption of maize/wheat in the Northern China Plain	• SEBS performed better during the wheat growing season than during the maize growing season. • The relative error in the estimation of LE was within 20% either within the wheat growing or maize growing season.
Elhag *et al.*, 2011	Determine total evaporation using SEBS	• SEBS total evaporation estimates were in good agreement with field based measurements. • The ability of the model to utilize satellite earth observation data with a high temporal resolution will assist decision makers to take into account the different plant growth phases and improve their real time water management strategies
Gibson *et al.*, 2011	Investigation of uncertainties associated with the pre-packaged version of SEBS in ILWIS	• The use of a coarse spatial resolution sensor is appropriate for catchment scale operations however at the field scale high spatial resolution imagery is required. • The pre-packaged version of SEBS in ILWIS was found to be most sensitive to; the land surface and air temperature gradient, choice of fractional vegetation cover formula, displacement height and height at which wind speed is measured, and the heterogeneity of the study area.

Table 2.4 Summary of key findings for limited list of case studies

STUDY	MAIN OBJECTIVE	SUMMARY OF KEY FINDINGS
Rwasoka *et al.*, 2011	Determine total evaporation using SEBS	• On average SEBS performed well for the plausibility and consistency check. • SEBS performed well for the Harare-Kutsage station and poorly for the Grassland station, this was attributed to spatial variability of temperature, heterogeneity of the land surface and roughness parameterization. • Overall the model was found to be a useful tool to estimate spatial total evaporation.
Muhammed, 2012	Application of satellite based total evaporation estimates in a hydrological model	• SEBS total evaporation estimates were found to be realistic when related to the seasonal conditions of the study area. • The comparison between streamflow volume estimates obtained using SEBS estimates of total evaporation and streamflow volume estimates obtained using the TOP model total evaporation estimates, produced satisfactory results with a Nash-Sutcliffe efficiency of 0.78 and a relative volume error of 0.59
Ma *et al.*, 2014	Determine the regional distribution of total evaporation in the NamCo region in the Tibetan Plateau	• The SEBS model over-estimated the total evaporation for by 39.50% and 38.90% for 11th June 2006 and 25th February 2008, respectively, when compared with eddy covariance measurements. • The comparison between the observed data and the SEBS estimates yielded, a root mean square error value of 0.7mm/day.
Mengistu *et al.*, 2014	Provide accurate field and satellite estimates of total evaporation for the calibration of hydro-meteorological models	• The SEBS daily total evaporation estimates using MODIS Terra images, as well as, Landsat 7 EM+ were higher than Eddy covariance daily total evaporation estimates for the corresponding days. • The SEBS Model over-estimated the daily total evaporation by approximately 15% for these days.

2.6 Integrating satellite earth observation and hydrological modelling

There has been a concerted global research effort to integrate satellite earth observation data with hydrological modelling over the past decade (Xu *et al.*, 2014). A large majority of the research with regards to this topic has been focused on; integrating satellite derived hydrological parameters, such as precipitation, surface soil moisture, leaf area index and total evaporation, with hydrological modelling (Xu *et al.*, 2014).

Xu *et al*. (2014) states that satellite earth observation can contribute to hydrological modelling applications, by providing estimates for a variety of hydro-meteorological parameters, through three possible methods; (i) applying the satellite earth observation data to model inputs, (ii) applying the satellite earth observation data to parameter estimation and (iii) applying the satellite earth observation data to a data assimilation problem.

According to Xu *et al*. (2014), the first of the aforementioned methods has been the historically dominant strategy, which has been applied, to facilitate the integration of satellite earth observation and hydrological modelling. With regards to this strategy, satellite earth observation can be used to provide hydrological models with information on catchment characteristics, satellite derived hydrologic variables required to drive the model and spatially representative data for forcing hydrological models.

* * * * * *

The research presented in the literature review assisted in the identification of; (i) a satellite based technique which can be used to estimate total evaporation and (ii) a potential strategy to assist in the integration of satellite earth observation data and hydrological modelling. These findings assisted in, informing the methodology used for this study.

The SEBS model was chosen to be applied in this study, to generate daily total evaporation estimates. These estimates would then be integrated and applied in a hydrological model, based on the historically dominant strategy described in Xu *et al*. (2014).

Chapter three will discuss the selection and description of the study area, whilst Chapter four will provide a detailed description of the methodology used to generate the SEBS daily total evaporation estimates and the approach used to integrate these estimates in the ACRU Model.

3. STUDY AREA

The Risk-based Operational Water Management Project (RISKOMAN) was established, to assist water managers and stakeholders in the identification, application and modification of efficient allocation policies for the Incomati Basin which is shared between South Africa, Swaziland and Mozambique (Ridell and Jewitt, 2010).

3.1 Description of the study area

The Inkomati Catchment is located in the Mpumalanga Province and partially in the Limpopo Province, both of which lie in the north-eastern half of South Africa. The Inkomati Catchment, which forms part of the international Incomati River Basin, borders the countries of Mozambique and Swaziland, on the east and south-east, respectively (Basson and Rossouw, 2003). There are three major catchments within the Inkomati Catchment i.e. the Komati, Crocodile and Sabie-Sands Catchments. In addition to this, two smaller catchments i.e. the Nwaswitsontso and Nwanedzi Catchments, are located in the conservation areas within South Africa (Kruger National Park) (DWAF, 2001). All the rivers within the Inkomati Catchment flow into the Incomati River. The Incomati River enters the Indian Ocean near Marracuene, after flowing through Mozambique (DWAF, 2001). Figure 3.1 illustrates the Inkomati Catchment, its sub-catchments and flow network.

The majority of the precipitation which falls within the Catchment occurs during the summer months. The mean annual precipitation (MAP) ranges between 400 mm to 1000 mm. In the mountainous regions of the Catchment, MAP may reach approximately 1500 mm (DWAF, 2001; Basson and Rossouw, 2003). Potential evaporation exceeds rainfall, which is accentuated in the drier reaches of the Catchment (Basson and Rossouw, 2003).

The Great Escarpment divides the Catchment into the Plateau region on the west and the Lowveld region in the East. As a result of this topographical divide, there are noticeably different climates within the region (Basson and Rossouw, 2003). The natural vegetation varies from scarce thornveld in the east and forestry along the Escarpment, to savannah vegetation in the Highveld (Basson and Rossouw, 2003). The geology of the region is complex and usually possesses a low water-bearing capacity (Basson and Rossouw, 2003). There are a large variety of land uses spread throughout the region, as well as numerous major storage dams (DWAF, 2001; Basson and Rossouw, 2003).

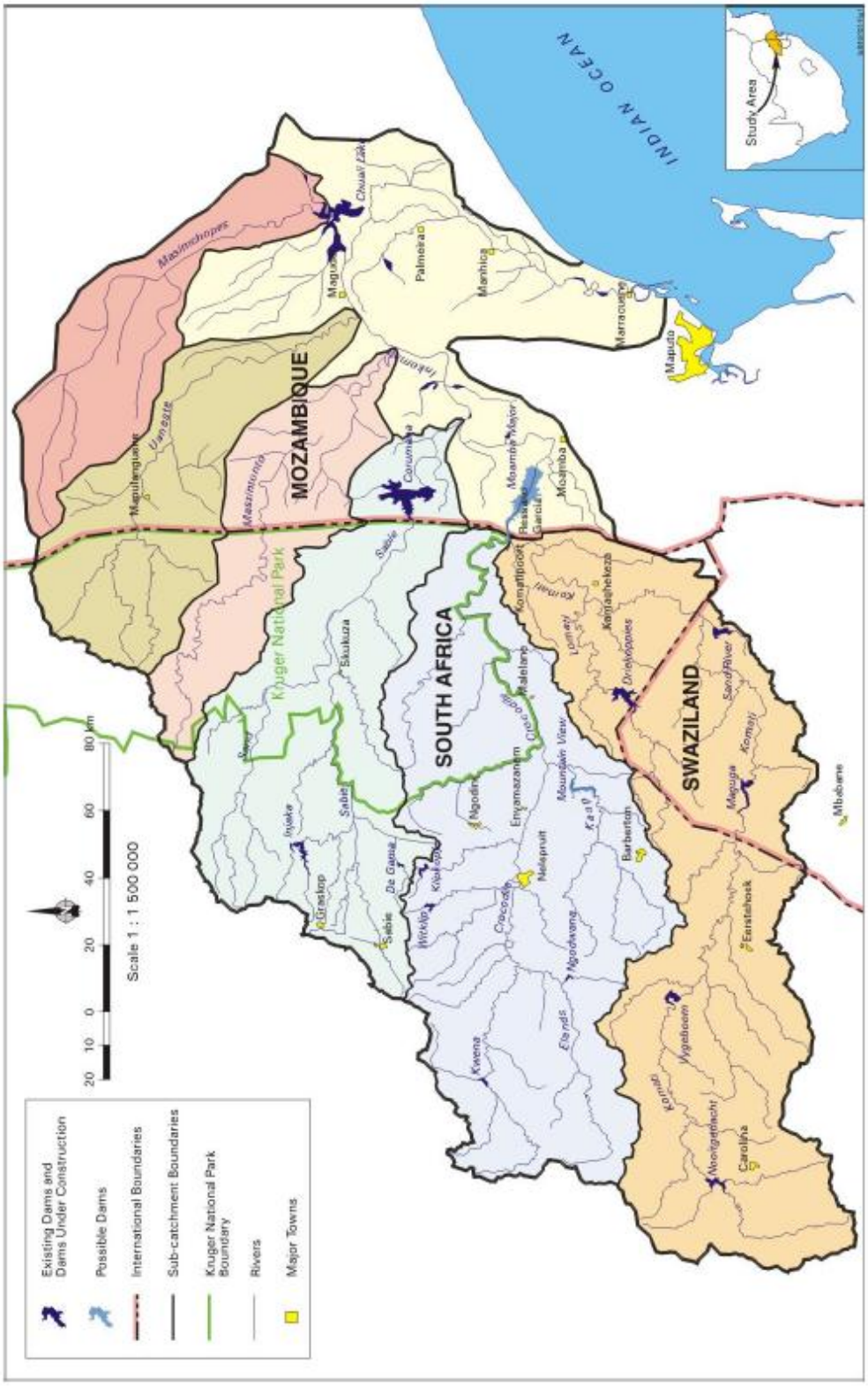

Figure 3.1 Location of the Inkomati Catchment within the Incomati Basin (After Jibs, 2011)

Two study sites, which are located within the Inkomati Catchment, were selected for this study i.e. the Komatipoort Research site and the X23_A quarternary catchment situated within the Kaap River Catchment. Figures 3.2 and 3.3, illustrate the location of these catchments within South Africa, respectively. The Komatipoort Research Site is located within the Inkomati Catchment in the north-eastern part of South Africa. The study site was selected based on the availability of meteorological data and observed daily total evaporation data. The sugarcane field within the Komatipoort Research Site is approximately 0.04 km^2. The surface renewal system and the eddy covariance flux tower which are discussed in the following chapter are situated within in this field at coordinates (25.59^0 S, 31.89^0 E).

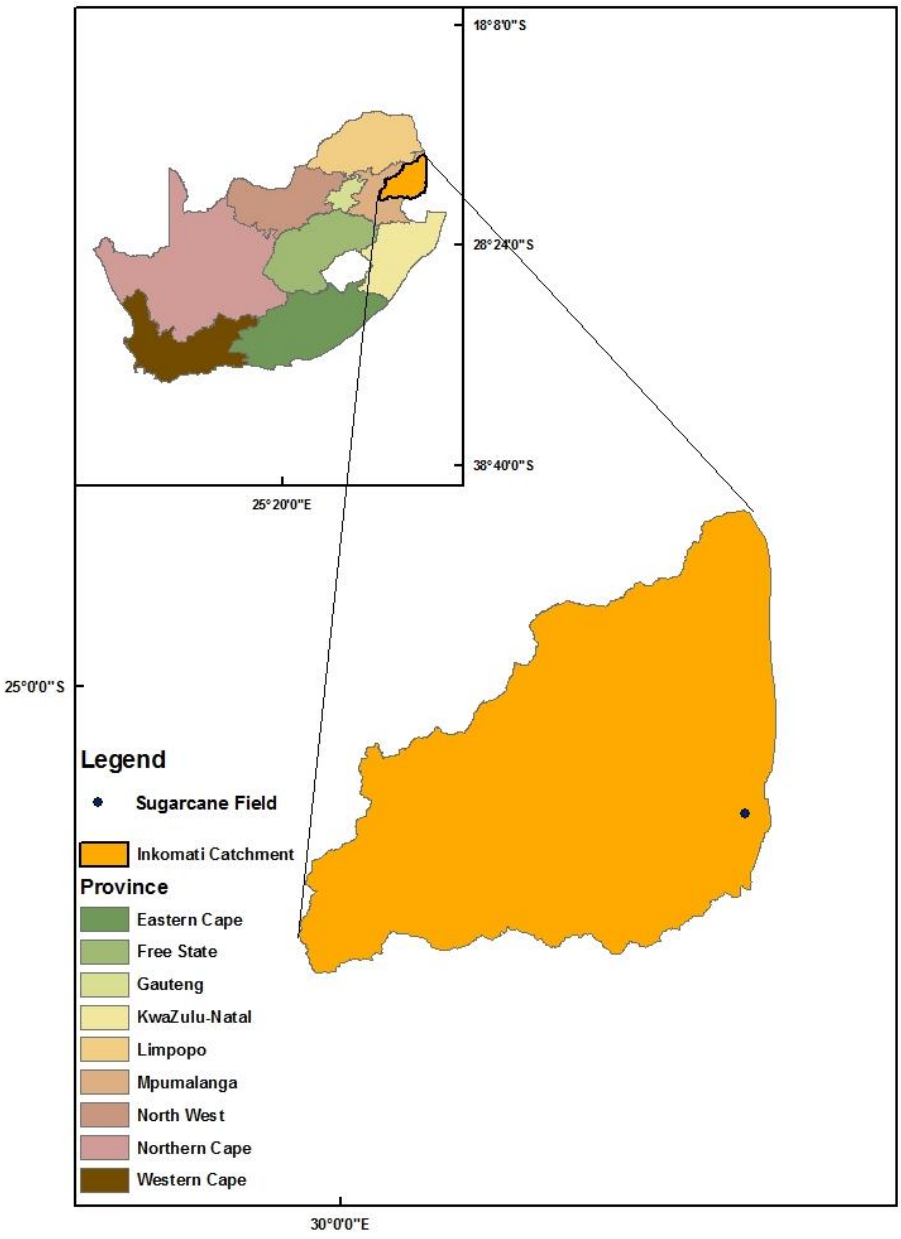

Figure 3.2 Location of the Komatipoort sugarcane field within the Inkomati Catchment

The X23_A quarternary catchment is situated within the Kaap River Catchment, which forms part of the Inkomati Catchment in the north-eastern part of South Africa. The catchment was selected based on the availability of nearby meteorological data and streamflow data, which coincided with the satellite-derived total evaporation estimates, which were processed for this study. The X23_A Catchment is located at coordinates (25.62^0 S, 30.75^0 E) and is situated at 1161 m above sea level, with an approximate area of 126.81 km^2. The mean annual precipitation (MAP) which the X23_A Catchment receives is approximately 1057 mm, with majority of the rainfall occurring during the summer months.

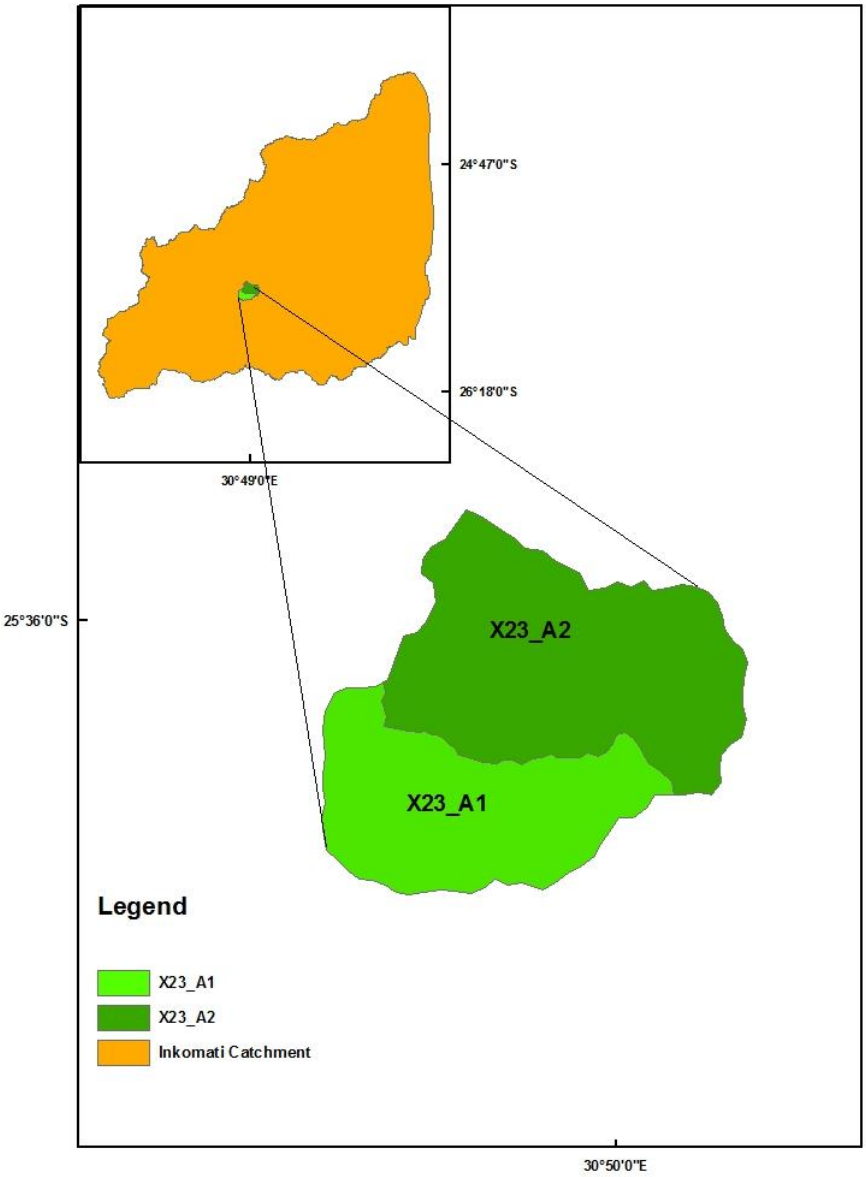

Figure 3.3 Location of the X23_A quarternary Catchment within the Inkomati Catchment

4. METHODOLOGY

4.1 General Methodology

The methodology which was applied in this study was divided into two sections, to answer the research questions posed in Chapter 1, which were listed as:

i. How do satellite-derived daily total evaporation estimates compare against *in situ* measurements obtained from a conventional technique?
ii. How can the satellite derived total evaporation estimates be incorporated into a hydrological model?
iii. How will simulated streamflow, using satellite-derived total evaporation estimates, compare against observed stream flow?

The first section was aimed at addressing research question one. The research carried out in this section, involved the application of the SEBS model, to generate daily total evaporation estimates. The total evaporation estimates generated by SEBS were compared with the observed historical daily total evaporation estimates for an irrigated sugarcane field situated in Komatipoort (Figure 3.2). The surface renewal technique was used, to obtain the historical daily total evaporation estimates. The satellite pixels located, in and around, the field site were selected as areas of interest and only the data within these pixels were used for the data comparison.

The methodology for Section One of the research work was divided into three phases. Phase One involved the collection of the SEBS input data. Historical satellite earth observation data and historical meteorological data were collected for the period 01st December 2011 to 25th November 2012. The choice of the time period for the collection of the satellite earth observation data was influenced by the availability of the historical observed data. Phase Two involved the pre-processing of the satellite earth observation data, which was collected in Phase One and Phase Three involved the use of the pre-processed data and the meteorological data as inputs, to the SEBS Model, to generate a daily total evaporation estimate.

Section Two of the research work was aimed at addressing the second and third research questions. The research conducted in this section involved, the application of SEBS total evaporation estimates for the period 01st December 2011 to 25th November 2012, as an input to the ACRU Model, to simulate the streamflow of the X23_A quarternary located within the Kaap Catchment. The average satellite pixel values located within the X23_A1 and X23_A2 sub-catchments were used to generate the daily total evaporation time series.

Due to the effects of cloud coverage, it was not possible to create a continuous total evaporation time series extending from the SEBS model. Therefore, these missing records needed to be infilled. A preliminary investigation was conducted, to identify a potential infilling technique, which could be used, to assist in the generation of a continuous total evaporation time series. Once the continuous total evaporation time series had been generated, two streamflow modelling scenarios, as well as two sensitivity analysis tests were performed using the ACRU Model.

In addition to the SEBS total evaporation data and the historical observed total evaporation data obtained from the surface renewal technique, historical rainfall and temperature data obtained from the Agricultural Research Council Institute for Soil, Climate and Water (ARC-ISCW), streamflow data obtained from the Department of Water Affairs (DWAF), soil characteristics from the national land type map, leaf area index (LAI) obtained from the MODIS products of MOD15A2 data and landcover data at 20 m resolution obtained from the SPOT 5 satellite, were used as inputs to ACRU.

Performance statistics were used, to analyse the results obtained from the comparisons between the total evaporation estimates, extending from the SEBS Model and the historical total evaporation estimates obtained from the surface renewal system, as well as for the comparisons between the two infilling techniques.

The statistics used in this study were the mean, median, relative volume error (RVE), root mean square error (RMSE), coefficient of determination (R^2) and a two sample t-test. These statistics have been used in a variety of studies in which satellite earth observation data are used to estimate total evaporation (Su, 2002; Jarmain et al., 2009; Yang *et al*., 2010; Elhag *et al*., 2011; Gibson et al., 2011; Rwasoka et al., 2012; Muhammed, 2012; Ma *et al*., 2014; Pardo *et al*., 2014).

The two sample t-test was conducted to assess if there was any significant difference between the means of the historical total evaporation estimates obtained from the surface renewal system and the total evaporation estimates extending from the SEBS Model, as well as to determine if there was any significant difference between the infilled data values and the known data values.

4.2 Satellite Earth Observation Data and Meteorological Data Inputs

Historical Moderate Resolution Imaging Spectroradiometer (MODIS) Terra images were used for this study, for the SEBS total evaporation estimation. Terra orbits the earth from a northerly to a southerly direction, passing the equator during the morning, (Muhammed, 2012). The spatial resolution of the data obtained from the MODIS sensors varies, depending on the product. MODIS Level 1_B calibrated radiances and a MODIS geo-location file were downloaded and used during the pre-processing phase of the study. MODIS Level 1_B data is calibrated, but not atmospherically corrected (Wang, 2010). The spatial resolutions of the products used in this study are displayed in Table 4.1.

Table 4.1 Spatial and temporal resolutions for each of the MODIS products used for the estimation of daily total evaporation (http://ladsweb.nascom.nasa.gov/data)

MODIS_ID	Terra level 1 product	Spatial Resolution	Temporal Resolution
MOD021KM	Level1_B calibrated radiances	1km	Daily
MOD03	Geolocation	1km	Daily

The images used in this study were primarily selected according to the extent of cloud coverage present within an image for a particular day. Images possessing little or no cloud coverage were selected. The rule used in the selection of images was that, only those images, which possessed less than approximately 30% (visual assessment) of cloud coverage over the study area, were selected.

Meteorological data for the study area (i.e. hourly solar radiation and hourly temperature data) were collected at co-ordinates 25^0 35' 40" S, 31^0 53' 33" E. These records were previously collected for the WRC study K5/2079//4 undertaken by Jarmain (2012) and Jarmain *et al.* (2013). However, this meteorological data did possess gaps. Consequently, hourly solar radiation and temperature data was obtained from the ARC-ISCW and used as a surrogate input for days in which there was no hourly solar radiation and temperature data available from the study undertaken by Jarmain (2012) and Jarmain *et al.* (2013).

In addition to the previously described meteorological parameters, ancillary meteorological data required for this study i.e wind speed, temperature and solar radiation were obtained from the ARC-ISCW, as well as the NASA earth observatory website (water vapor and aerosol optical thickness). The historical daily total evaporation records were provided by Dr C Jarmain. These records were previously collected at co-ordinates 25^0 35' 40" S, 31^0 53' 33" E for the WRC study K5/2079//4 by Jarmain (2012) and Jarmain *et al.* (2013).

4.3 Pre-processing and Post-processing of Satellite Earth Observation Data to be used in SEBS for the Estimation of Daily Total Evaporation

4.3.1 Pre-processing and post-processing of MODIS Level1_B data

The MODIS Level1_B data sourced for this study were in an orbit-based format, therefore they needed to be projected into a standard projection and format which would be compatible with Geographic Information System (GIS) software. The MODIS reprojection Swath Tool was used to convert both the MODIS Level1_B calibrated radiances and MODIS geolocation files into a geographic projection and Geotiff format, which is supported by ILWIS. During, this procedure only the relevant reflectance bands, which were required for further processing were exported into ILWIS (Wang, 2010; Timmermans, 2011). These bands are displayed in Table 4.2.

The MODIS Level 1_B data which were imported into ILWIS were given as a simplified integer number and therefore had to be converted into reflectances and radiances (Wang, 2010). Calibration coefficients consisting of scales and offsets are used in ILWIS, to perform the aforementioned conversion (Wang, 2010).

Calibration coefficients can be obtained from viewing the MODIS Level1_B data files in the HDF View 2.9 Software Tool. Band1_dn and Band3_dn to Band7_dn were converted to reflectances, whilst Band31_dn and Band32_dn were converted to radiances by, applying the relevant reflectance and radiance calibration coefficients (Wang, 2010). The solar and satellite zenith and azimuth angles also required correction. A scaling factor of 0.01 was applied to each of these bands (Wang, 2010).

Table 4.2 Representation of the 17 extracted reflectance bands and their output file names in ILWIS (Wang, 2010)

Input GeoTIFF filename	Output Filename in ILWIS
EV_250_Aggr1km_RefSB_b0.tif	Band1_dn
EV_250_Aggr1km_RefSB_b1.tif	Band2_dn
EV_500_Aggr1km_RefSB_b0.tif	Band3_dn
EV_500_Aggr1km_RefSB_b1.tif	Band4_dn
EV_500_Aggr1km_RefSB_b2.tif	Band5_dn
EV_500_Aggr1km_RefSB_b3.tif	Band6_dn
EV_500_Aggr1km_RefSB_b4.tif	Band7_dn
EV_1KM_RefSB_b11.tif	Band17_dn
EV_1KM_RefSB_b12.tif	Band18_dn
EV_1KM_RefSB_b13.tif	Band19_dn
EV_1KM_Emissive_b10.tif	Band31_dn
EV_1KM_Emissive_b11.tif	Band32_dn
SolarZenith.tif	sza_dn
SolarAzimuth.tif	saa_dn
SensorAzimuth.tif	vaa_dn
SensorZenith.tif	vza_dn
Height.tif	Height

The corrected reflectance, radiance, solar azimuth, satellite zenith, sensor zenith and sensor azimuth were then used as inputs to five processing phases in ILWIS i.e. computing the brightness temperature, A Simplified Method for the Atmospheric Correction of Satellite Measurements (SMAC), land surface albedo computation, land surface emissivity computation and the land surface temperature computation (Wang, 2010). The radiance values of Bands 31 and 32 were used to compute the brightness temperature by, converting radiances to black body temperatures (Wang, 2010).

This procedure is based on Planck's equation which is given as:

$$T_c = C_2/(\lambda_c \log((C_1/\lambda_c 5\pi L_s) + 1) \quad (4.1)$$

Where T_c is the brightness temperature from a central wavelength and λ_c is the sensors central wavelength.

The SMAC procedure derived by Rahman and Dedieu (1994) is used to correct all bands present in the visible channel i.e. Bands 1 to 7. The land surface albedo was computed utilizing the atmospherically corrected Bands 1 to 5, Band 7 and the formula derived by Liang (2001; 2002) given in Equations 4.2 as follows:

$$\alpha = (0.160 \times r1) + (0.291 \times r2) + (0.243 \times r3) + (0.116 \times r4) + (0.112 \times r5) + (0.018 \times r7) - 0.0015 \quad (4.2)$$

Where α is land surface albedo and r1, r2, r3, r4, r5, and r7 are bands present in the visible channel i.e. Bands 1 to 5 and Band 7.

The land surface emissivity was computed, using the atmospherically corrected Bands 1 and 2, as well the land surface albedo maps. This procedure is based on the algorithm described in Sobrinho *et al*. (2003) which fixes threshold values in the Normalized Difference Vegetation Index (NDVI) to differentiate between pixels i.e. bare soils pixels, vegetation pixels and a combination of bare soils and vegetation pixels.

In addition to, the land surface emissivity computation, emissivity difference, NDVI and vegetation proportion were also computed in ILWIS during this phase. The final phase involved computing the land surface temperature based on the formula by Sobrinho and Rassouni (2000). Water vapour values, which are required for the above mentioned formula, were not sourced for this study; instead the formula described in Li *et al*. (2003) was used to estimate water vapour values.

4.3.2 Estimation of daily total evaporation in SEBS

Meteorological data inputs such, as the air temperature, mean daily air temperature, mean daily wind speed, surface pressure and pressure at a reference height are used in conjunction with the satellite-derived raster maps to estimate daily total evaporation based on the algorithm derived by Su (2002).

Apart from the SEBS daily total evaporation map, additional maps are generated in ILWIS, once the SEBS model has been applied. These include the evaporative fraction, relative evaporation, soil heat flux, sensible heat flux at the dry limit, sensible heat flux at the wet limit, sensible heat flux, net radiation, latent heat flux, roughness height for momentum transfer, stability corrections, scalar roughness height for heat transfer, difference between LST and air temperature and the kb^{-1} value (Wang, 2010; Timmermans, 2011).

4.4 Estimation of daily total evaporation using the Surface Renewal Technique

The surface renewal technique is an energy balance technique which can be used to estimate the daily total evaporation (Savage *et al*., 2004). It requires knowledge of only a few parameters and is relatively low-cost, compared to other conventional techniques, therefore making it an attractive technique to use for the estimation of daily total evaporation (Jarmain *et al.*, 2013). The surface renewal technique is used to estimate the sensible heat flux.

The sensible heat flux is then combined with measurements of the soil heat flux and net radiation, to determine the latent heat flux as a residual of the simplified energy balance equation (Jarmain *et al.*, 2013). The surface renewal technique requires information pertaining to the vegetation type, measurement height, the air temperature gradient and a weighting factor (Jarmain *et al.*, 2013). The surface renewal technique requires calibration.

This is achieved by determining the weighting factor beforehand for the vegetation type, thermocouple size and measurement height and then comparing the estimated sensible heat flux against the sensible heat flux measured by an alternate technique (Jarmain *et al.*, 2013). Weighting factors are obtainable for a variety of vegetation types (Nile, 2010).

An eddy covariance system was installed *in situ* to determine the weigthing factors for a young short sugarcane crop during the period 24th July to 17th September 2012. The factors used for the remaining period and the various sugarcane growth stages were obtained from literature (Jarmain, 2013).

A graphic of the surface renewal system and eddy covariance flux tower is depicted in Figure 4.1. The surface renewal total evaporation data set used in this study was obtained by Dr C Jarmain for the WRC K5/2079//4study. The surface renewal system and eddy covariance flux tower was set up on a sugarcane field in Komatipoort Research Site (co-ordinates: 25^0 35' 40" S, 31^0 53' 33" E).

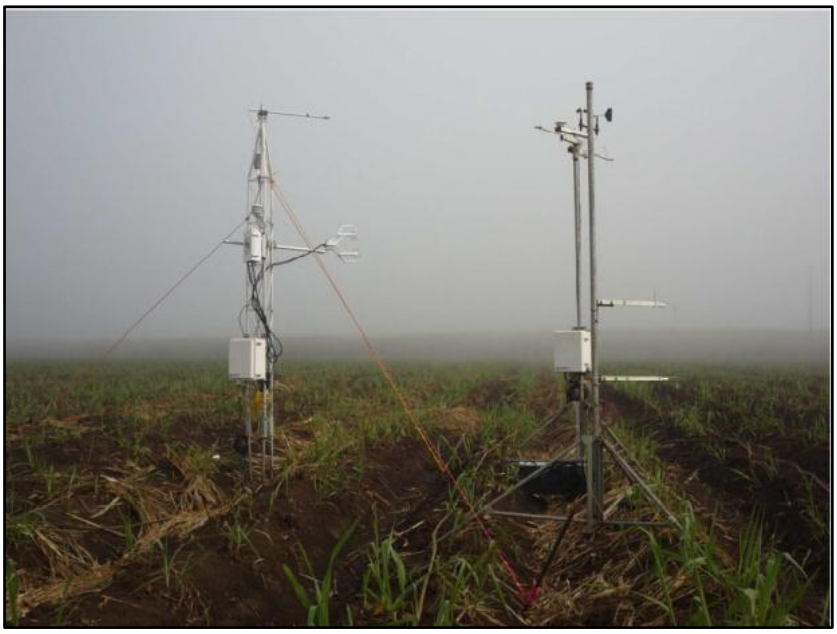

Figure 4.1 The surface renewal system (left) and the eddy covariance flux tower (right) used for calibration, installed in a sugarcane field in Komatipoort (Jarmain et al., 2013)

4.5 Application of the SEBS Model

The MODIS historical satellite earth observation data, as well as the historical meteorological data were used as inputs to the SEBS Model in order to conduct simulations to estimate the daily total evaporation. The SEBS model was used to estimate total evaporation on a daily time step for a period of 361 days i.e. from 01st December 2011 to 25th November 2012.

The daily total evaporation estimates generated through the use of MODIS Level 1_B satellite data were compared against observed historical daily total evaporation obtained through the use of the surface renewal technique.

A continuous daily total evaporation time series forms a fundamental component for the streamflow modelling component of the study, therefore MODIS Level1_B data was seen as the best option to be used for the estimation of daily total evaporation. An alternate to the use of MODIS Level 1_B data in the pre-packaged version of SEBS, is data obtained from the AATSR/MERIS sensors and Landsat. However, the temporal resolution of this data is far coarser than that of MODIS Level 1_B; therefore utilizing this data was not considered for this study.

In addition to the limited temporal availability of AATSR/MERIS data, the ENVISAT satellite which houses these two sensors was decommissioned in 2012, therefore only data captured before this period would have been available for processing. The validation data provided by Jarmain (2012) and Jarmain *et al.* (2013) is for the period 01st December 2011 to 25th November 2012. Consequently the use of AATSR/MERIS would have not been applicable for the scope of this project.

4.6 Infilling Techniques used to create a Continuous Daily Total Evaporation time series

Due to complete cloud coverage for twenty-eight days in the MODIS Level1_B data, it was impossible to generate a continuous daily total evaporation data set, using SEBS estimates of total evaporation. Therefore the use of an infilling technique was required to infill the missing data records within the time period 01st December 2011 to 25th November 2012.

The linear interpolation technique by Muhammed (2012) and the Kc_{act} technique by Santos *et al*. (2008) were applied in this study. These techniques were selected based on, the following criteria i.e. their relative ease of application and the data requirements of the technique. The description of each technique, as well as the methodological approach used to apply these techniques in this study will be further described in the following sub-sections.

4.6.1 The Linear Interpolation Technique

Muhammed (2012) applied a linear interpolation technique to infill missing data in a time series of daily total evaporation. Daily total evaporation estimates were generated by the SEBS Model. Muhammed (2012) used SEBS to populate a daily total evaporation time series which was to be used in the TOP model to conduct streamflow modelling simulations for the Gilgel Abay Catchment, Ethiopia. The daily total evaporation values generated for the days in which images possessed little or no cloud cover were used to infill the missing total evaporation records by interpolating between consecutive days for which daily total evaporation was known.

The aforementioned technique was used to infill the missing data in the SEBS total evaporation time series for this study which could be attributed to the presence of cloud cover. The linear interpolation technique described in Muhammed (2012) is given as:

$$ET_2 = [(ET_3-ET_1)/X_3-X_1)] (X_2-X_1) +ET_1 \quad (4.3)$$

Where ET_2 is the unknown daily total evaporation value (mm/day); ET_1 is the first known daily total evaporation value (mm/day); ET_3 is the next known daily total evaporation value; X_1 is the Julian day for ET_1; X_2 is the Julian day for ET_2 and X_3 is the Julian day for ET_3.

4.6.2 The Actual Crop Coefficient (Kc_{act}) Technique

The Kc_{act} technique derived and discussed in Santos *et al.* (2008) was used to incorporate total evaporation estimates derived from a satellite-based remote sensing technique i.e. Mapping Evapotranspiration with high Resolution and Internalized Calibration (METRIC) into a Water Balance Model, with the aim of improving irrigation scheduling in the Genil Cabra Irrigation Scheme, Spain. Santos *et al.* (2008) describes Kc_{act} as the ratio between total evaporation and the reference evaporation, which is determined using the standardized Penman-Monteith technique (ASCE-EWRI, 2005).

The Kc_{act} equation is given as:

$$Kc_{act} = AET/ET_0 \quad (4.4)$$

Where Kc_{act} is actual Kc; AET is total evaporation (mm/day) and ET_0 is reference evaporation

However, Kc_{act} differs from the Kc described by Allen *et al.* (1998) (Santos *et al.*, 2008). Santos *et al.* (2008) produced Kc_{act} images by dividing the total evaporation images produced in METRIC by the reference evaporation. Kc_{act} was interpolated between missing dates as the total evaporation images were temporally spaced at a minimum of 16 days. A spline was used to interpolate the values for the missing dates in order to account for the temporal progression of Kc_{act} which, in turn, was used to develop the Kc_{act} curves (Santos *et al.*, 2008). Due to the temporal spacing of images in the study undertaken by Santos *et al.* (2008), Kc_{act} values were obtained for every 16 days at minimum.

The MODIS Level 1_B images used in this study are available at a daily time step. Therefore, theoretically a Kc_{act} value could be generated on a daily basis for the entire time period, provided there was limited or no cloud cover on a particular day.

Although it is possible to generate a Kc_{act} value on a daily basis, this option was not exercised in this study. Instead, Kc_{act} values were generated approximately once every 10 days by dividing the MODIS Level 1_B image by the reference evaporation for that particular day. The reference evaporation data was obtained from the SASRI weather web for the period 01st January 2012 to 31st December 2012.

The choice of this temporal scale was based on the characteristics of the single crop coefficient approach. The crop coefficient can be described as a coefficient which expresses the difference in total evaporation between a particular crop and the reference grass (FAO, 1998). The differences between the crop and reference grass evaporation can be combined into a single coefficient or it can be divided into individual factors separately, describing the differences in soil water evaporation and transpiration between the crop and reference grass surfaces (FAO, 1998). The SEBS total evaporation estimate is a combined estimate of soil water evaporation and transpiration, therefore the single crop coefficient approach was seen as the most applicable approach to apply in this study (FAO, 1998).

The single crop coefficient approach is generally used to determine total evaporation for weekly or longer temporal periods. However, calculations using this coefficient may be undertaken on a daily basis (FAO, 1998). Suitable temporal scales for the application of the single crop coefficient are suggested in FAO (1998).

4.6.3 Application of the linear interpolation technique and the Kc_{act} technique

In order to assess which technique would be most suitable to infill the missing data in the SEBS total evaporation time series for the period 01st December 2011 to 25th November 2012, a preliminary investigation was undertaken involving two tests. A time period of six months i.e. from 01st January 2012 to 30th June 2012, was used to conduct the preliminary investigation.

The first test involved the use of the observed historical daily total evaporation record from the surface renewal system, which was obtained for the studies undertaken by Jarmain (2012) and Jarmain *et al.* (2013). Forty-five known total evaporation values obtained from the surface renewal system were hidden for the aforementioned time period. These values were treated as missing data. Seven of the forty-five days possessed complete cloud coverage, whilst a vast majority of the remaining thirty-eight days did possess some percentage of cloud coverage.

The linear interpolation technique and the Kc_{act} technique were then applied to these forty-five days to infill the missing data records. The forty-five days were selected randomly and the maximum number of consecutive days which required infilling was preset as three. The rationale behind this was due to the maximum number of consecutive days in which an SEBS total evaporation estimate could not be produced.

Tables 5.1 and 5.2 illustrate the comparison between the historical observed total evaporation for the respective days and the total evaporation values obtained through the use of infilling i.e. using linear interpolation and Kc_{act}, respectively.

The second test involved the use of the SEBS daily total evaporation estimates generated for the period 01st January 2012 to 30th June 2012. The equivalent forty-five random days to be in-filled in the first test were used here yet again. Known SEBS estimates of total evaporation were hidden and the linear interpolation technique and the Kc_{act} technique were applied to infill the missing data records. Tables 5.4 and 5.5 illustrate the comparison between the SEBS daily total evaporation for the respective days and the daily total evaporation values obtained through the use of infilling i.e. using linear interpolation and Kc_{act}, respectively.

The performance statistics outlined in Section 4.1 were used to analyse and interpret the results for each of these scenarios. A two sample t-test for a two tailed distribution with unequal variance was applied. The equation and t-distribution values used for this test are outlined in Larson and Farber (2003). The null hypothesis and alternate hypothesis were stated as:

Ho: Observed total evaporation = Infilled total evaporation

Ha: Observed total evaporation $\neq$ Infilled total evaporation

4.7 The Agricultural Catchments Research Unit (ACRU) Model

The ACRU4 Version of The Agricultural Catchments Research Unit (ACRU) model described in Clark *et al.* (2009) was chosen to be used in this study to conduct the streamflow modelling simulations, as it is has been applied extensively in South Africa and is listed by the South African Department of Water Affairs as one of the recommended hydrological models to be used. ACRU was developed by Schulze (1975) and has been frequently updated since its inception (Schulze, 1995; Jewitt and Schulze, 1999; Martinez *et al*., 2008; Warburton *et al*., 2010; Clark, 2013).

ACRU has been described as a "multi-purpose and multi-level integrated physical conceptual model that can simulate streamflow, total evaporation, land cover management and abstraction impacts on water resources at a daily time step" (Jewitt and Schulze, 1999). ACRU has been applied extensively, both locally and internationally, for a variety of purposes, some of which include crop yield estimation, irrigation scheduling, climate change analysis, land use change analysis, reservoir yield analysis and design hydrology (Schulze, 1995; Jewitt and Schulze, 1999; Martinez *et al*., 2008; Warburton *et al*., 2010; Clark, 2013).

4.7.1 General structure for daily multi-layer soil water budgeting in ACRU

ACRU is uniquely structured to determine how water is used within a catchment. This structure is known as the daily multi-layer soil water budget. The rainfall and/or irrigation which are not intercepted or contributing directly to stormflow, will first enter the surface layer of the earth and remain in the top soil horizon (Schulze, 1995). Once the top soil is saturated (field capacity), any additional moisture will percolate down into the sub-soil horizon/s.

The rate at which this takes place depends on the characteristics of the top soil horizon, for example, soil texture or wetness (Schulze, 1995). If the subsoil horizon/s reaches field capacity, any additional moisture will then drain into intermediate stores and ultimately contribute to groundwater. As a result, baseflow may then be generated. During, unsaturated conditions water may be redistributed either upwards or downwards, however the redistribution rate will be markedly slower than the rate which occurs during saturated conditions (Schulze, 1995).

Evaporation occurs from water which has been previously intercepted, as well as from the soil horizon/s. Within ACRU, evaporation which takes place from the soil horizon may be split into soil water evaporation from the top soil and transpiration, which includes all soil horizons where roots are present, or evaporation may be combined as total evaporation (Schulze, 1995). Plant transpiration is estimated, amongst other things, according to the atmospheric demand for water vapour which is based on the reference evaporation and the plant's growth stage (Schulze, 1995).

Stormflow generation within ACRU is based on the assumption that after the initial abstractions have taken place, the volume of runoff generated is dependent on the size of the rainfall event, as well as the antecedent soil water deficit at a critical response depth of the soil (Schulze, 1995). The critical response depth of the soil, amongst others, is a function of the prevailing runoff generating process, whilst the soil water deficit prior to a rainfall event is determined within ACRU on a daily basis, through the various multi-layer soil water budgeting procedures (Schulze, 1995).

It is important to note that not all of the stormflow generated in ACRU for a given rain event will be a same day response at the catchment outlet. Therefore stormflow in ACRU is separated into quickflow (i.e. a same day response) and delayed stormflow, which is dependent on soil characteristics and the catchment's properties (Schulze, 1995). Figure 4.2 depicts the daily multi-layer soil water budgeting in ACRU.

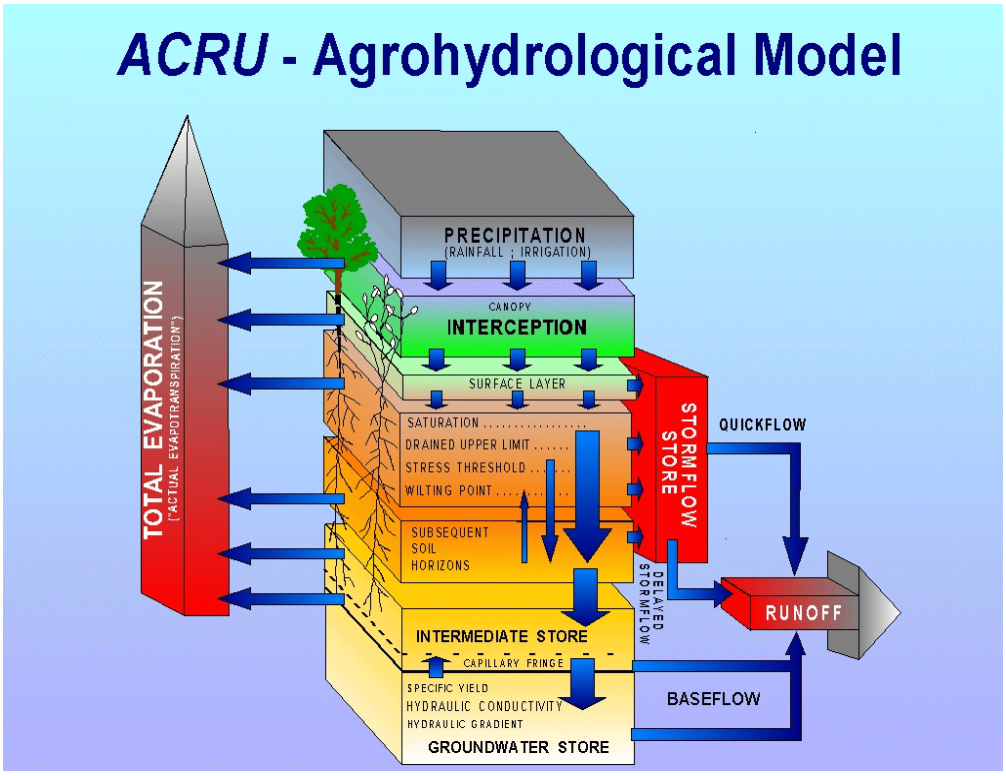

Figure 4.2 Multi-layer soil water budgeting through the partitioning and redistribution of soil water (Schulze, 1995)

4.7.2 Estimating total evaporation in the ACRU Model and the EVTR3 approach

Total evaporation may be modelled in one of two ways in the ACRU model, either by treating potential soil water evaporation and potential transpiration as a single entity, or estimating the potential soil water evaporation and potential transpiration components of potential evaporation separately (Schulze, 1995).

4.7.2.1 The EVTR1 routine

The estimation of total evaporation, by computing potential soil water evaporation and potential transpiration, as a single entity, is termed EVTR1 in the ACRU model (Schulze, 1995). Crop coefficient (K_c) values which are frequently used are stored in the ACRU Model, within a database for known land covers. These K_c values are then used in conjunction with reference evaporation data which is input to the model to estimate the potential evaporation (Schulze, 1995). The estimation of soil water evaporation and transpiration as a single entity is useful when the information required to estimate each of these parameters individually is not available (Schulze, 1995).

The EVTR1 technique was not applied in this study, as there was sufficient information available to estimate the soil water evaporation and transpiration components of total evaporation separately, therefore only a brief description of the EVTR1 procedure has been provided.

4.7.2.2 The EVTR2 routine

The estimation of total evaporation, by computing potential soil water evaporation and potential transpiration, as individual parameters, is termed EVTR2 in the ACRU model (Schulze, 1995). This option was selected to be applied in this study, as it allows for the soil water evaporation and transpiration components of total evaporation to be estimated with greater accuracy (Schulze, 1995).

For the EVTR2 option, the reference evaporation is entered as an input into the ACRU Model. On a day with interception losses, the interception loss is first determined in ACRU. This can be determined through the use of daily or monthly LAI information, based on the relationship outlined by von Hoyningen-Huene (1983) in (Schulze, 1995). This relationship is given, as follows:

$$Il = 0.30 + 0.27P_g + 0.13LAI - 0.013\ P^2_g + 0.0285P_g.LAI - 0.007LAI^2 \quad (4.5)$$

Where Il is interception loss (mm/day); P_g is gross daily rainfall (mm/day) and LAI is leaf area index (dimensionless).

Intercepted water, which still remains on the plant canopy from the previous day's rainfall, will be evaporated back to the atmosphere, using the available energy from the reference evaporation first. The remaining energy can then be used for soil water evaporation and transpiration processes (Schulze, 1995).

With regards to forests, this stored water from the previous day's rainfall has been found to evaporate at rates in excess of the available net radiation and potential evaporation. This is largely due to advection (Calder, 1982) and lower aerodynamic resistances of wet forest canopies (Rutter, 1967).

A conservative approach to estimate the enhanced wet canopy evaporation has been incorporated into ACRU, to simulate evaporation processes under forested conditions (Schulze, 1995). This relationship is given, as follows:

$$E_w = E_r(0.267LAI + 0.33) \quad (4.6)$$

Where E_w is enhanced wet canopy evaporation (mm); E_r is A-pan equivalent reference potential evaporation (mm) and LAI is leaf area index (dimensionless).

Once, the interception loss has been determined, it is removed from the initial reference evaporation store. The reduced reference evaporation store is then available to estimate potential soil water evaporation and potential transpiration (Schulze, 1995). If no interception losses occur for a particular day, the reference evaporation amount entered, as an input to ACRU will be used to estimate potential soil water evaporation and potential transpiration.

The potential transpiration can be determined in ACRU from LAI information, based on an adaptation of Ritchie (1972) procedures, which is detailed in Schulze (1995), as follows:

$$F_t = 0.7 \times LAI^{0.5} - 0.21 \quad (4.7)$$

Where F_t is the fraction of total available transpiration (dimensionless) and LAI is leaf area index (dimensionless).

However, if LAI information is not available, the decision support database for known land covers can be used. K_c values which are stored in this database can be used to determine LAI, using the equation derived by Angus (1987), based on information given in Kristensen (1974) (Schulze, 1995)

The fraction of transpiration cannot exceed 95% of the potential evaporation; therefore the lower and upper limits of the fraction of transpiration are set as 0.00 and 0.95, respectively. The potential transpiration can then be determined, as follows:

$$PT = F_t \times ET_0 \quad (4.8)$$

Where PT is potential transpiration (mm/day); F_t is the fraction of total available transpiration (dimensionless) and $ET_{0\ is}$ reference evaporation (mm/day).

The potential transpiration which is determined from the above equation may be suppressed, due to the effects of enhanced atmospheric CO_2 concentrations. The levels of potential transpiration suppression in ACRU are dependent on the nature of the plants present i.e C_3 or C_4 plants (Schulze, 1995). The potential transpiration from the plant is apportioned to the A-Horizon and B-Horizon based on the proportion of the root mass distributions present within the respective layers.

Soil water evaporation is assumed to occur from the top soil only in ACRU (Schulze, 1995). Potential soil water evaporation in ACRU can be estimated either as a residual of the available energy not used for the estimation of potential transpiration, or from considerations of the effects, which shading from the above ground vegetation has on the soil surface (Schulze, 1995). The latter approach is used in ACRU for irrigation simulations and will therefore not be discussed further, as this option was not exercised in this study. The potential soil water evaporation is estimated, as a residual in ACRU's "dryland" (rainfed) routine (Schulze, 1995), as follows:

$$P_{SWE} = E_r \times (1-F_t) \qquad (4.9)$$

Where P_{SWE} is potential soil water evaporation (mm); E_r is A-pan equivalent reference potential evaporation (mm) and F_t is the fraction of total available transpiration (dimensionless).

The potential soil water evaporation, which is determined from the aforementioned equation, may be suppressed, due to the effects of surface cover such as mulch, litter or surface rocks (Schulze, 1995).

The actual soil water evaporation is calculated in two stages in ACRU, according to Ritchie (1972). During the first stage, when the soil is wet, soil water evaporation is limited only by the available energy at the surface; therefore the actual soil water evaporation is equal to the potential soil water evaporation.

The stage two evaporation process begins, when the accumulated soil water evaporation exceeds the stage 1 upper limit (Schulze, 1995). The stage 1 upper limit is estimated in ACRU (Schulze, 1995), as follows:

$$U_1 = 9(\alpha_s - 3)^{0.42} \quad (4.10)$$

Where U_1 is stage 1 upper limit of SWC (mm) and α_s is soil water transmission parameter.

While the stage two soil water evaporation is estimated in Schulze (1995), by:

$$E_s = \alpha_s t_d^{0.5} - (t_d - 1)^{0.5} \quad (4.11)$$

Where E_s is stage two soil water evaporation (mm/day); α_s is soil water transmission parameter and t_d is time (days).

Once the stage two soil water evaporation commences, soil water evaporation begins to decline rapidly.

The actual transpiration in ACRU can be equal to the potential transpiration or it may be less than the potential transpiration, due to limited/excess of soil water. During conditions of limited soil water availability, the actual transpiration is estimated in ACRU (Schulze, 1995), as follows:

$$E_{tA} = Ep_{tA} (\theta_A - \theta_{PWPA})/ (f_s \text{ x } PAW_A) \quad (4.12)$$

Where E_{tA} is actual transpiration of the A-Horizon (mm/day); E_{ptA} is potential transpiration of the A-Horizon (mm/day); θ_A is SWC of the A-Horizon (mm); θ_{PWPA} is SWC of the A-Horizon at permanent wilting point (mm); PAW_A is plant available water (PAW) for the A-Horizon (mm) and f_s is fraction of PAW at which stress sets in due to soil water deficit.

While under conditions of soil water excess, actual transpiration is estimated, as:

$$E_{tA} = Ep_{tA}[0.7(\theta_{POA} - \theta_A)/ (\theta_{POA} - \theta_{DULA}) + 0.3] \quad (4.13)$$

Where E_{tA} is actual transpiration of the A-Horizon (mm/day); E_{ptA} is potential transpiration of the A-Horizon (mm/day); θ_{POA} is SWC of the A-Horizon at saturation (mm); θ_A is SWC of the A-Horizon (mm) and θ_{DULA} isSWC of the A-Horizon at the drained upper limit (mm).

The same form of the equation will apply for the B-Horizon in both cases.

The ACRU model operates on the assumption that "roots look for water, water does not look for roots" (Schulze, 1995). Based on this premise, once the daily actual transpiration has been determined for the respective soil horizons, the daily actual transpiration may be adjusted horizon-by-horizon, when one of the soil horizons experiences a greater deficiency in soil moisture than the other (Schulze, 1995).

During such conditions the model has been encoded, so that the horizon which is not experiencing stress, will contribute more to daily actual transpiration than what was initially computed, by accounting for the proportion of root mass available in the horizon for transpiration (Schulze, 1995). This however, is only possible if the plant is in an active stage of growth (Schulze, 1995).

Once, the actual soil water evaporation and actual transpiration have been determined, the soil water content within each of the soil horizons is adjusted (Schulze, 1995). Figure 4.3 provides a simplistic representation of the EVTR2 procedure.

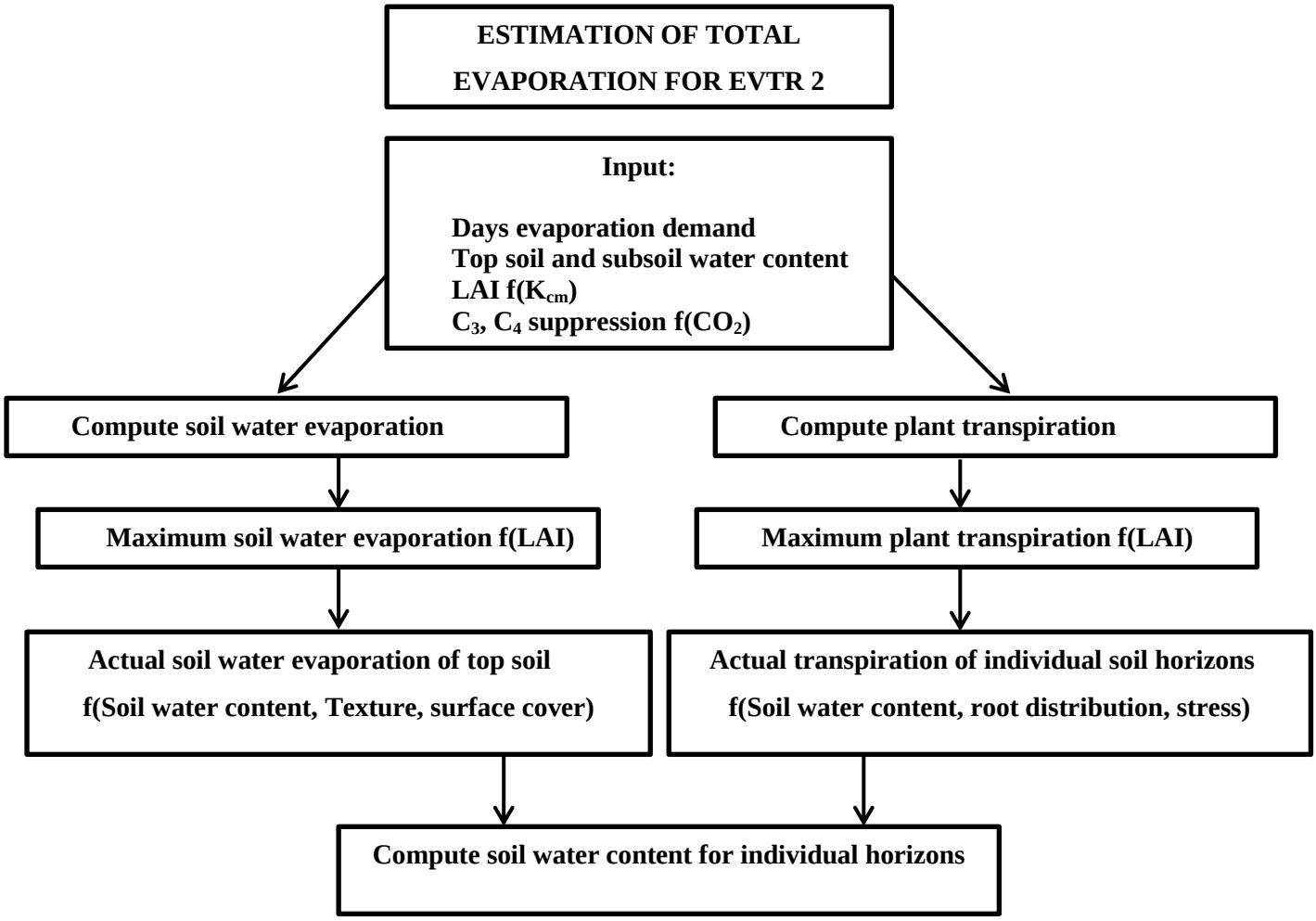

Figure 4.3 Estimation of total evaporation within ACRU for option EVTR2 (After Schulze, 1995)

4.7.2.3 The EVTR3 approach

The ACRU4 Version of the ACRU Model described in Clarke *et al.* (2009) does not accommodate actual total evaporation, as an input. Therefore, in order to utilize the SEBS total evaporation estimates, as an input to ACRU, a new routine was required, to be added to the model. This routine was termed EVTR3. This new approach was needed because neither option EVTR1 or EVTR2 had the capacity of handling total evaporation as an input.

The total evaporation is used as an input to ACRU for the EVTR3 approach, however before it can be used to perform various hydrological simulations; it must be apportioned accordingly to interception losses, actual transpiration and soil water evaporation.

On a day with interception losses, the interception loss is first determined in ACRU. This can be determined through the use of daily or monthly LAI information. Interception loss can be determined from LAI data based on the relationship outlined by von Hoyningen-Huene (1983) in (Schulze, 1995), detailed in Equation 4.5.

Once, the interception loss has been determined, it is removed from the initial actual total evaporation store. The reduced actual total evaporation store is then available to determine actual soil water evaporation and actual transpiration. If no interception losses occur for a particular day, the actual total evaporation amount entered as an input to ACRU will be used to determine actual soil water evaporation and actual transpiration.

The actual transpiration for the EVTR3 procedure can be determined in ACRU, based on an adaptation of Ritchie (1972) procedures, detailed in Equation 4.7. The fraction of total available transpiration is then used to determine the daily actual transpiration, which is given as:

$$A_{trans} = AET \times F_t \quad (4.14)$$

Where A_{trans} is actual transpiration (mm/day); AET is total evaporation (mm/day) and F_t is the fraction of total available transpiration.

The actual transpiration which occurs from the A-Horizon and B-Horizon is determined, based on the plant root fraction. For example if 60 % of the roots are situated within the A-Horizon, then 60% of the actual transpiration calculated in Equation 4.14, will occur from the A-Horizon, whilst the remaining 40 % will occur from the B-Horizon.

The root fraction parameter values used for the EVTR3 option are a user-defined value. The ACRU decision support database for known land covers can be used to assist in determining representative root fraction values.

The actual soil water evaporation can be estimated as a residual of the available energy not used for the estimation of actual transpiration and is given, as follows:

$$A_{swe} = AET \times (1-F_t) \quad (4.15)$$

Where A_{swe} is actual soil water evaporation (mm/day); AET is total evaporation (mm/day) and F_t is the fraction of total available transpiration.

Soil water evaporation is assumed to take place from the top soil horizon only. Once, the actual soil water evaporation and actual transpiration have been determined, the soil water content within each of the soil horizons is adjusted.

It is important to note that the actual total evaporation which is input to the model may not be equal to the actual total evaporation output by the model, as the soil water content of the A-Horizon and B-Horizon, which is estimated within the model may not be able to meet the actual total evaporation demand being specified.

4.7.3 ACRU configuration

The delineation of sub-catchments in the Inkomati Catchment (X23) was based on a quinary shapefile obtained from DHI (Fregzi, 2012b), originating from a report undertaken by Mallory and Beater, which was commissioned by the Department of Water Affairs (DWAF) (DWAF, 2009). Twenty sub-catchments were identified within this quinary shapefile, and of these twenty, two sub-catchments were further sub-divided, based on the location of the proposed Mountain View (Haumann, 2008) and Concession Creek (Theron, 2006) Dams. A 20 m DEM received from the Inkomati Catchment Management agency was used to delineate the new sub-catchments and rivers, to create the X23_A shapefile used in this study (Thornton-Dibb *et al*., 2013).

The ACRU Model was configured for the X23_A quarternary located within the Kaap River Catchment. The details pertaining to model inputs, such as climate, elevation, soils, landuse and ancillary model inputs are described in the proceeding sub-sections.

4.7.3.1 Sub-catchment and HRU configuration

The ACRU Model was configured by extracting the X23_A quarternary catchment, which is located within the X23 tertiary catchment (Thornton-Dibb *et al*., 2013). The sub-catchments, the flow network and the area of the quarternary and its sub-catchments are shown in Figures 4.4 and 4.5, respectively and Table 4.3. The X23_A coverage was then used as an input to the ACRU Grid extractor (Lynch and Kiker, 2001), which is an extension of ArcView that is used to extract rainfall correction factors, soils and land type information required as inputs to the ACRU Model (Thornton-Dibb *et al*., 2013).

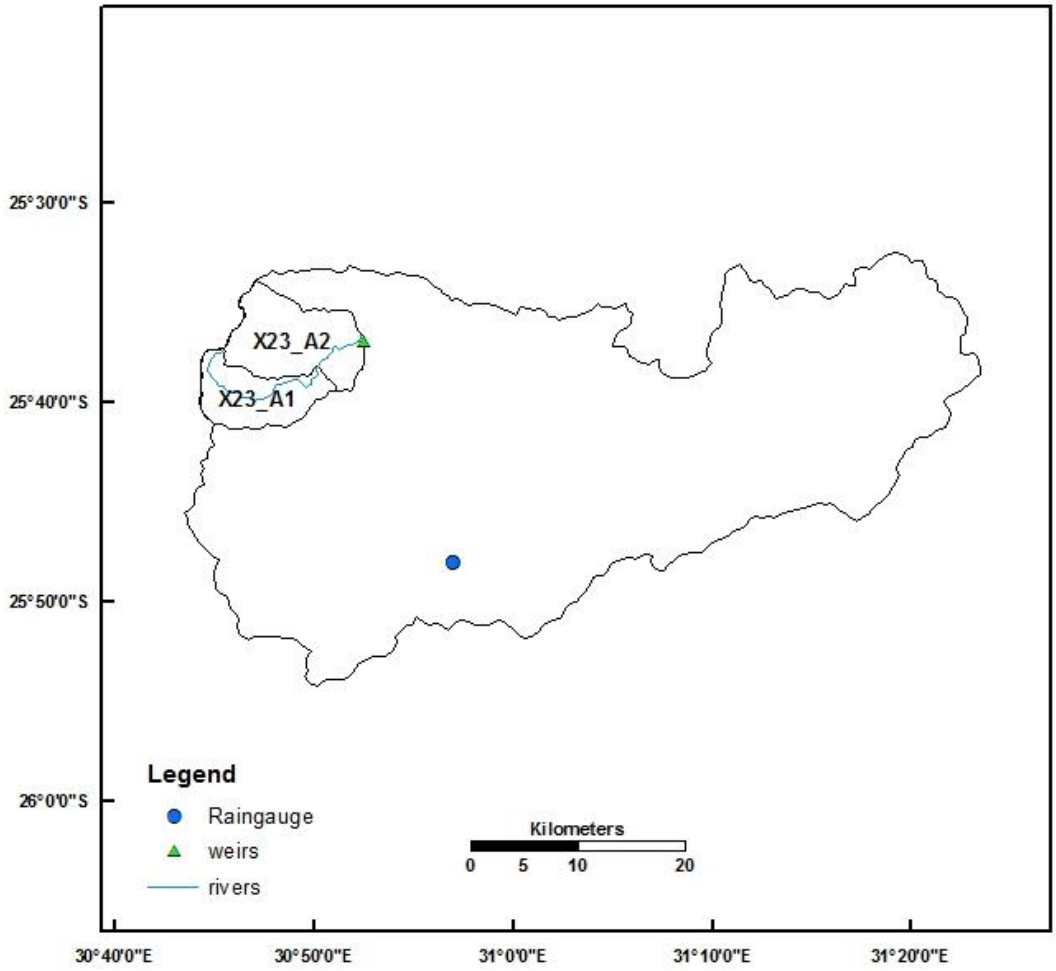

Figure 4.4 Location of the X23A Quaternary Catchment, sub-catchments, flow gauging weir and rain gauge

Table 4.3 X23_A quarternary catchment and sub-catchment areas

Quarternary catchment		**Subcatchment**	
ID	**Area (km^2)**	**ID**	**Area (km^2)**
X23_A	126.86	X23_A1	51.66
		X23_A2	75.2

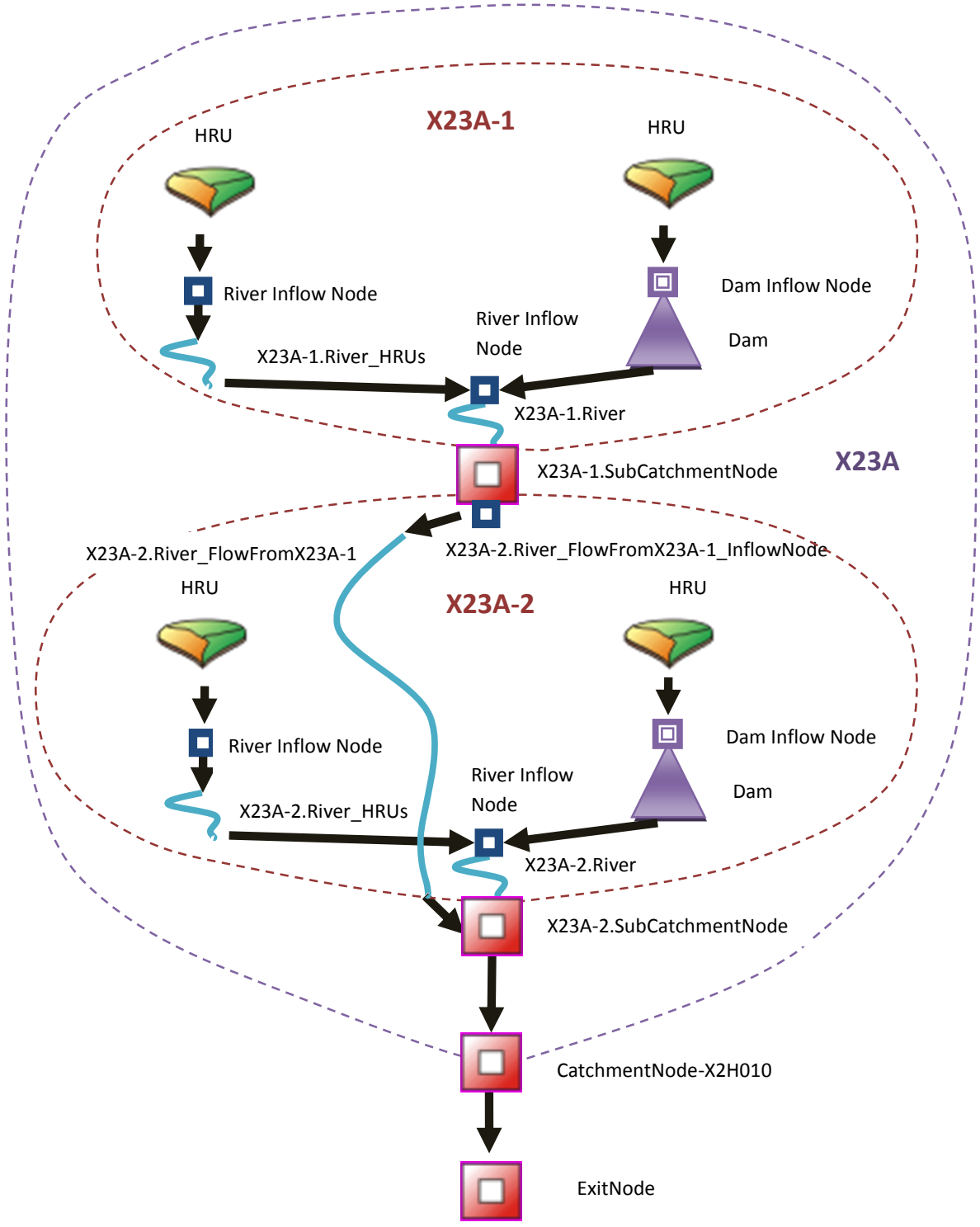

Figure 4.5 X23_A flow network (Thornton-Dibb, 2014)

4.7.3.2 Historical observed climate data

Rainfall is the chief driver input to the ACRU model. Rain gauges located within the quarternary did not possess rainfall records which corresponded to the time period that was to be used for the modelling of streamflow in the X23_A quarternary i.e. 01st December 2011 to 25th November 2012. The nearest rain gauge which possessed the required rainfall record, formed part of an ARC-ISCW automatic weather station located at coordinates: 25°.81 S and 31°.01 E, at an altitude of 703 m, a mean annual precipitation of 681 mm and 80.7 % reliability (Thornton-Dibb *et al*., 2013). This station was selected as the driver station for the quarternary. Rainfall values can be corrected using the gridded MAP. The MAP is represented by a degree grid (Schulze *et al.*, 2008) and is illustrated in Figure 4.6.

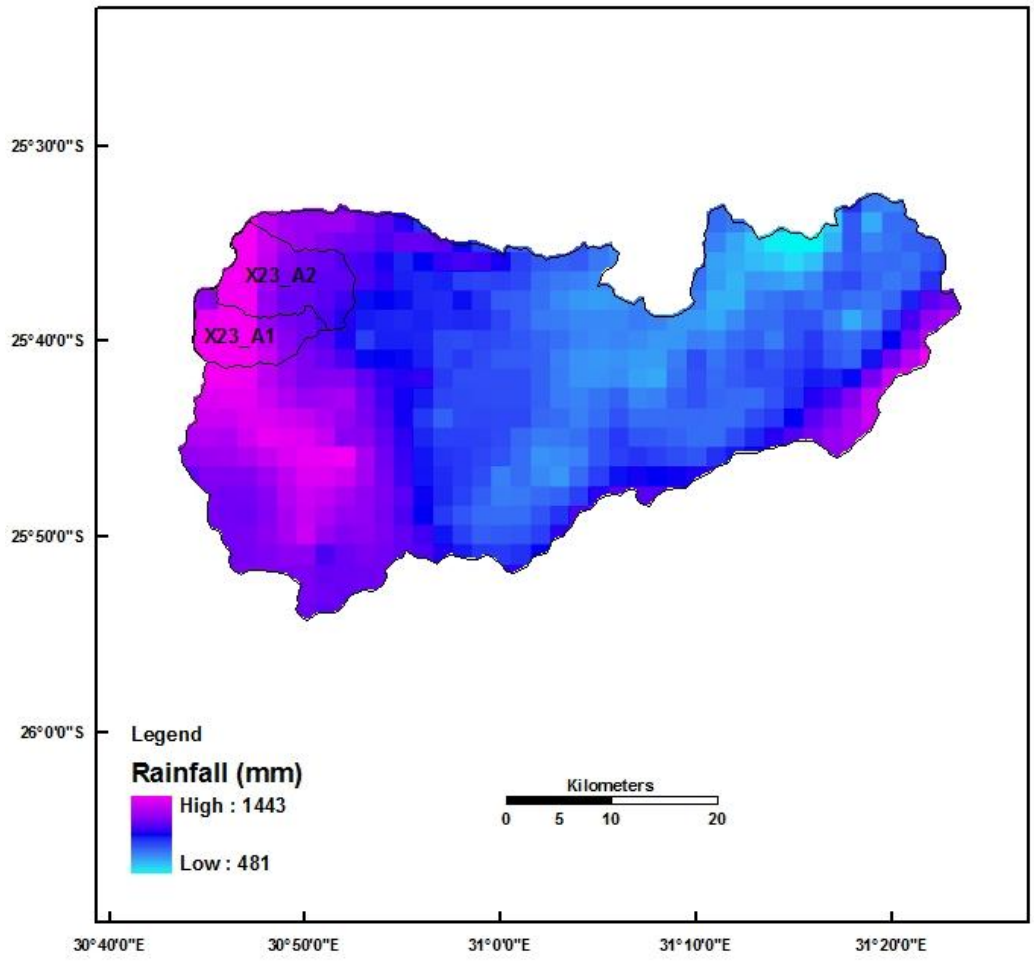

Figure 4.6 Distribution of mean annual precipitation (MAP) over the X23 tertiary catchment

The rainfall values for this station were not corrected in ACRU, as the length of record (7 years) was not adequate to generate representative rainfall correction factors. A length of record of 20 years or longer is the suggested time period for the generation of correction factors. Daily temperature and daily Penman-Monteith reference evaporation data were also acquired from the ARC-ISCW weather station. The SEBS total evaporation time series was obtained, by determining the average of the satellite pixel values located within the X23_A1 and X23_A2 sub-catchments. A sample of the SEBS total evaporation estimates for a random day in winter and summer is illustrated in Figure 4.7.

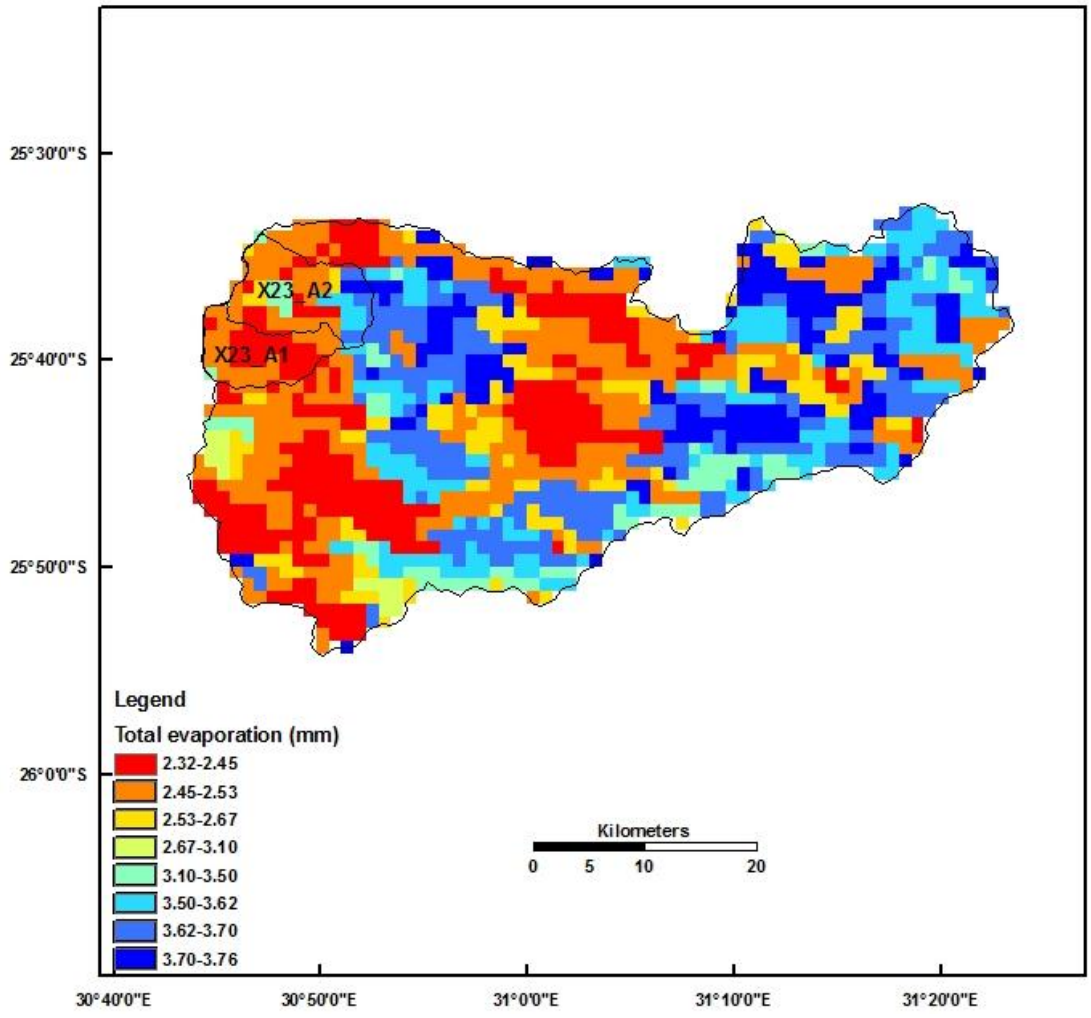

Figure 4.7 Variation of SEBS total evaporation over the X23 tertiary catchment

Observed streamflow values were obtained by downloading the weir records from the Department of Water Affairs database. Streamflow depths were downloaded for the gauging weir X2H010 located at coordinates 25^{o}.615 S, 30^{o}.875 E (Thornton-Dibb *et al*., 2013). Quality control and error checking of the data was undertaken for the study by Thornton-Dibb *et al*. (2013). The observed values of rainfall, temperature, FAO Penman-Monteith reference evaporation and streamflow were then used to compile a climate file, which was used to input the relevant climate data and to drive the ACRU Model.

4.7.3.3 Elevation

The variation in altitude over the quarternary catchment X23_A, represented by the national 200 m Digital Elevation Model (DEM) for South Africa is represented in Figure 4.8. The elevation for each of the sub-catchments was extracted from the DEM at a 200 m resolution and used as an input to ACRU (Thornton-Dibb *et al*., 2013).

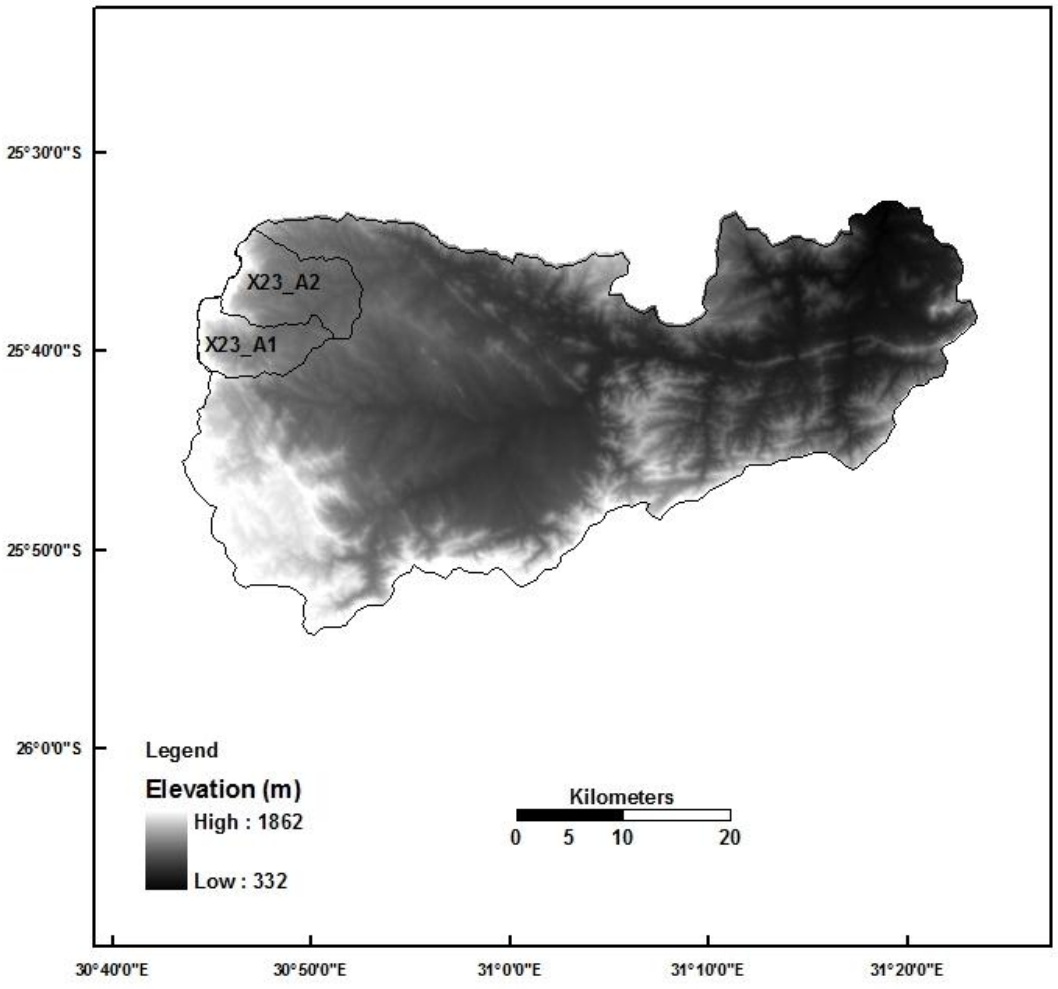

Figure 4.8 Variation of altitude over the X23 tertiary catchment

4.7.3.4 Soils and land use

The hydrological soils information required as an input to ACRU were extracted from the Land Type map (Schulze *et al.*, 2008). The soil parameters which were extracted and used as inputs to ACRU included the wilting point, field capacity and porosity for the A-horizon and B-horizon, as well as the depth and drainage response fractions for the aforementioned horizons (Thornton-Dibb *et al.*, 2013). The broad soils classification used to extract the soil parameters required as inputs to ACRU, are displayed in Figure 4.9.

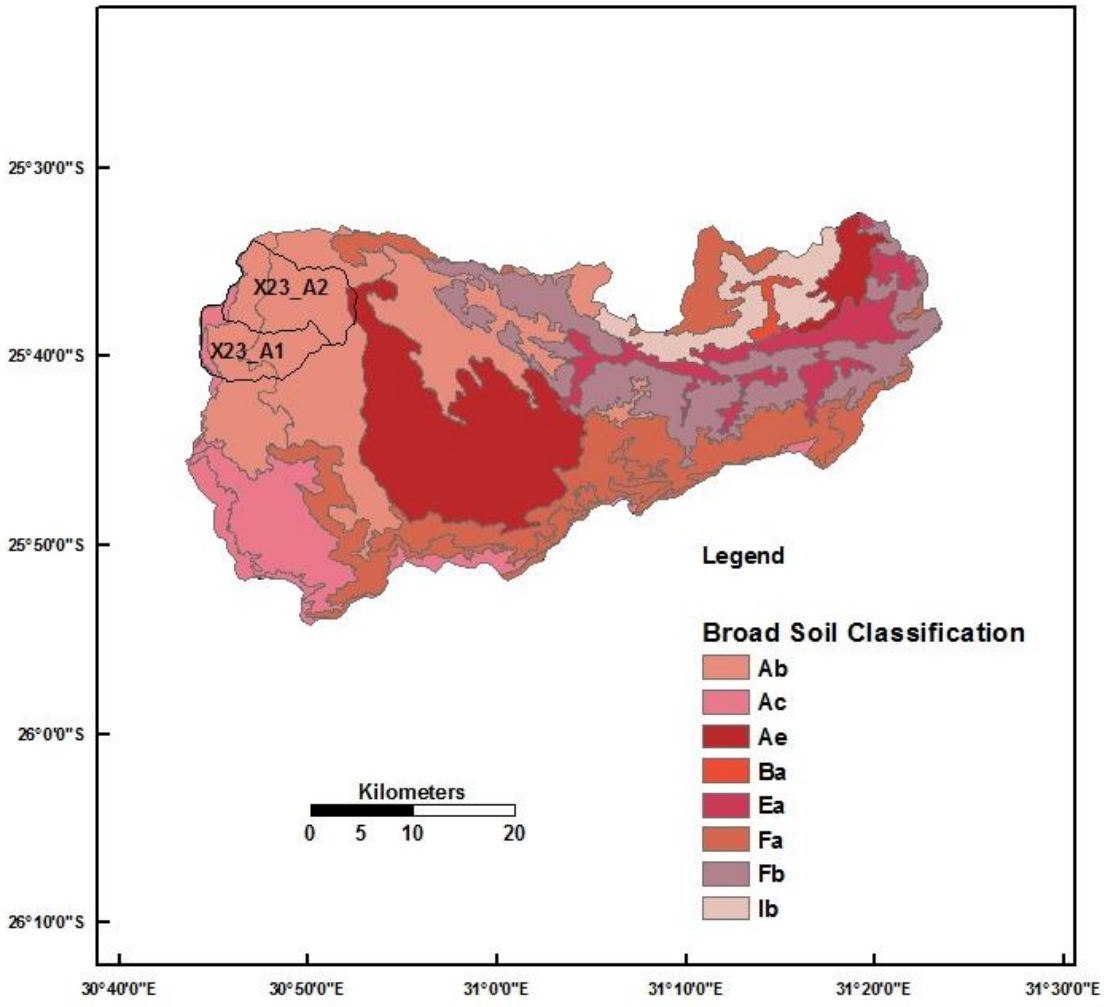

Figure 4.9 Broad soil classification within the X23 tertiary catchment (after ISCW, 2005)

The land use information was obtained from a Spot 5 satellite image at a 20 m resolution. A number of varying land uses were identified within each of the sub-catchments. However, due to the differences in the spatial resolution of the MODIS Level 1_B (1 km) images used, as inputs to SEBS, to generate daily total evaporation estimates, the total evaporation for each of the varying land covers could not be accurately accounted for.

This phenomenon is illustrated in Figures 4.10 and 4.11. Figure 4.10 illustrates the SEBS total evaporation which was calculated for the quarternary catchment X23_A. The 1 km pixels highlighted in this figure were then overlaid onto the landcover map in Figure 4.11, to illustrate the limited inter-field variation detected by the MODIS Level1_B data.

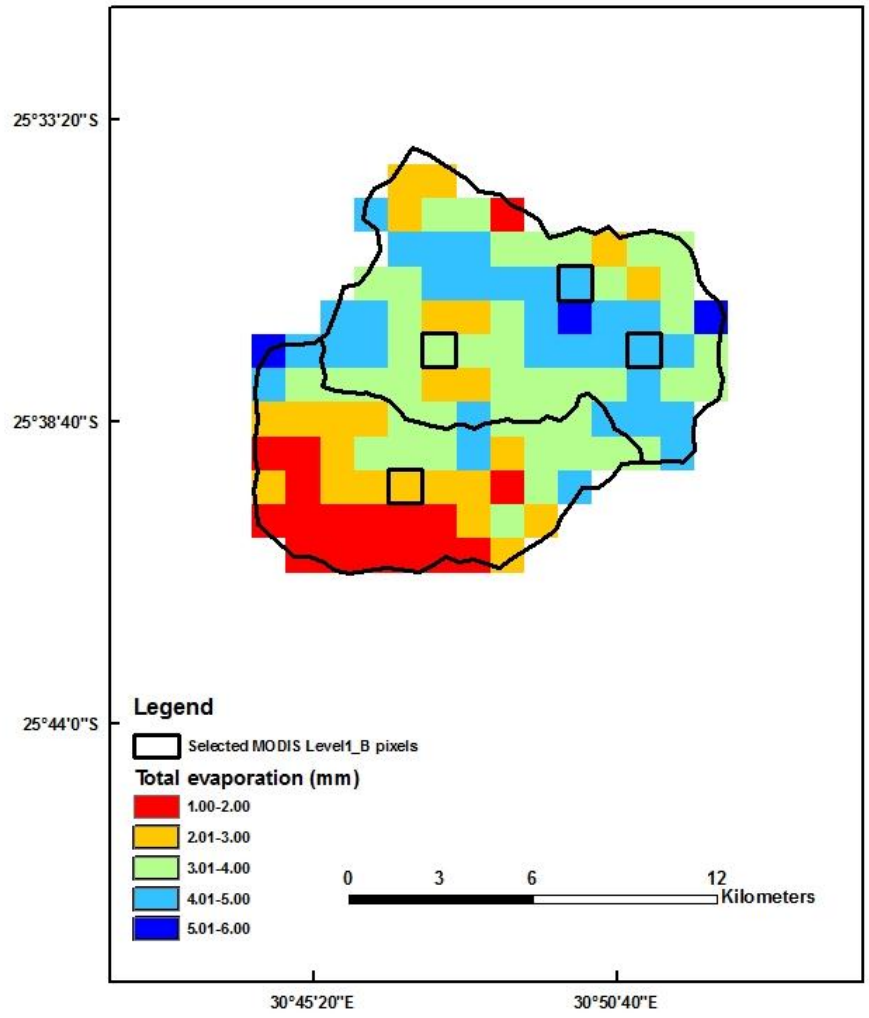

Figure 4.10 An illustration of the SEBS total evaporation (mm) estimated at a resolution of 1km for the quarternary catchment X23_A

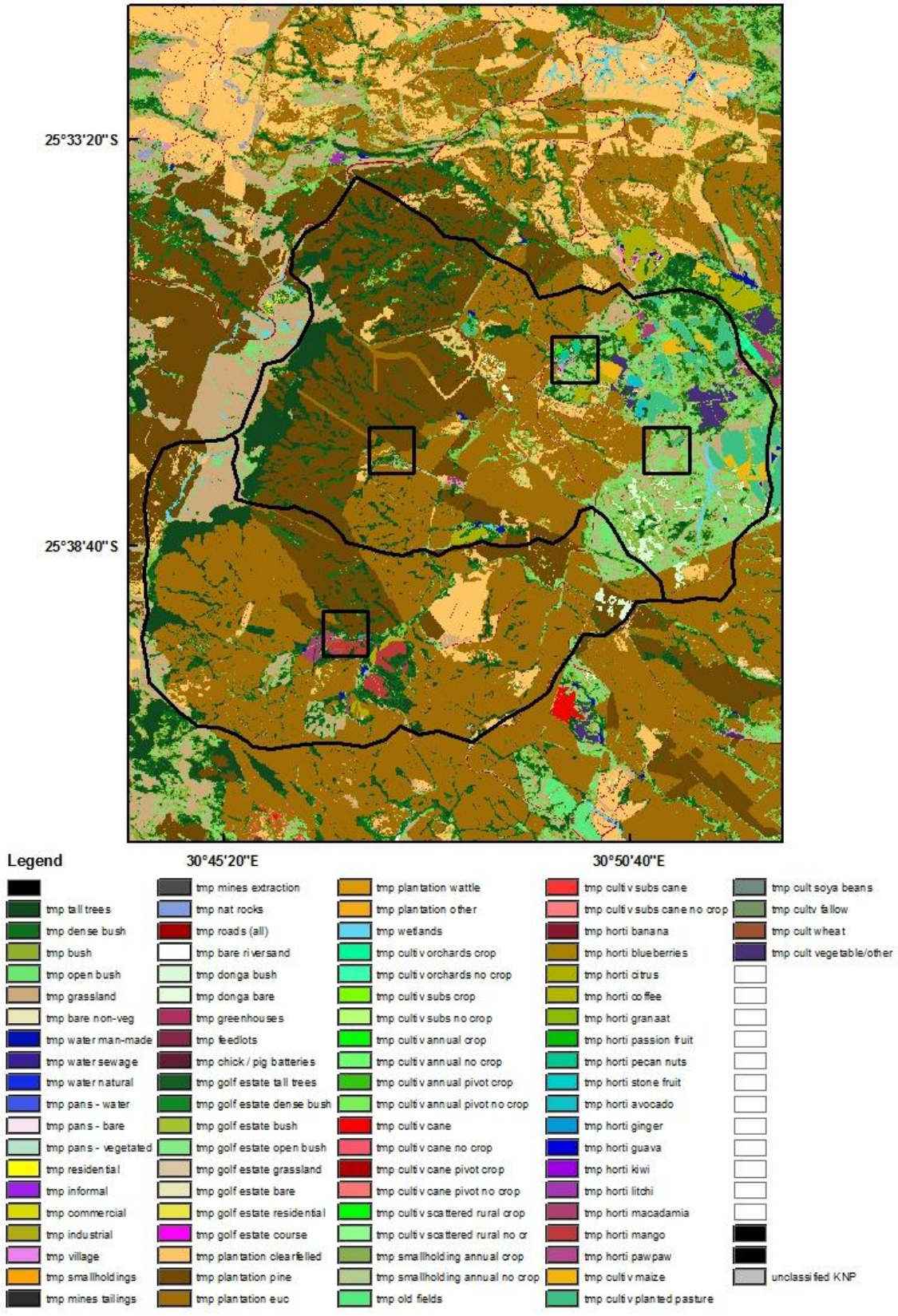

Figure 4.11 **An illustration of the spatial coverage for the selected MODIS Level1_B pixels in comparison to the land uses present within the quarternary catchment X23_A**

The selected pixels in Figure 4.10 provide a total evaporation estimate at a spatial resolution of 1 km^2. Within this pixel, as shown in Figure 4.11, it can be seen that there are various land covers which are present. Each of these land covers may possess differing total evaporation. The total evaporation estimate provided by SEBS in this instance, therefore may not be a representative estimation of the different land covers present within the quarternary X23_A.

In order to overcome this limitation the model had to be configured in a relatively simplistic manner. The quarternary catchment X23_A was modelled at the sub-catchment level and a homogenous land cover would be assumed for the Hydrological Response Units (HRU's) within the X23_A1 and X23_A2 sub-catchments. The landcover which possessed the largest area contribution within each sub-catchment was selected to represent the landuse in each of the sub-catchments.

Forestry contributes to more than 65% of the total area within the quarternary catchment X23_A and more than 75% and 60% of the total area within the sub-catchments X23_A1 and X23_A2 respectively. Eucalyptus plantations accounted for more than 65% and 41% of the forestry, present in sub-catchments X23_A1 and X23_A2, respectively. Therefore it was decided that eucalyptus plantations would be used to represent the landuse in each of the sub-catchments. The area contribution of each land use within the sub-catchments is shown in Table 4.4. These were determined, using the tabulate area function in ArcGIS 9.3.

The sub-catchments X23_A1 and X23_A2 were further sub-divided into two HRU's. The land cover present within each of these HRU's would remain the same i.e. each HRU would possess eucalyptus plantations as the land cover. The sub-division of each of the sub-catchments was used to assist in the configuration of the flow network into a logical sequence which is representative of the river flow; this is represented in Figure 4.4.

Table 4.4 Landuse area contribution within the X23_A sub-catchments

Land Use	X23_A-1 (km^2)	X23_A-2 (km^2)	X23_A (km^2)
Forest (indigenous)	4.25	6.71	10.96
Thicket, Bush land, Bush Clumps, High Fynbos	5.78	16.36	22.15
Unimproved (natural) Grassland	3.55	5.79	9.34
Bare Rock and Soil (natural)	0.23	1.07	1.30
Water bodies (manmade)	0.07	0.11	0.17
Urban / Built-up (residential)	0.15	0.35	0.50
Mines & Quarries (mine tailings, waste dumps)	0.00	0.00	0.00
Forest Plantations (clear-felled)	2.51	1.85	4.36
Forest Plantations (Pine spp)	7.35	18.50	25.85
Forest Plantations (Eucalyptus spp)	26.37	19.32	45.70
Wetlands	0.15	0.25	0.40
Cultivated, permanent, commercial, dry land	0.03	3.88	3.90
Cultivated, commercial, irrigated	1.21	1.03	2.24
Total area	**51.66**	**75.20**	**126.86**

4.7.3.5 LAI

The LAI data used in this study was downloaded from the MODIS products of MOD15A2 for the period 01st December 2011 to 25th November 2012. The MOD15A2 product is available at a spatial resolution of one km and an eight-day temporal resolution. The MOD15A2 product is archived in the NASA HDF EOS data format (Muhammed, 2012). The MODIS reprojection tool was used to reproject and convert the data to a Geo-tiff format, which was compatible with ArcGIS. A correction factor of 0.1 was applied to the data, to obtain LAI values in m^2/m^2.

The LAI values were assumed to remain constant over the eight-day period and based on this assumption, a daily LAI time series for the period 01st December 2011 to 25th November 2012 was generated. The LAI values for the aforementioned time period were added to the climate file. An example of the LAI for the quarternary catchment X23_A is shown in Figure 4.12.

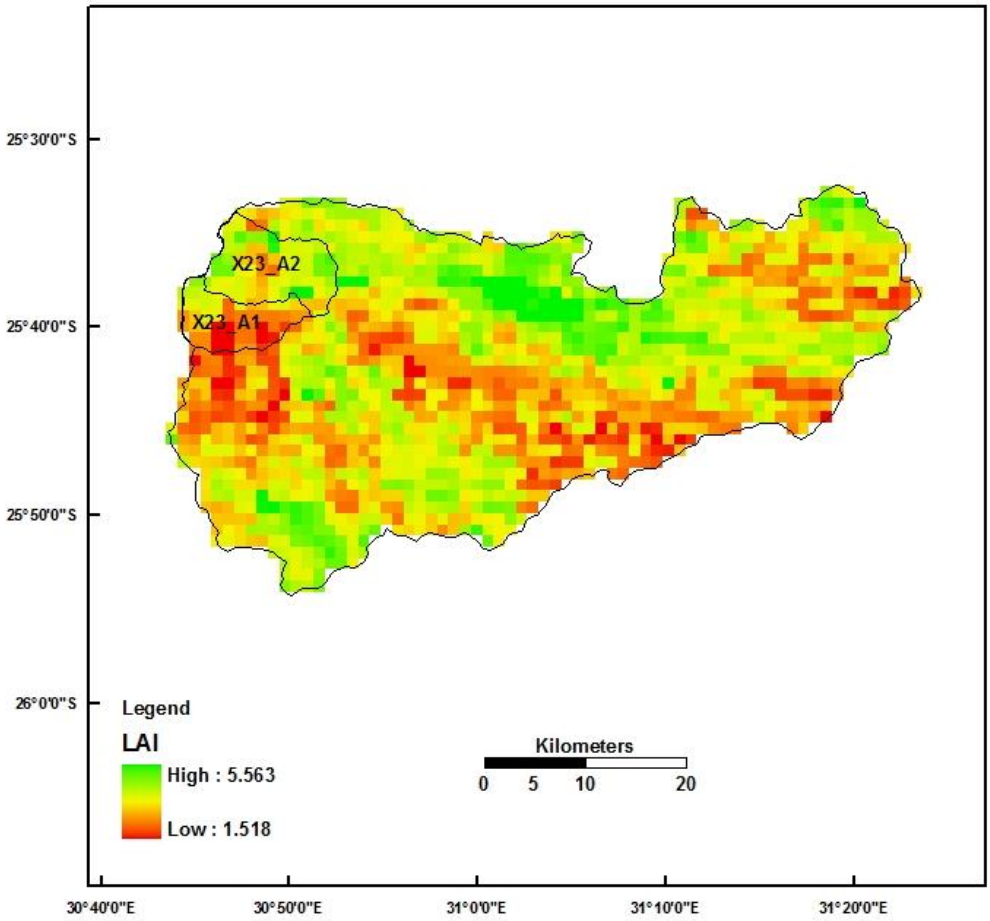

Figure 4.12 LAI values over the X23_A quarternary on the 03rd December 2011

4.7.3.6 Dams and water bodies

A database of registered dams housed on the Department of Water Affairs Website was downloaded to identify the dams within the X23_A quarternary (DWA, 2012a). A Google earth file is included within the database, to facilitate the location of these dams within the X23_A quarternary (Thornton-Dibb *et al*., 2013). The files in the database were only accurate to the nearest second of a degree and as a result, some of the locations specified in the file did not correspond to the dams identified using Google Earth. Five unidentified dams were situated within the X23_A1 and X23_A2 sub-catchments (Thornton-Dibb *et al*., 2013).

The dams located in the X23_A quarternary within the database were linked with the dams identified within Google Earth, as well as the water bodies identified by the Spot 5 land use map. A single virtual dam was created per sub-catchment and used in the ACRU configuration. The creation of the virtual dam was based on the aggregation of water bodies and dams located within the respective sub-catchments (Thornton-Dibb *et al*., 2013).

4.7.4 Streamflow modelling scenarios and sensitivity analysis tests

The configuration of the ACRU Model discussed in the previous sub-section was used to conduct two streamflow modelling scenarios and two sensitivity analysis tests. The first streamflow modelling scenario involved the application of Penman-Monteith reference evaporation data as the evaporation input to the ACRU Model, whereas the second streamflow modelling scenario involved the use of the SEBS total evaporation time series as the evaporation input to the ACRU model.

The first sensitivity analysis test which was performed focused on assessing the sensitivity of the ACRU model to the initial baseflow store value. The second sensitivity analysis test focused on the sensitivity of the ACRU Model to the root fraction parameter values required for the EVTR3 option. A detailed description of each of the streamflow modelling scenarios and sensitivity analysis tests will be outlined in the following sub-sections.

4.7.4.1 Scenario One: streamflow modelling using daily FAO Penman-Monteith reference evaporation estimates

The first scenario involved comparing the simulated streamflow, which was attained using the FAO Penman-Monteith Reference evaporation data, against observed streamflow. The flow network of the quarternary catchment X23_A and its sub-catchments are displayed in Figure 4.5. The MAP and hydrological soils information which was extracted using the ArcView grid extractor was used to populate the ACRU model. A climate file was added to each HRU to provide the relevant climatic data required to drive the model. It is important to note that the climate data used in the climate file pertains to the ARC-ISCW weather station located at coordinates 25.81 S and 31.01 E.

This weather station is not situated within the quarternary catchment X23_A; however, it was the only station in close proximity which possessed the required climatic data to conduct streamflow modelling simulations for the period 01st December 2011 to 25th November 2012. A sample of the climate file used, as an input to ACRU is shown in Table 4.5. The vegetation parameters pertaining to eucalyptus plantations were used to populate the HRU's menu and these were obtained from the ACRU decision support database for known land covers.

Table 4.5 Sample of climate file used

Station ID	Date	Rfl (mm)		Tmax (^{o}c)		Tmin (^{o}c)		FAO ref_evap (mm)		Streamflow (mm)				LAI	
30765	20111201	0.51		32.68		18.90		4.13		0.2419				1.70	
30765	20111202	1.02		30.20		19.89		3.11		0.2814				1.70	
30765	20111203	13.72		22.26		16.84		1.43		0.2718				1.70	

The daily temperature and daily FAO Penman-Monteith reference evaporation values stored in the climate file were corrected within ACRU. The daily temperature values were subjected to an altitudinal correction, based on the lapse rate region for the Limpopo Province (Schulze and Maharaj, 2004) and the base elevation of the respective sub-catchment. A correction factor of 1.2, suggested in Schulze (1995) for K_c values from Doorenbos and Pruitt (1977), was applied to the daily FAO Penman-Monteith reference evaporation, to produce daily A-pan equivalent values which are required by ACRU. Soil water evaporation and transpiration can be modelled as a single entity (EVTR1) or as separate entities (EVTR2) within ACRU. The EVTR2 option was chosen for this scenario.

Once all the relevant information had been input into ACRU, simulations were undertaken. The time period used to conduct the streamflow modelling in ACRU was from the 01st of December 2011 to 25th November 2012. This time period was selected due to the length of record of the SEBS daily total evaporation estimates and the MODIS LAI data processed for this study.

However, the model was initially run using only the historical observed climate data from the ARC-ISCW automatic weather station for the period 28th September 2006 to 29th September 2013. This was done in order to determine an initial baseflow store value for the 01st December 2011. An assumption was made that this value would be somewhat more representative than conducting simulations with the baseflow store beginning at a value of zero.

During this initial simulation, K_c values were used instead of the MODIS LAI values, as the MODIS LAI values were only available from the 01st of December 2011 to 25th November 2012. Once the initial baseflow store value was determined for the 01st December 2011, streamflow simulations were undertaken, using the historical observed climate data and the MODIS LAI data for the period 01st of December 2011 to 25th November 2012. The simulated streamflow for this simulation was compared with the observed streamflow. The results of these simulations are discussed in Section 6.1.

4.7.4.2 Scenario Two: streamflow modelling using SEBS daily total evaporation estimates

The configuration of ACRU and the inputs used in scenario one was once again used in this scenario. However changes were made to the vegetation parameters and the evaporation data used as inputs to the model. Instead of using the daily FAO Penman-Monteith reference evaporation, as an input to ACRU, to determine actual soil water evaporation and actual transpiration, the daily SEBS total evaporation estimates were used. A sample of the climate file used as an input to ACRU is shown in Table 4.6. Daily FAO Penman-Monteith reference evaporation was still used as an input to ACRU however this was only used to estimate open water evaporation as SEBS has rarely been applied and validated for the estimation of open water evaporation (Abdelrady, 2013). In order to estimate open water evaporation using satellite earth observation data, an adaptation of the SEBS model is required (Su *et al*., 2001).

Once the actual total evaporation values were successfully incorporated, ACRU was run for the period 01st of December 2011 to 25th November 2012, to estimate streamflow. The simulated streamflow for this simulation was compared with the observed streamflow. These results are discussed in Section 6.1.

Table 4.6 Sample of climate file used

Station ID	Date	Rfl (mm)		Tmax (°c)		Tmin (°c)		FAO ref_evap (mm)		Streamflow (mm)		SEBS ET (mm)		LAI	
30765	20111201	0.51		32.68		18.90		4.13		0.2419		6.08		1.70	
30765	20111202	1.02		30.20		19.89		3.11		0.2814		0.23		1.70	
30765	20111203	13.72		22.26		16.84		1.43		0.2718		3.12		1.70	

4.7.4.3 Sensitivity analysis test 1: initial baseflow store value

ACRU was configured to simulate streamflow in Scenario One and Scenario Two, using an initial baseflow store value for the 01st of December 2011, which was determined by conducting an initial simulation, using only the historical observed climate data from the ARC-ISCW automatic weather station for the period 28th September 2006 to 29th September 2013.

An assumption was made that this value would be somewhat more representative of the observed conditions rather than conducting simulations with the initial baseflow store beginning at 0 mm. The initial baseflow store value was determined to be 400 mm for the 01st of December 2011.

In order to test the validity of the aforementioned assumption, a sensitivity analysis was performed by conducting five simulations to assess the effect of what a specified initial baseflow value has on the simulated streamflow. The ACRU configuration used for Scenario Two was used for all five simulations. The initial specified baseflow store specified was 0 mm, which was increased by 200 mm increments for each of the four simulations thereafter. These results are discussed Section 6.2.

4.7.4.4 Sensitivity analysis test 2: root fraction parameter values

As detailed previously in sub-section 4.7.3.4, a number of varying land uses were identified from a Spot 5 satellite image at a 20 m resolution. However, the HRU's in ACRU were configured to represent only eucalyptus plantations. The root fraction parameters pertaining to eucalyptus were used as this was the dominant land use present within each of the sub-catchments that were being modelled. It was assumed that because the average SEBS total evaporation within each sub-catchment was used, the root fraction parameter for the dominant landuse in each sub-catchment could be used for the EVTR3 routine.

The root fraction parameter values pertaining to this vegetation type were used to conduct simulations for the first and second scenarios, as well as for the first sensitivity analysis test for the EVTR3 routine.

Although the HRU's are being modeled as eucalyptus plantations, the SEBS daily actual total evaporation estimate is a mixed pixel estimate of actual total evaporation i.e. the actual total evaporation estimate produced per pixel by SEBS may account for other vegetation types. This is due to the coarse resolution of the MODIS Level 1_B data processed in SEBS, to generate the daily actual total evaporation estimate. The assumption that eucalyptus would be used to represent the landuse in each of the sub-catchments will not affect the representation of the SEBS total evaporation used as an input to ACRU.

The EVTR3 option in ACRU does not require detailed land use information,, however the root fraction parameter values plays an important role in determining the amount of actual transpiration, which occurs from the A-Horizon and from the B-Horizon, as well as the soil water evaporation, which occurs from the A-Horizon. As a result, inaccuracies may be introduced to simulated outputs by incorporating root fraction parameter values pertaining to a single land use.

A sensitivity analysis was performed to assess the effect which the root fraction parameter variable associated with a specific land cover (in this case eucalyptus) has on certain hydrological parameters for the EVTR3 option. The configuration of ACRU used in Scenario Two was used to conduct the sensitivity analysis. Three simulations were performed using the minimum (eucalyptus plantation), average and maximum (wetland grasses) A-Horizon root fraction values present in the X23_A quarternary catchment.

The results for this sensitivity analysis are discussed in Section 6.3. Table 4.7 shows the A-Horizon rooting fraction for the various land uses in the X23_A quarternary catchment. The B-Horizon rooting fraction for the various land uses in the X23_A quarternary catchment is determined as:

$$\text{B-Horizon rooting fraction} = 1 - \text{A-Horizon rooting fraction}$$

Table 4.7 A-Horizon root fractions for varying land uses in the X23_A quarternary catchment

Root Fraction A-horizon												
Landuse	**Jan**	**Feb**	**Mar**	**Apr**	**May**	**Jun**	**Jul**	**Aug**	**Sep**	**Oct**	**Nov**	**Dec**
Bare rock	0.90	0.90	0.90	0.94	0.94	0.94	0.94	0.94	0.92	0.92	0.90	0.90
Com Dryland	0.77	0.75	0.81	0.93	1.00	1.00	1.00	1.00	1.00	1.00	0.99	0.86
Indig Forest	0.70	0.70	0.70	0.70	0.70	0.70	0.70	0.70	0.70	0.70	0.70	0.70
Clearfelled Forest	0.65	0.65	0.65	0.65	0.65	0.65	0.65	0.65	0.65	0.65	0.65	0.65
Euc Forest	0.65	0.65	0.65	0.65	0.65	0.65	0.65	0.65	0.65	0.65	0.65	0.65
Pine Forest	0.66	0.66	0.66	0.66	0.66	0.66	0.66	0.66	0.66	0.66	0.66	0.66
Thicket and bush	0.80	0.80	0.90	0.90	0.90	0.90	0.90	0.90	0.90	0.80	0.80	0.80
Grassland	0.90	0.90	0.90	0.94	0.98	1.00	1.00	1.00	1.00	0.95	0.90	0.90
Urban	0.80	0.80	0.80	0.90	1.00	1.00	1.00	1.00	0.90	0.90	0.80	0.80
Wetland grasses	1.00	1.00	1.00	1.00	1.00	1.00	1.00	1.00	1.00	1.00	1.00	1.00

5. RESULTS AND DISCUSSION: SEBS DATA SET

5.1 Application of the Linear Interpolation Technique and the Kc_{act} Technique to the Observed Data Set

As detailed in Section 4.6.3, the linear interpolation technique and Kc_{act} technique were tested on the surface renewal total evaporation data set and the SEBS total evaporation data set, respectively. The first test involved applying the two techniques to the surface renewal data set. Tables 5.1, 5.2 and 5.3 indicate the results of the investigations. The use of the linear infilling technique to estimate the missing observed daily total evaporation values yielded positive results.

The relative volume error between the observed total evaporation and the linear infilled total evaporation indicates that the linear interpolation technique over-estimates total evaporation by approximately 2%. The R^2 and RMSE values are 0.67 and 0.90, respectively. These statistics, as well as the results of the t-test indicate a fairly good agreement between the known surface renewal values and the linear infilled surface renewal values and show no significant difference between their means.

Table 5.1 A comparison of observed total evaporation vs infilled total evaporation using linear interpolation for 45 random days during the period 01st January 2012 to 30th June 2012

	Surf Ren ET (mm)	Linear Int ET (mm)	RVE (%)
Total	122.16	124.33	-1.78
Average	2.71	2.76	-18.56
Median	2.76	2.56	
Variance	2.47	2.06	
Std Dev	1.57	1.43	
Max	6.07	6.00	
Min	0.42	0.63	
R^2	0.67		
RMSE	0.90		

The use of the Kc_{act} technique to estimate the missing observed daily total evaporation values yielded positive results. The relative volume error between the observed total evaporation and the Kc_{act} infilled total evaporation indicates that the Kc_{act} interpolation technique under-estimates total evaporation by approximately 1%. The R^2 and RMSE values are 0.85 and 0.60, respectively. These statistics, as well as the results of the t-test indicate a good agreement between the known surface renewal values and the Kc_{act} infilled surface renewal values and show no significant difference between their means.

Table 5.2 A comparison of observed total evaporation vs infilled total evaporation using Kc_{act} for 45 random days during the period 01st January 2012 to 30th June 2012

	FAO56 Ref ET (mm)	Surf Ren ET (mm)	Kc_{act} ET (mm)	RVE (%)
Total	163.70	122.16	121.17	0.81
Average	3.64	2.71	2.69	-9.21
Median	3.50	2.76	2.49	
Variance	1.75	2.47	2.19	
Std Dev	1.32	1.57	1.48	
Max	6.70	6.07	6.03	
Min	1.60	0.42	0.65	
R^2		0.85		
RMSE		0.60		

The observed total evaporation estimates and the infilled estimates were accumulated for the period 01st January 2012 to 30th June 2012 and are illustrated in Figure 5.1. Both the techniques appear to be in fairly good agreement with the observed data for the forty-five random days and they are able to capture the trends of the observed data. The results of the t-tests shown in Table 5.3 indicate that the null hypothesis can be accepted for both the techniques at the 95% interval.

Table 5.3 A two sample t-test for the difference between means, comparison of linear infilling and observed data, as well as Kc_{act} and observed data

Technique	T-test (p-value)	Rejection region for null hypothesis (95% confidence)	Accept /Reject
Linear Int	1	$p < 0.05$	Accept
Kc_{act}	0.95	$p < 0.05$	Accept

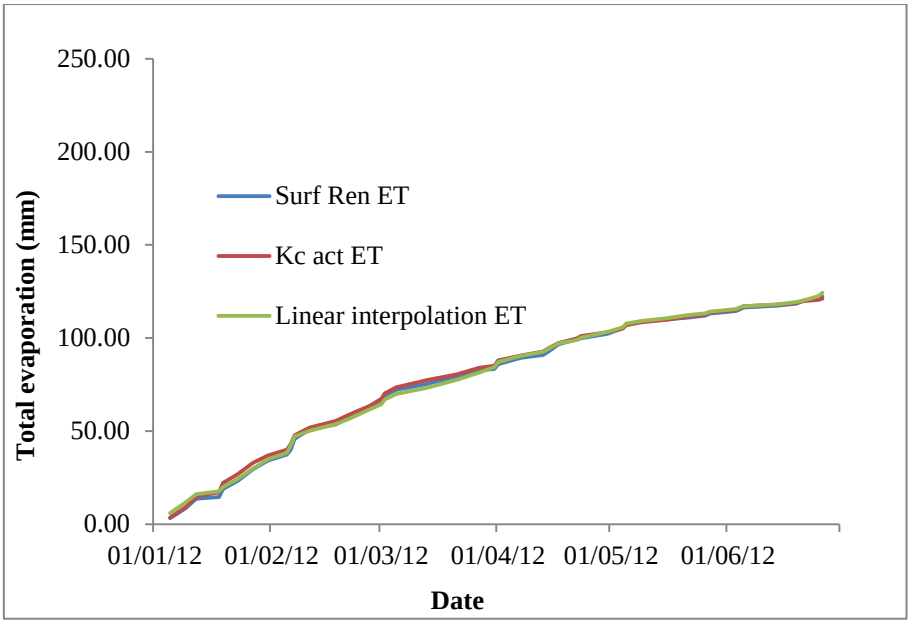

Figure 5.1 A comparison of accumulated observed total evaporation vs accumulated infilled total evaporation using linear interpolation and Kc_{act} for 45 random days during the period 01st January 2012 to 30th June 2012

5.2 Application of the Linear Interpolation Technique and the Kc_{act} Technique to the SEBS Data Set

The second test involved applying the two techniques to the SEBS data set. Tables 5.4, 5.5 and 5.6 indicate the results of the investigation. The use of the linear infilling technique to estimate the missing SEBS daily total evaporation values yielded contrasting results.

The relative volume error between the SEBS total evaporation and the linear infilled total evaporation indicates that the linear interpolation technique under-estimates total evaporation by approximately 3%, indicating a fairly good comparison. This was further supported by the results of the t-test shown in Table 5.6, which indicate that there is no significant difference between their means. However the R^2 and RMSE values of 0.27 and 1.54, respectively, indicate a poor agreement between the known SEBS values and the linear infilled SEBS values.

Table 5.4 A comparison of SEBS total evaporation vs infilled total evaporation using linear interpolation for 45 random days during the period 01st January 2012 to 30th June 2012

	SEBS ET (mm)	Linear Int ET (mm)	RVE (%)
Total	201.12	195.49	2.80
Average	4.47	4.34	-19.78
Median	4.34	4.07	
Variance	3.24	1.40	
Std Dev	1.80	1.18	
Max	8.75	8.15	
Min	0.00	2.09	
R^2	0.27		
RMSE	1.54		

The use of the Kc_{act} technique to estimate the missing SEBS daily total evaporation values yielded poor results. The relative volume error between the SEBS total evaporation and the Kc_{act} infilled total evaporation indicates that the Kc_{act} interpolation technique under-estimates total evaporation by approximately 30%. The R^2 and RMSE values are 0.37 and 1.96, respectively. These statistics, as well as the results of the t-test indicate a poor agreement between the known SEBS values and the Kc_{act} infilled SEBS values.

Table 5.5 A comparison of SEBS total evaporation vs infilled total evaporation using Kc_{act} for 45 random days during the period 01st January 2012 to 30th June 2012

	FAO56 Ref ET (mm)	SEBS ET (mm)	Kc_{act} ET (mm)	RVE (%)
Total	163.70	201.12	141.68	29.55
Average	3.64	4.47	3.15	21.69
Median	3.50	4.34	3.05	
Variance	1.75	3.24	1.99	
Std Dev	1.32	1.80	1.41	
Max	6.70	8.75	5.85	
Min	1.60	0.00	1.33	
R^2		0.37		
RMSE		1.96		

Table 5.6 A two sample t-test for the difference between means, comparison of linear infilling and SEBS data, as well as Kc_{act} and SEBS data

Technique	T-test (p-value)	Rejection region for null hypothesis (95% confidence)	Accept /Reject
Linear Int	0.7	$p < 0.05$	Accept
Kc_{act}	0	$p < 0.05$	Reject

The SEBS total evaporation estimates and the infilled estimates were accumulated for the period 01st January 2012 to 30th June 2012 and are illustrated in Figure 5.2. Both techniques have been shown to perform poorly on the known SEBS data set. The linear interpolation technique closely follows the trends of the SEBS data, whilst the Kc_{act} technique compares less favourably.

The linear interpolation technique marginally under-estimates the total evaporation value specified in the SEBS data set, whereas the Kc_{act} technique largely under-estimates the total evaporation value specified in the SEBS data set. Taking into consideration the results obtained for each of the tests, the linear interpolation technique was chosen to infill the missing data in the SEBS daily total evaporation time series, which was to be generated for the quarternary catchment X23_A.

The Kc_{act} technique performed well in the first test, when Kc_{act} was calculated for a homogenous landcover (sugarcane) at a point scale. However for the second test, the Kc_{act} was calculated from the SEBS total evaporation which was estimated at a 1 km spatial resolution. Other landuses which are present within the 1 km pixel could have contributed to the total evaporation resulting in a mixed pixel estimate of total evaporation. Taking into consideration the results of the two tests the heterogeneity of the pixel and scale at which Kc_{act} was determined could have had a significant influence on the performance of the technique, as the performance of the Kc_{act} technique markedly decreased when it was applied to estimate the artificially removed SEBS total evaporation.

The linear interpolation technique was influenced only by the known total evaporation values. Consequently, a more favourable comparison was identified between the linear interpolation technique and the known SEBS total evaporation values, as it was able to better capture the trends displayed by the known SEBS values.

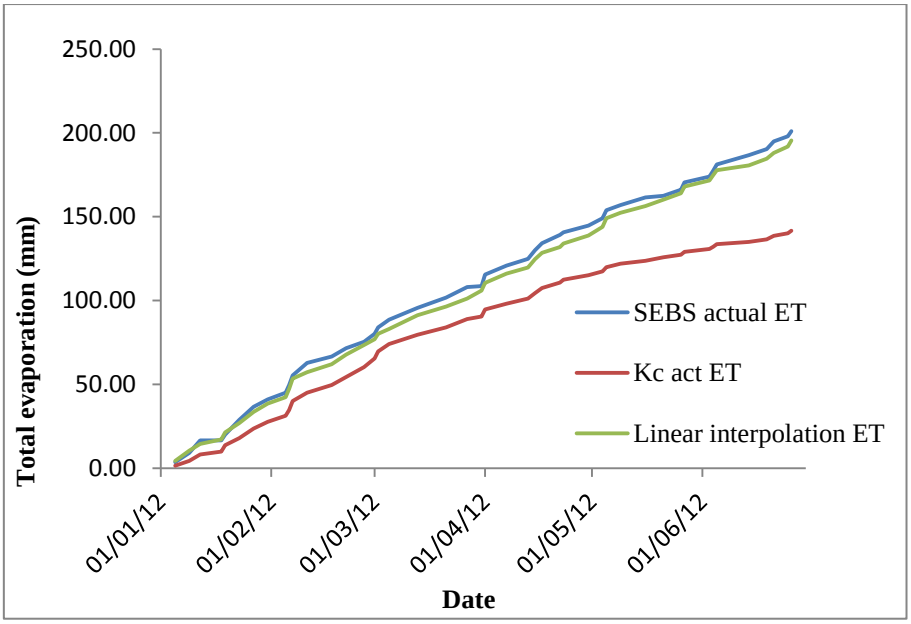

Figure 5.2 A comparison of accumulated SEBS total evaporation vs accumulated infilled total evaporation using linear interpolation and Kcact for 45 random days during the period 01st January 2012 to 30th June 2012

Complete cloud coverage within the MODIS Level 1_B images, resulted in no daily total evaporation values being generated for twenty-eight days of the entire SEBS time series. The linear infilling technique was applied to these days, in order to create a complete total evaporation time series to validate the SEBS total evaporation against the surface renewal total evaporation and to create a complete total evaporation time series required for the modelling of the Kaap Catchment.

5.3 Comparison of SEBS Daily Total Evaporation Estimates against Observed Historical Daily Total Evaporation Estimates

The daily total evaporation estimates generated by SEBS for the time period 01st December 2011 to 25th November 2012 were compared with observed historical surface renewal estimates for the corresponding time period. Tables 5.7 and 5.8 provide the monthly statistical comparisons between the SEBS estimates and the surface renewal technique, whilst Table 5.9 provides the statistical comparison for the entire data collection period.

The comparison between the SEBS daily total evaporation estimates and the Surface Renewal daily total evaporation estimates show considerable variations over the entire time period. The relative volume error between the SEBS total evaporation estimates and the surface renewal total evaporation estimates indicates that SEBS over-estimates total evaporation for the entire time period, except for the month of December. The SEBS total evaporation estimates and the surface renewal total evaporation estimates are in fairly good agreement for December, January and February. The relative volume error between the two techniques during this period is less than 20%.

The poor correlation between the observed data and the SEBS daily total evaporation estimates begins from the month of March onwards, until September. With the exception of the month of March, the relative volume error between the SEBS total evaporation estimates and the surface renewal total evaporation estimates is close to 100% or exceeds 100%. This indicates that the total evaporation estimates generated by SEBS are close to double that of the total evaporation which is observed. The correlation between the observed data and the SEBS daily total evaporation estimates then begins to improve from October onwards.

The monthly comparisons between the SEBS estimates and the observed data indicate that the SEBS model possesses bias, when estimating daily total evaporation for the study area. The model possesses the tendency to perform better during the warmer phases of the time period. The results of the t-test, presented in Table 5.10 further serve to confirm this observation.

Table 5.7 A statistical comparison of SEBS total evaporation estimates vs surface renewal total evaporation estimates from 01st December 2011 to 31st May 2012

Month		Surf Ren ET (mm)	SEBS ET (mm/d)	RVE (%)	Month		Surf Ren ET (mm)	SEBS ET (mm)	RVE (%)
Dec-11	**Total**	135.52	125.98	7.04	**Mar-12**	**Total**	105.31	149.47	-41.93
	Average	4.37	4.06	11.84		**Average**	3.40	4.82	-44.44
	Median	4.71	4.32			**Max**	4.55	8.15	
	Variance	2.65	6.79			**Min**	0.80	0.61	
	Std Dev	1.63	2.61			**Median**	3.61	4.72	
	Max	6.75	8.15			**Variance**	0.74	3.53	
	Min	0.38	0.06			**Std Dev**	0.86	1.88	
	RMSE	1.79				**RMSE**	2.20		
Jan-12	**Total**	143.41	164.48	-14.69	**Apr-12**	**Total**	73.84	134.73	-82.46
	Average	4.63	5.31	-15.71		**Average**	2.46	4.49	-93.89
	Max	7.40	9.68			**Max**	4.10	6.93	
	Min	0.49	0.00			**Min**	0.42	0.79	
	Median	4.75	5.63			**Median**	2.49	4.91	
	Variance	2.40	6.38			**Variance**	0.69	1.91	
	Std Dev	1.55	2.53			**Std Dev**	0.83	1.38	
	RMSE	2.10				**RMSE**	2.34		
Feb-12	**Total**	122.50	145.66	-18.90	**May-12**	**Total**	54.01	121.48	-124.95
	Average	4.22	5.02	-20.49		**Average**	1.74	3.92	-144.40
	Max	5.87	7.52			**Max**	3.72	5.66	
	Min	1.15	0.03			**Min**	0.67	0.85	
	Median	4.55	5.45			**Median**	1.65	3.96	
	Variance	1.74	4.47			**Variance**	0.46	1.05	
	Std Dev	1.32	2.11			**Std Dev**	0.68	1.02	
	RMSE	1.89				**RMSE**	2.37		

The null hypothesis is accepted during the warmer periods of the time series at the 95% confidence level, indicating that there is no significant difference between the means between the surface renewal total evaporation estimates and the SEBS total evaporation estimates. However, during the colder periods of the time series, the null hypothesis is rejected at the 95% confidence level, indicating a significant difference between the means between the surface renewal total evaporation estimates and the SEBS total evaporation estimates.

A possible reason for this occurrence is that the SEBS model provides higher uncertainties for dryer regions (Timmermans, 2014). The colder periods in the time series are the dryer periods and this is when the SEBS total evaporation estimates are in extremely poor agreement with the surface renewal total evaporation estimates.

Table 5.8 A statistical comparison of SEBS total evaporation estimates against surface renewal total evaporation estimates from 01st June 2012 to 25th November 2012

Month		Surf Ren ET (mm)	SEBS ET (mm)	RVE (%)	Month		Surf Ren ET (mm)	SEBS ET (mm)	RVE (%)
Jun-12	**Total**	35.16	94.77	-169.56	**Sep-12**	**Total**	71.14	116.78	-64.16
	Average	1.17	3.16	-203.15		**Average**	2.37	3.89	-203.41
	Max	2.92	5.38			**Max**	4.53	9.58	
	Min	0.39	0.57			**Min**	0.09	0.00	
	Median	1.07	3.35			**Median**	2.58	4.09	
	Variance	0.24	0.77			**Variance**	2.43	5.89	
	Std Dev	0.49	0.88			**Std Dev**	1.56	2.43	
	RMSE	2.17				**RMSE**	2.55		
Jul-12	**Total**	35.24	79.62	-125.96	**Oct-12**	**Total**	85.58	93.32	-9.04
	Average	1.14	2.57	-141.37		**Average**	2.76	3.01	-4.77
	Max	2.49	4.93			**Max**	6.56	7.96	
	Min	0.39	0.00			**Min**	0.55	0.00	
	Median	1.03	2.89			**Median**	2.65	2.55	
	Variance	0.19	1.58			**Variance**	1.56	5.81	
	Std Dev	0.43	1.26			**Std Dev**	1.25	2.41	
	RMSE	1.89				**RMSE**	1.79		
Aug-12	**Total**	42.48	103.40	-143.40	**Nov-12**	**Total**	84.58	117.58	-39.02
	Average	1.37	3.34	-168.67		**Average**	3.38	4.70	-41.11
	Max	2.13	5.58			**Max**	5.50	9.59	
	Min	0.72	0.00			**Min**	1.20	0.00	
	Median	1.33	3.58			**Median**	3.62	4.45	
	Variance	0.12	2.12			**Variance**	1.64	7.30	
	Std Dev	0.34	1.46			**Std Dev**	1.28	2.70	
	RMSE	2.52				**RMSE**	2.50		

This trend can also be seen in the time series comparison between SEBS and the Surface Renewal technique illustrated in Figure 5.3. The SEBS Model estimates are in good agreement with the observed data from December to March. However, from March to August this relationship becomes consistently poorer and then begins to improve again from September onwards. Although there is a poor correlation between the observed data and the SEBS daily total evaporation estimates, the seasonal trends which are displayed in the observed data set, are captured within the SEBS daily total evaporation time series.

Table 5.9 A statistical comparison of SEBS estimates against Surface Renewal estimates from 01st December 2011 to 25th November 2012

Time period		Surf Ren ET (mm)	SEBS ET (mm)	RVE (%)
01st Dec 2011 : 25th Nov 2012	**Total**	988.76	1447.27	-46.37
	Average	2.74	4.01	-89.66
	Median	2.42	3.95	
	Variance	2.66	4.50	
	Std Dev	1.63	2.12	
	Max	7.40	9.68	
	Min	0.09	0.00	
	R2	0.33		
	RMSE	2.19		

The R^2 and RMSE values are 0.33 and 2.19, respectively. These statistics, as well as the results of the t-test, shown in Table 5.11, indicate a poor agreement between the known SEBS total evaporation estimates and the surface renewal total evaporation estimates for the entire time period. The null hypothesis is rejected at the 95% confidence level, indicating that there is a significant difference between the means of surface renewal total evaporation estimates and the SEBS total evaporation estimates for the entire time period.

Table 5.10 A two sample t-test for the difference between means, monthly comparisons between Surface Renewal and SEBS total evaporation estimates

Time period	T-test (p-value)	Rejection region for null hypothesis (95% confidence)	Accept /Reject
Dec-11	0.58	$p < 0.05$	Accept
Jan-12	0.21	$p < 0.05$	Accept
Feb-12	0.91	$p < 0.05$	Accept
Mar-12	0.00	$p < 0.05$	Reject
Apr-12	0.00	$p < 0.05$	Reject
May-12	0.00	$p < 0.05$	Reject
Jun-12	0.00	$p < 0.05$	Reject
Jul-12	0.00	$p < 0.05$	Reject
Aug-12	0.00	$p < 0.05$	Reject
Sep-12	0.01	$p < 0.05$	Reject
Oct-12	0.61	$p < 0.05$	Accept
Nov-12	0.03	$p < 0.05$	Reject

The comparison between the SEBS daily total evaporation estimates and the surface renewal total evaporation estimates for the entire duration of time period indicates a very poor relationship. The SEBS total evaporation estimates and the surface renewal estimates were accumulated for the entire time period i.e. 01st December 2011 to 25th November 2012, which is illustrated in Figure 5.4. The relative volume error between the SEBS total evaporation estimates and the surface renewal evaporation estimates indicates that SEBS over-estimates total evaporation for the entire time period by approximately 47%.

The poor relationship between the SEBS estimates and the observed data is largely attributed to the difference in the spatial resolution at which SEBS total evaporation estimates are generated and surface renewal total evaporation estimates are captured. This may be further compounded by the scattering and absorption of radiation by cloud coverage in the MODIS Level1_B images, the infilling of missing data in the observed record and the SEBS total evaporation time series, as well as the up-scaling from instantaneous total evaporation to daily total evaporation

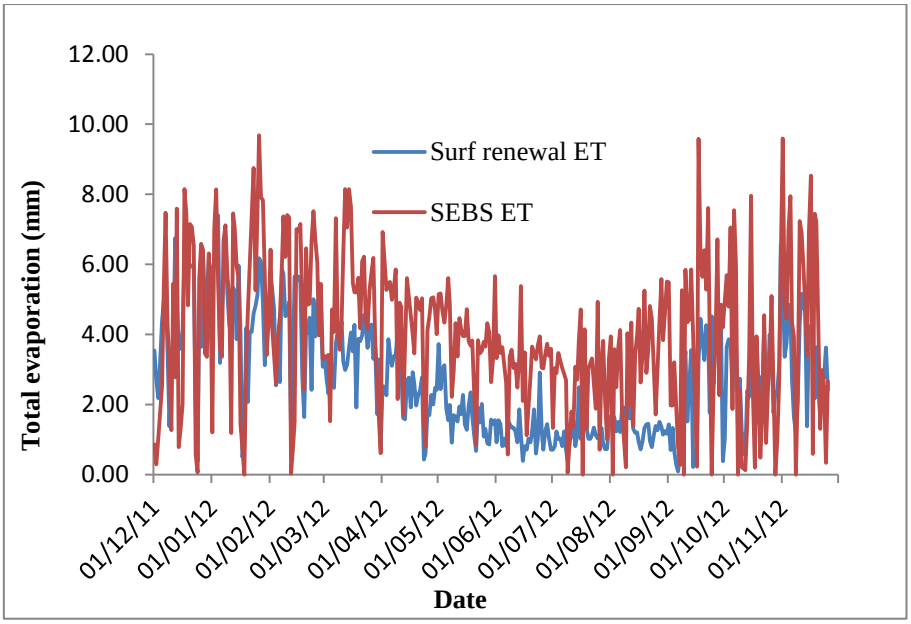

Figure 5.3 A time series comparison between SEBS daily total evaporation estimates and Surface Renewal daily total evaporation estimates

The number of clear sky MODIS level1_B images available for the study area during the period 01st December 2011 to 25th November 2012 was limited. A large majority of the images for this time period possessed a percentage of cloud coverage.

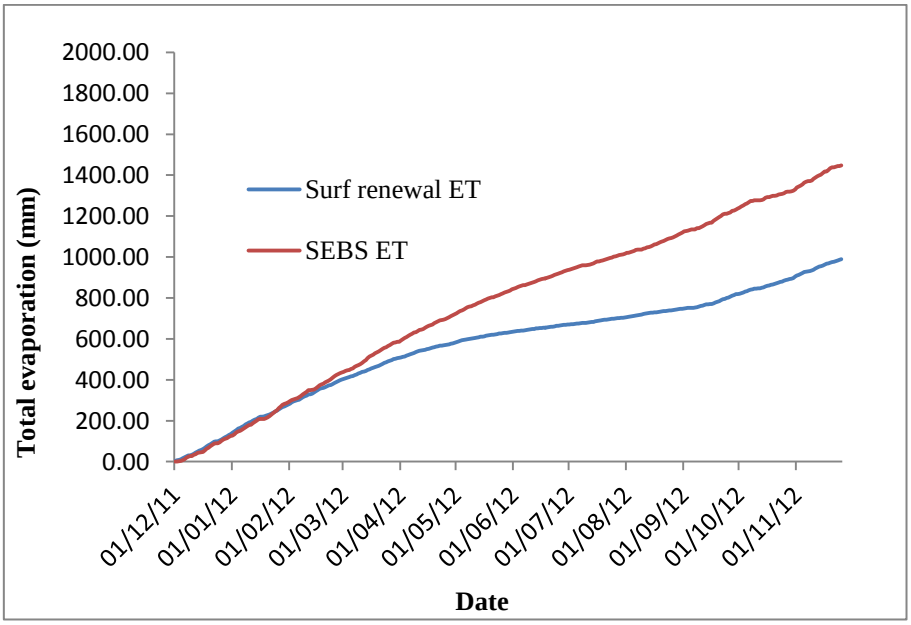

Figure 5.4 A comparison of accumulated SEBS total evaporation estimates vs surface renewal total evaporation estimates for the period 01st December 2011 to 25th November 2012

The scattering and absorption of radiation, by clouds will affect the accuracy of the data captured for the optical and thermal bands, which are used during the SMAC, albedo, land surface emissivity, and land surface temperature computations within SEBS. These maps are key inputs to the SEBS model. Therefore inaccuracies associated with these inputs will be further exacerbated during the computation of daily total evaporation within SEBS.

The surface renewal time series which was used for the validation component of the study was not a complete record. Approximately 25% of the 361 day record was infilled, this was due to the surface renewal system being removed just prior to harvesting and just after crop reestablishment (30th May 2012-28th July 2012), as well as a short period in January 2012 (10th-30th) (Jarmain, 2014). The infilling of the total evaporation data for the aforementioned time periods may not have produced accurate estimates. Consequently comparing the SEBS total evaporation estimates to these values, which possess some level of uncertainty, could lead to unfavourable results.

The SEBS estimates were generated through the use of MODIS Level 1_B data which are collected at a spatial resolution of 1 km, whereas the surface renewal technique operates at a point scale. The SEBS total evaporation estimate which is provided is therefore inclusive of total evaporation values from all landuses which are present within the 1 km pixel, whilst the surface renewal technique only provides an estimate of total evaporation at the point in which it is situated.

Table 5.11 A two sample t-test for the difference between means, comparisons between Surface renewal and SEBS total evaporation estimates for the time period 01st December 2011 to 25th November 2012

Time period	T-test (p-value)	Rejection region for null hypothesis (95% confidence)	Accept /Reject
Dec 2011 : Nov 2012	0	$p < 0.05$	Reject

According to McCabe and Wood (2006), MODIS has a restricted ability to capture the spatial variability of energy fluxes at the field level. Coarse resolution satellite earth observation data may be appropriate for the partitioning of energy at the catchment scale, however at the field scale, high resolution spatial data is required in order to adequately detect inter-field variations (Gibson *et al.*, 2011). Figures 5.5 and 5.6 illustrate this phenomenon.

Figure 5.5 illustrates the SEBS total evaporation which was calculated for the sugarcane field in the Komatipoort Research Site. The 1 km pixel highlighted in this figure is then overlaid onto the landcover map in Figure 5.6, to illustrate the limited interfiled variation detected by the MODIS Level1_B data. Consequently, it is expected that, more often than not, there will be an unfavourable comparison between the SEBS estimate and the observed data due to the differences in the spatial resolution at which the estimate is produced.

The use of finer resolution imagery to estimate total evaporation could assist in improving the comparisons between the surface renewal total evaporation and the SEBS total evaporation. If finer resolution imagery is unavailable, the application of downscaling techniques can be applied to the coarse resolution imagery to improve the representation of the SEBS total evaporation estimate. However the application of a downscaling technique was not within the scope of this study and was therefore not applied.

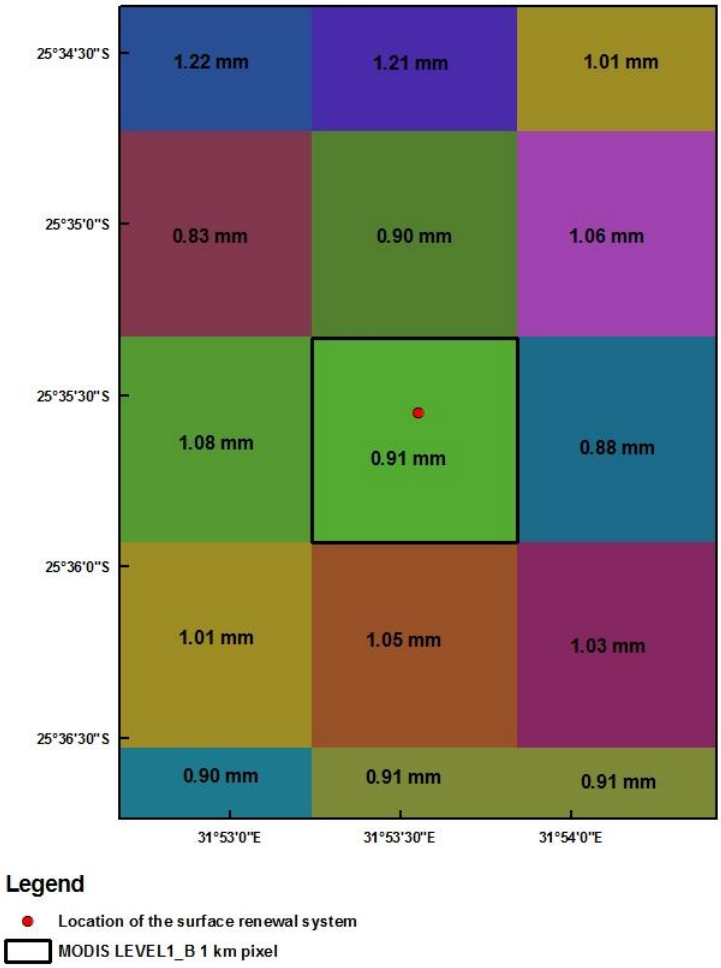

Figure 5.5. An illustration of the SEBS total evaporation (mm) estimated at a resolution of 1km for the sugarcane field in the Komatipoort Research Site

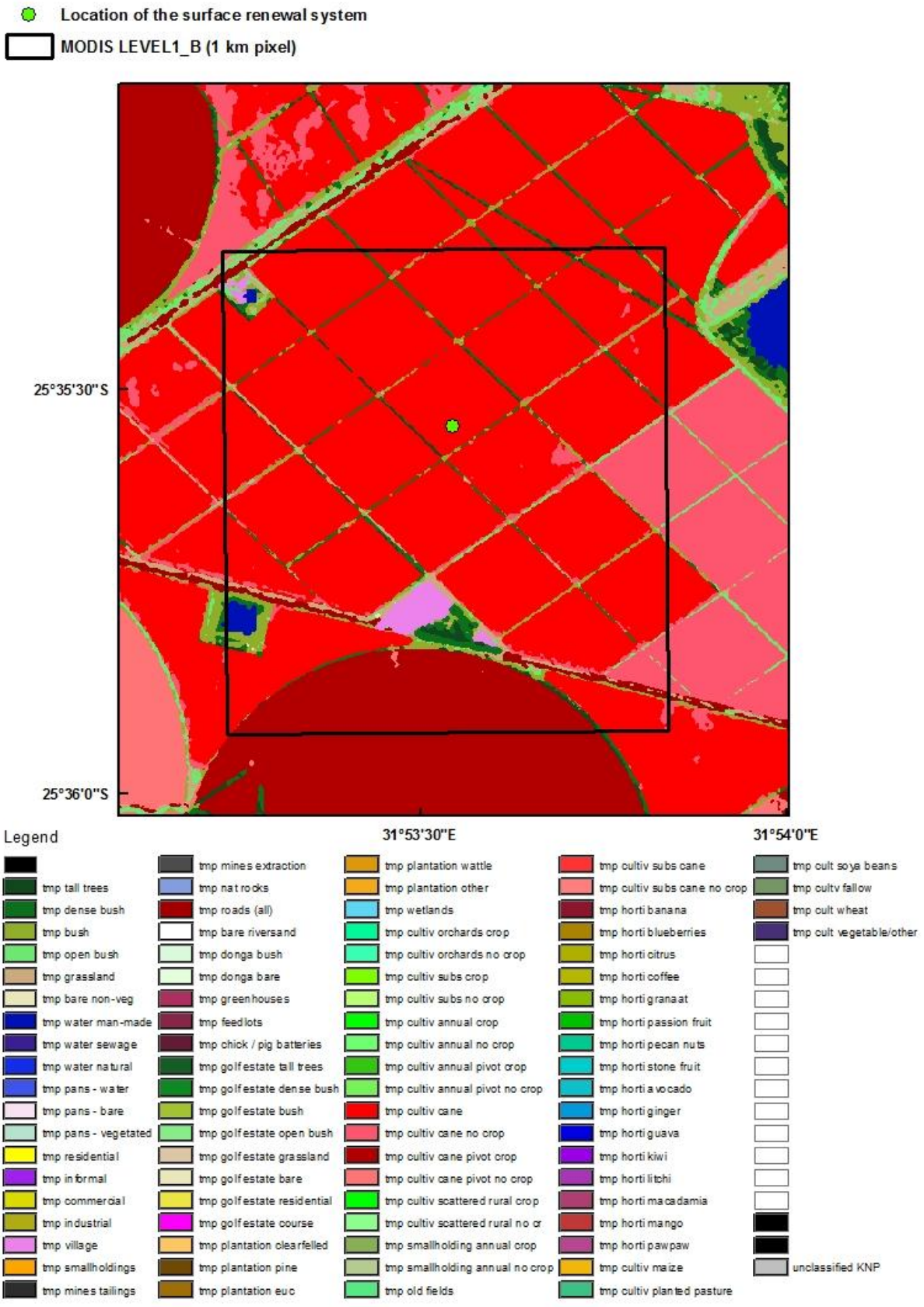

Figure 5.6 An illustration of the spatial coverage for the selected MODIS Level1_B pixel in comparison to surface renewal system

6. RESULTS AND DISCUSSION: ACRU STREAMFLOW MODELLING

The ACRU Model is able to provide a variety of simulated output. However, only the hydrological parameters, which are expected to be most affected, by the changes implemented in each of the scenarios, as well as the sensitivity analysis tests, will be analysed. The analysis involved identifying trends in these parameters, which occurred throughout the duration of the time series.

6.1 A Comparison of Results Obtained for Scenario One and Scenario Two

The ACRU model configuration for Scenario One and Scenario Two were identical, with the only exception being the evaporation option used within the model. This was done in order to determine the effects which the EVTR3 option would have on hydrological parameters. An analysis of the key hydrological parameters, which are affected by the choice of evaporation option selected in ACRU (i.e. the actual total evaporation, soil water content, interception evaporation and runoff) were undertaken, to assess if the EVTR3 approach is not conceptually flawed. The results displayed in Figures 6.1 to 6.9 and Tables 6.1 to 6.6, are for the HRU upstream of the dam in the X23_A2 sub-catchment.

Figure 6.1 illustrates the total evaporation which is output by ACRU (GAET) for the EVTR2 and EVTR3 option, as well as the observed total evaporation input to ACRU (AET) for the EVTR3 option. The AET and GAET for the EVTR3 option are not equal. This is due to the soil water content of the A-Horizon and B-Horizon within the model not being able to meet the actual total evaporation demand being specified. The use of MODIS Level 1_B data could have resulted in an overestimation of the SEBS total evaporation. In addition to this the degree of uncertainty associated with the SEBS total evaporation estimates during dryer periods is higher, therefore the SEBS total evaporation estimates during the winter period of the time series could be inaccurate.

The soils ability to meet the evaporation demand being specified could have been exceeded and as a result the total evaporation which was input to the model was constrained.The constraints to the total evaporation input can be limited or made obsolete through the use of finer resolution satellite imagery for the estimation of total evaporation. Finer resolution satellite imagery would allow for greater inter-field variations in total evaporation to be accounted for thereby assisting in providing a more representative representation of the total evaporation estimated within SEBS. Downscaling of coarse scale imagery can also be used to assist in improving the representativeness of the SEBS total evaporation estimate.

The underestimation of soil water levels and the use of rainfall data which possesses a degree of uncertainty could have also contributed to the AET and GAET for EVTR3 option not being equal. The rainfall data used to drive the streamflow simulation in quarternary catchment X23_A was obtained from a raingauge located at a great distance from the study site and separated by differences in topography and altitude. No correction factors where applied to the rainfall data set due to the length of record. Rainfall is the chief contributor to soil water recharge. As a result the soil water levels which are estimated within the model could be inaccurate due to the uncertainties associated with the rainfall data.

The trend identified in Figure 6.1 illustrates that the GAET output for the EVTR2 option and the EVTR3 option appear to be in reasonably good agreement, with the GAET for EVTR3 being marginally higher. This observation is further confirmed by the results of the statistical analyses shown in Tables 6.1 and 6.2.

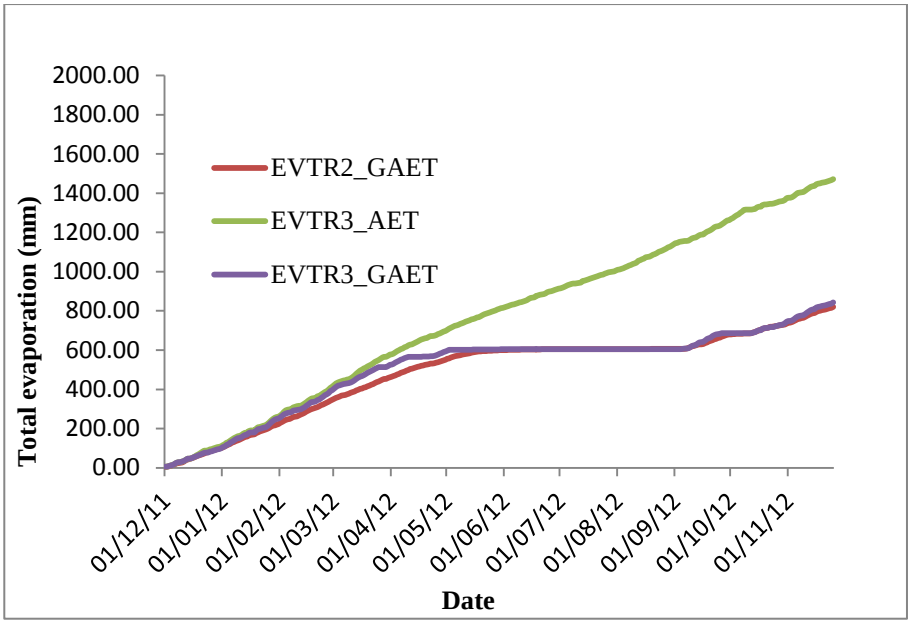

Figure 6.1 A comparison of accumulated observed total evaporation used as an input for EVTR3 vs accumulated actual total evaporation for EVTR2 and EVTR3

Table 6.1 Statistical comparison between EVTR2 GAET and EVTR3 AET and GAET

Actual evapotranspiration (mm)			
	EVTR2	EVTR3	
	GAET	AET	GAET
Total	819.96	1470.94	842.37
Mean	2.27	4.07	2.33
Med	2.29	3.84	1.35
RMSE		2.80	1.64
RVE (%)		-79.39	-2.73
R^2		0.18	0.63

The relative volume error between the EVTR2 GAET and EVTR3 GAET option indicates that the accumulated total evaporation for the EVTR3 option is 2.73% higher than that simulated for EVTR2. The R^2 and RMSE error values for the daily actual evaporation comparisons between the EVTR2 GAET and EVTR3 GAET are 0.63 and 1.64, respectively.

A two tailed t-test was conducted in order to understand how significant the difference between the EVTR2 GAET and EVTR3 GAET is. The null hypothesis and alternate hypothesis were stated as:

$$Ho: EVTR2\ GAET = EVTR3\ GAET$$

$$Ha: EVTR2\ GAET \neq EVTR3\ GAET$$

The results of the t-test, shown in Table 6.2, indicate that there is no significant difference between the GAET simulated for the EVTR2 option and the EVTR3 option.

Table 6.2 A two sample t-test for the comparison between daily GAET for EVTR2 and EVTR3

T-test (p value)	Rejection region for null hypothesis (95% confidence level)	Accept/Reject
0.72	$p < 0.05$	Accept

Quickflow and baseflow are the two major contributors to runoff within a catchment; therefore these parameters were selected in ACRU to understand the runoff contribution to streamflow for each of the evaporation options used. Figure 6.2 represents the baseflow contribution to runoff for the EVTR2 and EVTR3 options.

The baseflow contribution for EVTR2 is fractionally higher than that for EVTR3. This is possibly due to the reduced soil moisture storage, which occurs as a result of the increased GAET experienced for EVTR3. The changes in soil moisture storage in the A and B horizons for the EVTR2 and EVTR3 options are illustrated in Figures 6.3 and 6.4, respectively, and Table 6.3.

The quickflow contribution for the EVTR2 and EVTR3 option is illustrated in Figure 6.5. The quickflow contribution for EVTR3 is marginally higher than that of EVTR2. This is attributed to the variation in interception losses which occur for each of the evaporation options. Even though the technique used to determine the interception loss for EVTR2 and EVTR3 is identical, EVTR2 has a greater interception loss than EVTR3, which is illustrated in Figure 6.6.

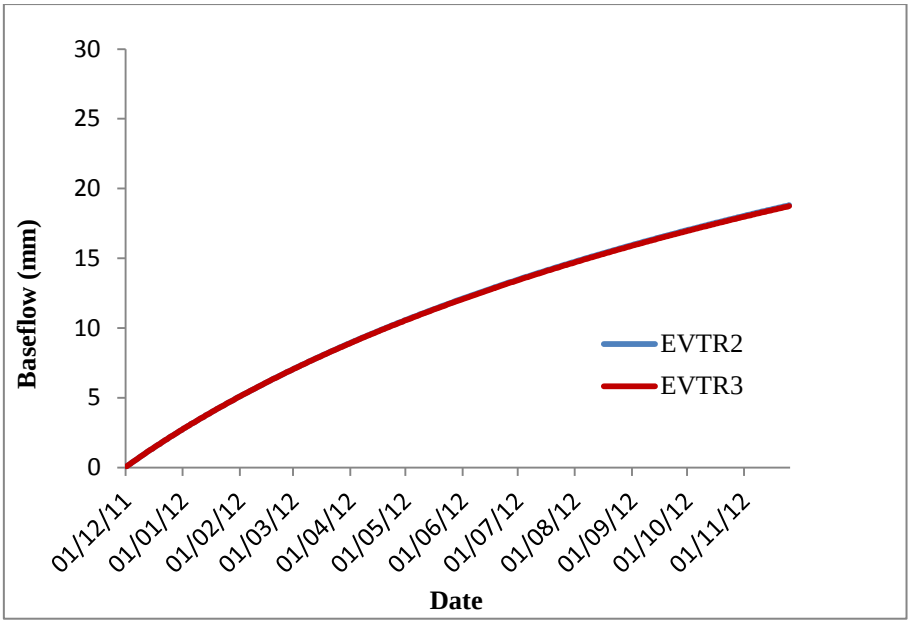

Figure 6.2 A comparison of accumulated baseflow for EVTR2 and EVTR3

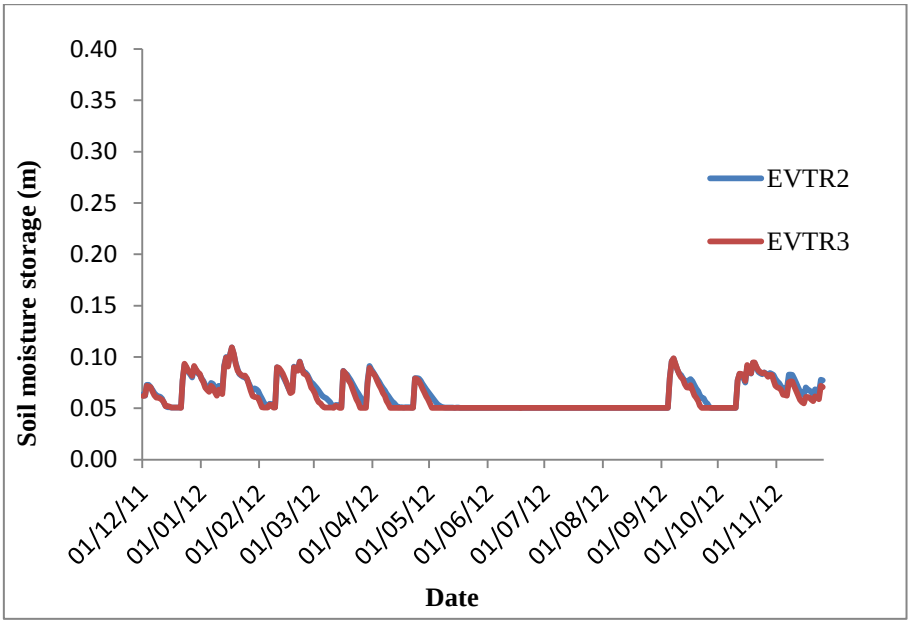

Figure 6.3 A comparison of change in A-Horizon soil moisture storage for EVTR2 and EVTR3

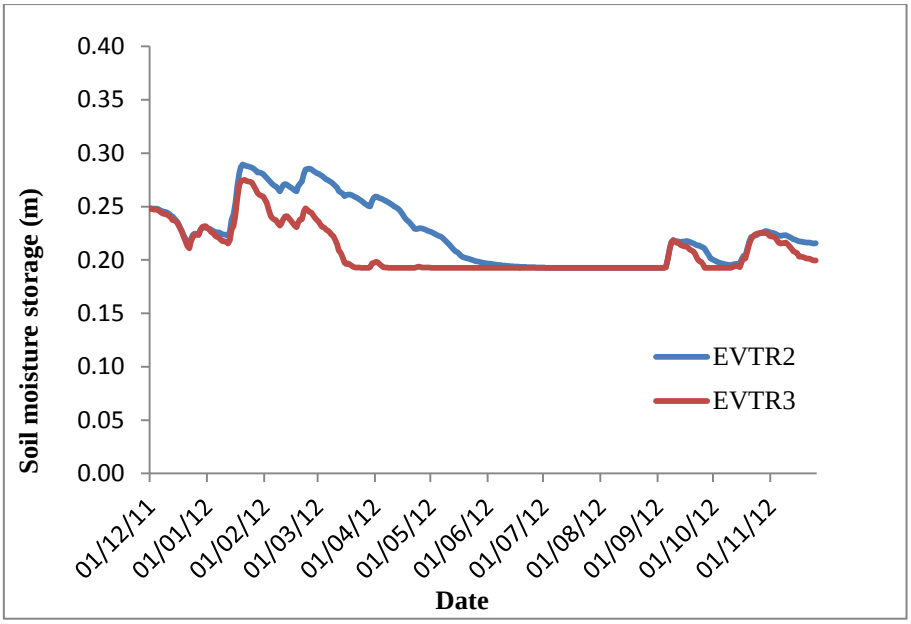

Figure 6.4 A comparison of change in B-Horizon soil moisture storage for EVTR2 and EVTR3

The reason attributed to the higher interception losses for EVTR2 is due to the observed total evaporation for EVTR3 being less than the interception storage for 26 days of the time period being modelled, whereas for EVTR2, the potential evaporation was less than the interception storage for 18 days of the time period being modelled.

This implies that the interception, which is stored on the plant canopy for specific days during the time period being modelled, will be completely evaporated for eight days more for EVTR2, as opposed to EVTR3. These are represented in Figures 6.7 and 6.8, respectively.

The increased loss of water to interception evaporation for EVTR2 results in the plant canopy having a greater capacity to store intercepted water, thereby reducing the amount of rainfall that will reach the soil surface and contribute to quickflow.

Table 6.3 A comparison between initial and final soil moisture storages for EVTR2 and EVTR3

Soil Moisture storage A-Horizon (mm)			Soil Moisture storage B-Horizon (mm)		
	EVTR2	**EVTR3**		**EVTR2**	**EVTR3**
Final	77.39	70.81	**Final**	215.63	199.41
Initial	66.50	66.50	**Initial**	249.60	249.60
Δ	10.89	4.31	**Δ**	-33.97	-50.19

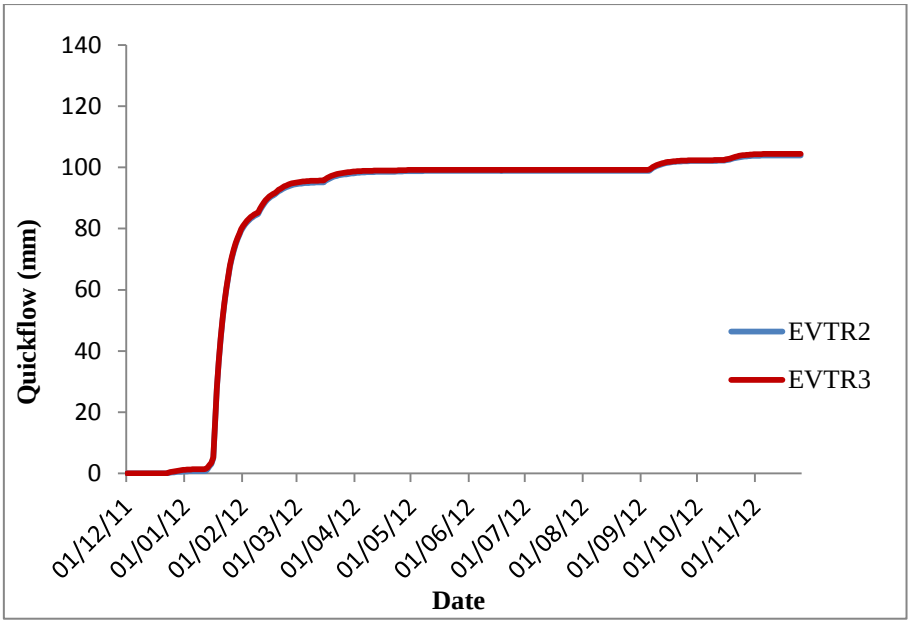

Figure 6.5 A comparison of accumulated quickflow for EVTR2 and EVTR3

The differences in the baseflow and quickflow for the EVTR2 and EVTR3 options are minimal. However, the difference in the quickflow generated for EVTR2 and EVTR3 is greater than the difference in the baseflow generated for the EVTR2 and EVTR3. Thus, the runoff generated for the EVTR3 option is higher than the runoff generated for EVTR2. The differences in baseflow, quickflow and runoff are displayed in Table 6.4 and the runoff for EVTR2 and EVTR3 is illustrated in Figure 6.9.

The coupling of SEBS and ACRU may introduce uncertainties to the outputs simulated by ACRU, due to uncertainties which can be associated with both the SEBS and ACRU models. The validation component of the study was done in order to understand the uncertainties associated with the SEBS total evaporation estimates. The uncertainties associated with the ACRU model prior to its modification to accommodate the EVTR3 routine were not considered.

However once all the various hydrological parameters had been analysed for the X23_A2 sub-catchment, a water balance calculation was done for the X23_A2 sub-catchment for both the EVTR2 and EVTR3 scenarios, in order to ensure that all inputs to the subcatchment are balanced by outputs leaving the subcatchment, thereby validating the model and the evaporation routines being used.

Although this does not provide a true reflection/representation as to the degree of uncertainty associated with the parameters/variables estimated within the model, it did provide an indication that the processes which are being simulated within the model are being represented correctly.

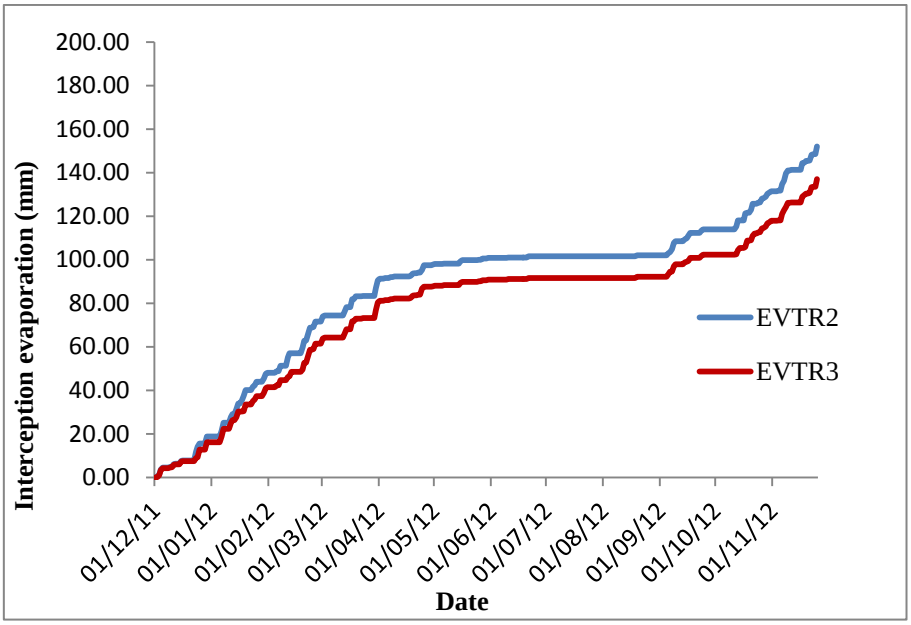

Figure 6.6 A comparison of accumulated interception evaporation output by ACRU for EVTR2 and EVTR3

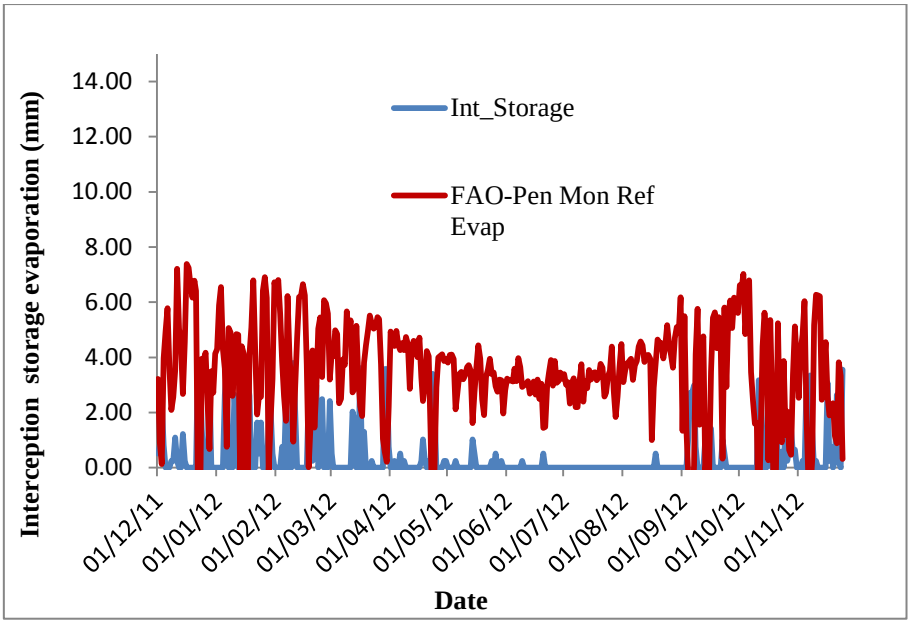

Figure 6.7 A comparison between the interception storage output by ACRU for EVTR2 and daily FAO Penman-Monteith reference evaporation used as an input for EVTR2

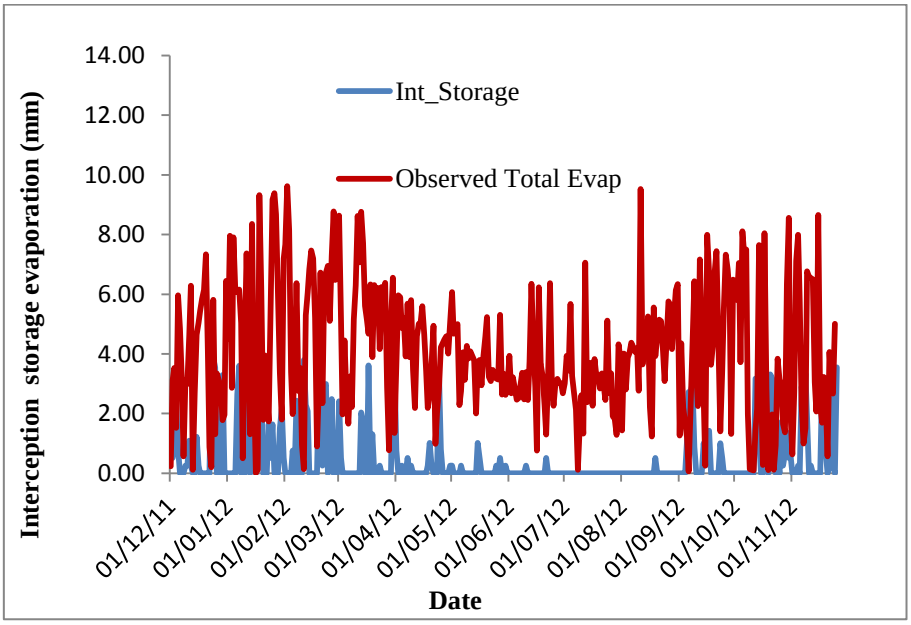

Figure 6.8 A comparison between the interception storage for EVTR3 and the daily observed total evaporation used as an input for EVTR3

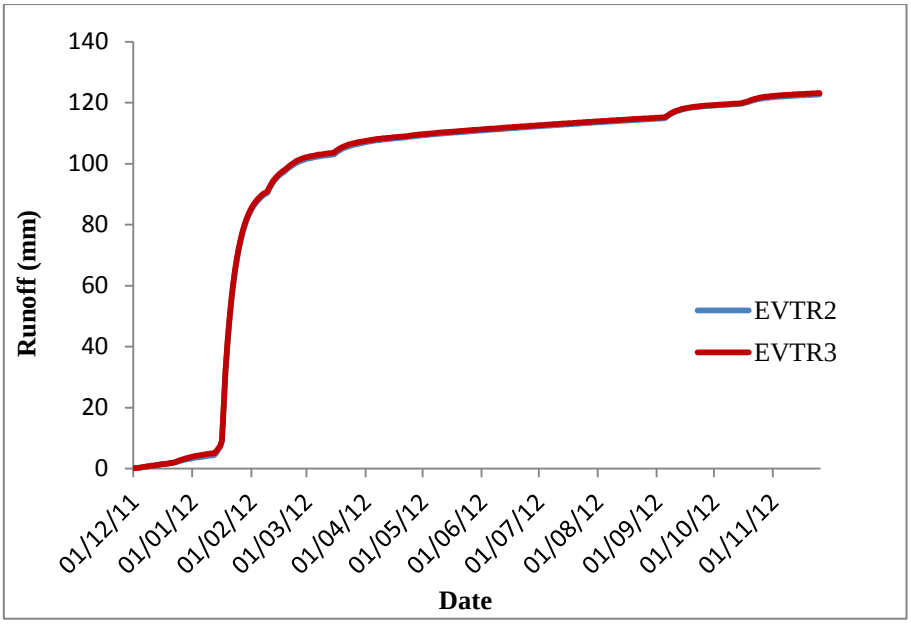

Figure 6.9 A comparison of accumulated runoff for EVTR2 and EVTR3

Table 6.4 A comparison between accumulated baseflow, quickflow and runoff for EVTR2 and EVTR3

	Baseflow	Quickflow	Runoff
EVTR2	18.81	103.93	122.74
EVTR3	18.74	104.45	123.19
Difference	0.07	0.52	0.45

The relevant hydrological parameters were selected and a simple equation was used to perform the water balance calculation i.e. Inputs – Outputs = 0. The inputs and outputs used for this equation are shown in tables 6.5 and 6.6 for EVTR2 and EVTR3, respectively.

Table 6.5 Parameter values used for the EVTR2 water balance calculation

Inputs and outputs for water balance calculation (mm)							
Input	**Output**	**Input**	**Input**	**Input**	**Input**	**Output**	**Input**
RFL	**GAET**	**Δ INTSTO**	**Δ RUNCO**	**Δ STO1**	**Δ STO2**	**URFLOW**	**Δ DELSTS**
901.05	819.96	0.00	-18.65	10.89	-33.97	122.74	0.00

Table 6.6 Parameter values used for the EVTR3 water balance calculation

Inputs and outputs for water balance calculation (mm)							
Input	**Output**	**Input**	**Input**	**Input**	**Input**	**Output**	**Input**
RFL	**GAET**	**Δ INTSTO**	**Δ RUNCO**	**Δ STO1**	**Δ STO2**	**URFLOW**	**Δ DELSTS**
901.05	842.37	0.00	-18.71	4.31	-50.19	123.19	0.00

Where RFL is rainfall (mm); GAET is actual total evaporation simulated in ACRU (mm); Δ INTSTO is difference between the initial and final interception storage (mm); Δ RUNCO is difference between the initial and final baseflow storage (mm); Δ STO1 is difference between the initial and final A-Horizon storage (mm); Δ STO2 is difference between the initial and final B-Horizon storage (mm); is URFLOW is runoff (mm) and Δ DELSTS is delayed stormflow store (mm).

The results for the water balance calculation for both EVTR2 and EVTR3 were rounded off to the nearest millimetre. A final answer of 0 mm was obtained for both EVTR2 and EVTR3, indicating that the model is performing as expected for both evaporation options in ACRU. The results presented in the preceding Figures and Tables indicate that the EVTR3 evaporation technique is not flawed conceptually. Therefore this technique can be used for the estimation of streamflow in ACRU.

In order to assess the performance of the two evaporation techniques used in ACRU to simulate streamflow i.e. EVTR2 and EVTR3, observed streamflow volumes for the X23_A quaternary catchment were compared to the simulated streamflow for the X23A quaternary catchment. A statistical analysis and graphical analysis was undertaken for each of the aforementioned outputs. These results are displayed in Figures 6.10 to 6.11 and Tables 6.7 to 6.10.

Daily streamflow values were accumulated to represent the streamflow for the time period that the simulation was conducted (i.e. 01st December 2011 to 25th November 2012) and these are represented in Figure 6.10. The total flow appears to be adequately simulated for both the EVTR2 and EVTR3 options. The statistical analyses for each of these scenarios are presented in Table 6.7.

Table 6.7 Statistical comparison between simulated daily and total flows vs observed daily and total flows

Streamflow (mm)			
	Obs	**EVTR2**	**EVTR3**
Total	138.02	123.34	123.78
Mean	0.38	0.34	0.34
Med	0.31	0.06	0.06
RMSE		1.05	1.05
RVE (%)		10.63	10.32
R^2		0.41	0.41

The total flow simulated using the EVTR2 option compared fairly well against the observed total flow. The relative volume error indicates that ACRU under-simulates the total flow by 10.63%. However, the daily flow comparisons are less favourable with a R^2 and RMSE error values of 0.41 and 1.05, respectively.

The total flow simulated using the EVTR3 option compared fairly well against the observed total flows. The relative volume error indicates that ACRU under-simulates the total flow by 10.32%. However, the daily flow comparisons are less favourable, with R^2 and RMSE error values of 0.41 and 1.05, respectively.

The R^2 and RMSE error values for the daily flow comparisons indicate that flow values simulated for the EVTR2 and EVTR3 option do not compare as favourably with the observed daily flow values, when compared to the simulated total flow and observed total flow comparisons. Figure 6.11 illustrates the simulated daily flow for the EVTR2 and EVTR3 option, as well as the observed daily flow.

The general trend represented in Figure 6.11 indicates that there is a general under-simulation of streamflow for both the EVTR2 and EVTR3 option in ACRU. The high streamflow simulated during the month of January is attributed to the high precipitation which occurred during this period. However, this response does not appear to be captured in the observed streamflow record, which is possibly due to instrumentation malfunction or the rainfall data used for the modelling of the catchment.

The rainfall station which was used to drive the streamflow simulation in the quarternary catchment X23_A was not situated within close proximity to the catchment. No rainfall correction factors were applied to the data from this raingauge due to the length of the rainfall record. It is possible that the magnitude of this rainfall event did not occur within the catchment therefore explaining why it was not captured within the observed streamflow record.

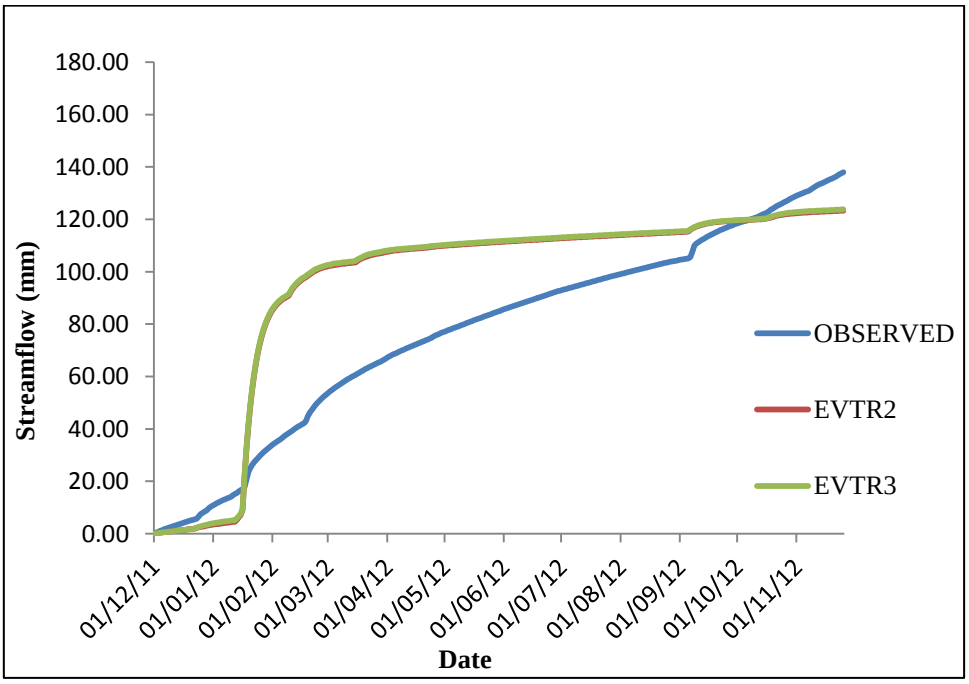

Figure 6.10 A comparison of accumulated observed streamflow and accumulated simulated streamflow for the X23_A quaternary

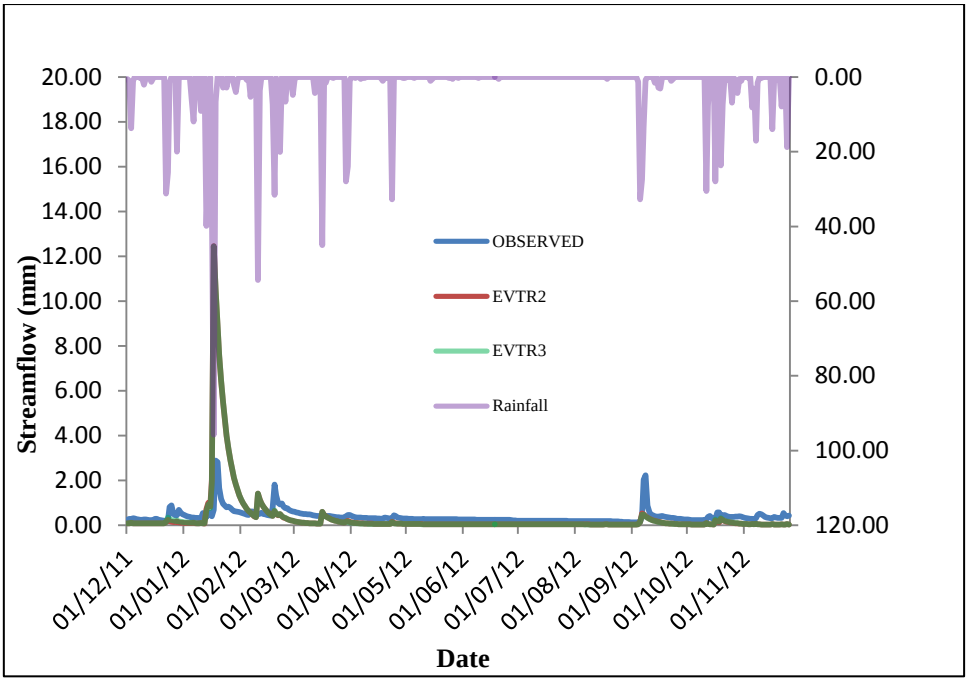

Figure 6.11 A comparison of daily observed streamflow and daily simulated streamflow for the X23_A quaternary

A frequency analysis of the simulated daily flows for the EVTR2 and EVTR3 option, as well as the observed daily flows was conducted to further understand the difference between the daily simulated flow output and the observed daily flow. The results of the frequency analysis are presented in Tables 6.8 and 6.9 and indicate the relative volume error between the observed daily flows and simulated daily flows for low flows (80%), moderate flows (50%) and high flows (20%). A positive result indicates an under-simulation, whilst a negative result indicates an over-simulation.

Table 6.8 Percentage difference between simulated daily flows for EVTR2 and observed daily flows

RVE (%) between observed vs simulated streamflow for EVTR2												
Percentile	**Oct**	**Nov**	**Dec**	**Jan**	**Feb**	**Mar**	**Apr**	**May**	**Jun**	**Jul**	**Aug**	**Sep**
20	65.78	87.88	68.89	-461.70	-3.98	53.61	74.71	81.00	82.28	80.10	79.89	47.59
50	81.69	89.61	65.50	-133.10	11.52	66.11	78.57	82.05	81.89	80.20	80.43	74.86
80	84.62	90.13	63.48	72.55	26.71	76.76	80.59	82.40	82.50	80.40	78.66	82.82

Table 6.9 Percentage difference between simulated daily flows for EVTR3 and observed daily flows

RVE (%) between observed vs simulated streamflow for EVTR3												
Percentile	**Oct**	**Nov**	**Dec**	**Jan**	**Feb**	**Mar**	**Apr**	**May**	**Jun**	**Jul**	**Aug**	**Sep**
20	61.89	87.18	62.67	-463.51	-3.73	54.02	76.15	81.00	82.68	80.10	79.89	49.20
50	80.60	89.61	65.50	-133.98	8.69	66.59	79.50	82.42	81.89	80.69	80.43	75.43
80	85.04	90.13	63.48	69.47	26.09	76.50	81.25	82.77	82.50	80.40	78.66	83.21

The results of the frequency analysis are fairly similar and further serve to confirm the observation that streamflow is being under-simulated within ACRU. Low flows, moderate flows and high flows for both the EVTR2 and EVTR3 options are generally under-simulated, when compared with the observed low, moderate and high flows.

However, the high flows in January and February, as well as the moderate flows in January are being largely over-simulated. This is attributed to the effect of high rainfall in the month of January not being captured in the observed streamflow, which could be due to uncertainties associated with; the streamflow data, the rainfall data used for the modelling of the catchment or a combination of both.

The general under-simulation is attributed to the configuration of vegetation within the sub-catchments. The vegetation selected to be present in each of the HRU's was eucalyptus plantations. Commercial afforestation is a known streamflow reduction activity in South Africa. Therefore, the simplistic configuration used in ACRU (i.e. selecting eucalyptus plantations) to represent the land use of the entire X23_A quaternary catchment, was expected to yield lower streamflow volumes.

A two tailed t-test was conducted in order to understand how significant the difference between the observed and simulated streamflow is for, both the EVTR2 and EVTR3 options. The results of the t-test are shown in Table 6.10. The null hypothesis and alternate hypothesis were stated as:

Ho: Observed streamflow = Simulated streamflow

Ha: Observed streamflow ≠ Simulated streamflow

Table 6.10 Two sample t-test for the comparison between daily simulated streamflow and daily observed streamflow for EVTR2 and EVTR3

Evaporation Routine	T-test (p value)	Rejection region for null hypothesis (95% confidence level)	Accept/Reject
EVTR2	0.54	$p < 0.05$	Accept
EVTR3	0.55	$p < 0.05$	Accept

Although, ACRU has been shown to under-simulate streamflow for both the EVTR2 and EVTR3 options, the results of the t-test, indicate that there is no significant difference between the simulated streamflow and observed streamflow for either evaporation routine.

6.2 Sensitivity Analysis Test 1: Initial Baseflow Store Value

ACRU was configured to simulate streamflow in Scenario One and Scenario Two, using an initial baseflow store value for the 01st of December 2011, which was predetermined by conducting a simulation, using only the historical observed climate data from the ARC-ISCW automatic weather station for the period 28th September 2006 to 29th September 2013.

An assumption was made that this initial baseflow store value would produce simulated streamflow values which are more representative of the observed conditions, rather than conducting simulations using an initial baseflow store value of 0 mm.

The results discussed in this section will attempt to identify how sensitive ACRU is with regards to the initial baseflow store value. Daily observed and simulated streamflow depths were accumulated for the period 01st December 2011 to 25th November 2012. These are illustrated in Figure 6.12. The general trend identified in Figure 6.12, indicates that, as the initial baseflow store value is increased, the resultant streamflow depth increases as well. This observation is further confirmed by the results presented in Table 6.11.

The general trend identified in the previous section for the comparison between the observed and simulated streamflow for EVTR2 and EVTR3, was that ACRU generally under-simulated daily streamflows for the entire time period and largely over-simulated streamflow during the month of January. A frequency analysis test was conducted to better understand the effects that the initial baseflow store value, specified in ACRU would have on the daily simulated streamflow.

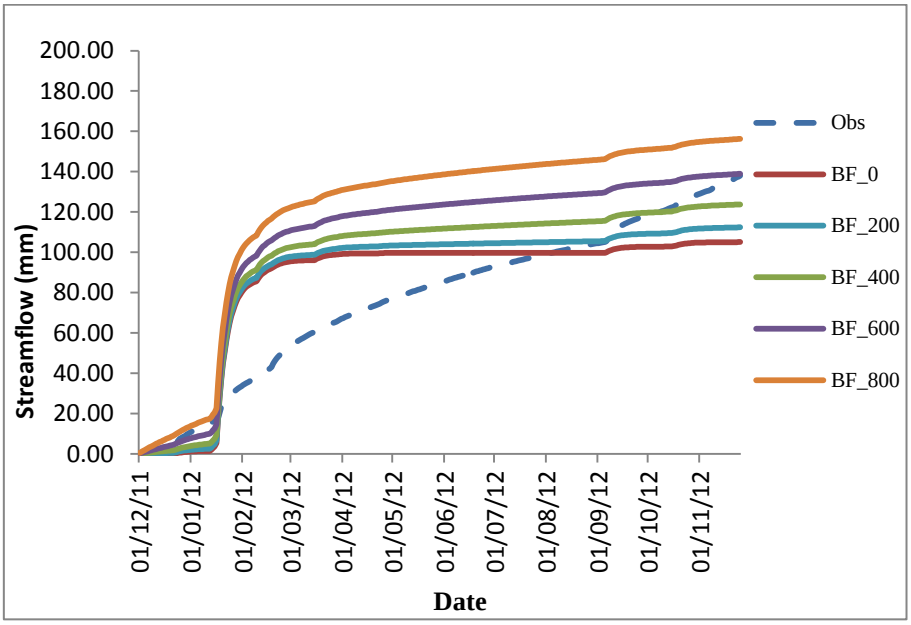

Figure 6.12 A comparison of accumulated observed streamflow and accumulated simulated streamflow in the X23_A quaternary for varying initial baseflow store values

The results of this analysis are shown in Tables 6.12 to 6.16 and indicate the relative volume error between the observed daily flows and simulated daily flows for low flows (80%), moderate flows (50%) and high flows (20%).

Table 6.11 Statistical comparison between simulated daily and total flows vs observed daily and total flows

Streamflow (mm)						
	Obs Streamfow	**BF_0**	**BF_200**	**BF_400**	**BF_600**	**BF_800**
Total	138.02	105.09	112.40	123.78	138.94	156.26
Mean	0.38	0.29	0.31	0.34	0.38	0.43
Med	0.31	0.01	0.03	0.06	0.09	0.12

The results of the frequency analysis shown in Tables 6.12 to 6.16 indicate that, low flows, moderate flows and high flows are generally being under-simulated in ACRU when compared with the observed low flows, moderate flows and high flows, with the exception of the high flows in January and February, as well as the moderate flows in January.

Table 6.12 Percentage difference between simulated daily flows for BF_0mm and observed daily flows

RVE (%) between observed vs simulated streamflow for initial baseflow store of 0mm												
Percentile	**Oct**	**Nov**	**Dec**	**Jan**	**Feb**	**Mar**	**Apr**	**May**	**Jun**	**Jul**	**Aug**	**Sep**
20	69.90	95.34	80.89	-454.74	4.84	65.66	92.24	98.92	100.00	100.00	100.00	57.47
50	89.34	98.52	100.00	-121.30	20.39	81.52	96.27	99.63	100.00	100.00	100.00	87.71
80	98.29	99.68	100.00	91.88	39.96	92.69	98.68	100.00	100.00	100.00	100.00	96.18

Table 6.13 Percentage difference between simulated daily flows for BF_200mm and observed daily flows

RVE (%) between observed vs simulated streamflow for initial baseflow store of 0.02												
Percentile	**Oct**	**Nov**	**Dec**	**Jan**	**Feb**	**Mar**	**Apr**	**May**	**Jun**	**Jul**	**Aug**	**Sep**
20	66.02	90.91	75.11	-457.62	1.86	61.24	85.92	91.76	92.91	91.75	91.30	53.56
50	84.97	94.07	89.92	-125.70	16.13	76.07	89.44	93.04	92.59	91.58	91.85	80.86
80	92.31	95.22	89.57	84.59	34.99	86.68	92.11	93.26	92.92	91.96	90.85	90.08

Table 6.14 Percentage difference between simulated daily flows for BF_400mm and observed daily flows

RVE (%) between observed vs simulated streamflow for initial baseflow store of 0.04												
Percentile	**Oct**	**Nov**	**Dec**	**Jan**	**Feb**	**Mar**	**Apr**	**May**	**Jun**	**Jul**	**Aug**	**Sep**
20	61.89	87.18	62.67	-463.51	-3.73	54.02	76.15	81.00	82.68	80.10	79.89	49.20
50	80.60	89.61	65.50	-133.98	8.69	66.59	79.50	82.42	81.89	80.69	80.43	75.43
80	85.04	90.13	63.48	69.47	26.09	76.50	81.25	82.77	82.50	80.40	78.66	83.21

Table 6.15 Percentage difference between simulated daily flows for BF_600mm and observed daily flows

RVE (%) between observed vs simulated streamflow for initial baseflow store of 0.06												
Percentile	**Oct**	**Nov**	**Dec**	**Jan**	**Feb**	**Mar**	**Apr**	**May**	**Jun**	**Jul**	**Aug**	**Sep**
20	58.74	84.15	40.00	-472.99	-12.05	44.58	64.94	68.82	71.65	68.93	69.57	45.52
50	77.05	85.76	13.57	-146.83	-2.13	54.74	67.39	70.70	71.60	69.80	70.11	71.14
80	78.63	86.31	10.43	42.58	12.84	62.92	68.42	71.16	72.08	70.35	68.29	77.48

Table 6.16 Percentage difference between simulated daily flows for BF_800mm and observed daily flows

RVE (%) between observed vs simulated streamflow for initial baseflow store of 0.08												
Percentile	**Oct**	**Nov**	**Dec**	**Jan**	**Feb**	**Mar**	**Apr**	**May**	**Jun**	**Jul**	**Aug**	**Sep**
20	56.55	82.28	-5.56	-484.75	-21.61	35.34	53.74	58.42	62.99	60.19	61.41	42.76
50	74.59	83.38	-67.83	-161.97	-13.83	43.36	56.52	60.81	62.96	61.39	63.04	68.00
80	74.36	83.76	-70.43	5.32	-1.86	49.09	57.24	62.17	64.17	62.31	60.37	73.28

An increase in the initial baseflow store results in a decrease in the degree of general under-simulation. However, an increase in the initial baseflow store results in a higher degree of over-simulation for the high flows in January and February, as well as the moderate flows in January, with the greatest effect being seen for an initial baseflow store of 800 mm.

Taking into consideration the results presented and discussed in this section, it can be concluded that the initial baseflow store value specified in ACRU has a direct influence on the daily streamflow which is simulated. Therefore, it is necessary to possess *apriori* knowledge on the initial baseflow, to ensure the simulated output is representative of the system being modelled.

6.3 Sensitivity Analysis Test 2: Root Fraction Parameter Values

As described previously, with regards to the EVTR3 option in ACRU, the root fraction parameter values play an important role in determining the amount of soil water evaporation and actual transpiration which occurs from the A-Horizon and from the B-Horizon. As a result, inaccuracies may be introduced to the simulated output, by incorporating root fraction parameter values pertaining to a single land use, when there are multiple land uses within the catchment. A sensitivity analysis was performed to assess the effect which the root fraction parameter variable has on certain hydrological parameters for the EVTR3 option. The results discussed in this section pertain to the HRU upstream of the dam in the X23_A2 sub-catchment.

The effect of the root fraction parameter on soil moisture storage is shown in Table 6.17 and illustrated in Figures 6.13 and 6.14, respectively. The change in soil moisture storage in the A-Horizon does not seem to be greatly affected by the choice of root fraction parameter values used, as the increase in soil moisture storage is fairly similar for all three of the root fraction parameter choices.

However, the change in the B-Horizon soil moisture storage shows a greater degree of variation. The minimum A-Horizon root fraction (RF-MIN) option, which is representative of the A-Horizon root fraction for eucalyptus plantations, shows the greatest decrease in soil moisture storage, whereas the maximum A-Horizon root fraction (RF-MAX), which is representative of the A-Horizon root fraction for wetlands, shows the smallest decrease in soil moisture storage. This was expected, as eucalyptus plantations have the majority of their roots in the B-Horizon and can therefore extract more water from this horizon.

Table 6.17 Comparison between initial and final soil moisture storages for EVTR3, using differing A-Horizon root fraction options

Soil moisture storage A-Hor (mm)				Soil moisture storage B-Hor (mm)			
	RF-MIN	**RF-AVG**	**RF-MAX**		**RF-MIN**	**RF-AVG**	**RF-MAX**
Final	71.69	69.95	71.40	**Final**	143.92	150.50	201.08
Initial	66.50	66.50	66.50	**Initial**	249.60	249.60	249.60
Δ	5.19	3.45	4.90	**Δ**	-105.68	-99.10	-48.52

The effect of the root fraction parameter on soil water evaporation is shown in Table 6.18 and illustrated in Figure 6.15. The highest soil water evaporation occurs for RF-max, whilst RF-min and the average A-Horizon root fraction (RF-AVG) display similar soil water evaporation losses. Soil water evaporation for EVTR3 is determined as the difference between the GAET and actual transpiration. Therefore, the higher the actual transpiration, the lower the soil water evaporation and vice versa.

The lowest actual transpiration occurs for RF-MAX, whilst RF-MIN and RF-AVG display similar actual transpiration, with RF-MIN being marginally higher. This is illustrated in Table 6.19 and Figure 6.16. This occurrence justifies the soil water evaporation losses for the different root parameter options which have been discussed previously.

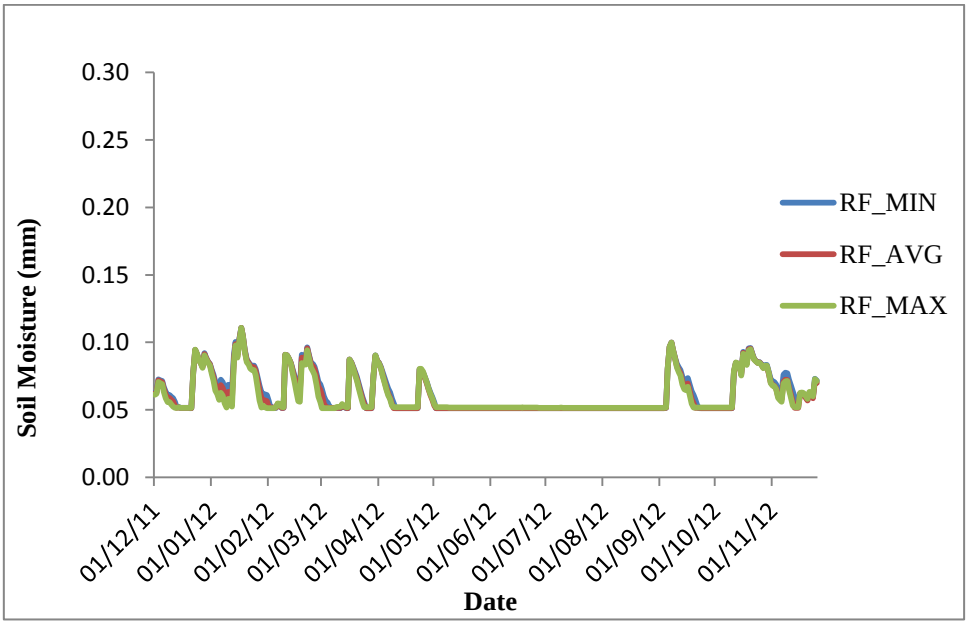

Figure 6.13 A comparison of change in A-Horizon soil moisture storage for EVTR3, using differing A-Horizon root fraction options

The effect of the root fraction parameter on runoff is illustrated in Table 6.20 and Figure 6.17. The total runoff generated for the RF-MIN and RF-AVG options is identical. This is largely due to similar losses of water to soil water evaporation and transpiration.

The contribution of water to the two major components of runoff i.e. baseflow and quickflow, for the RF-max option is higher than the RF-MIN and RF-AVG rooting fraction parameters due to, the smaller loss of water to transpiration and soil water evaporation. As a result, the runoff generated for the RF-max option is the highest of the three rooting fraction parameter options used to conduct the sensitivity analysis.

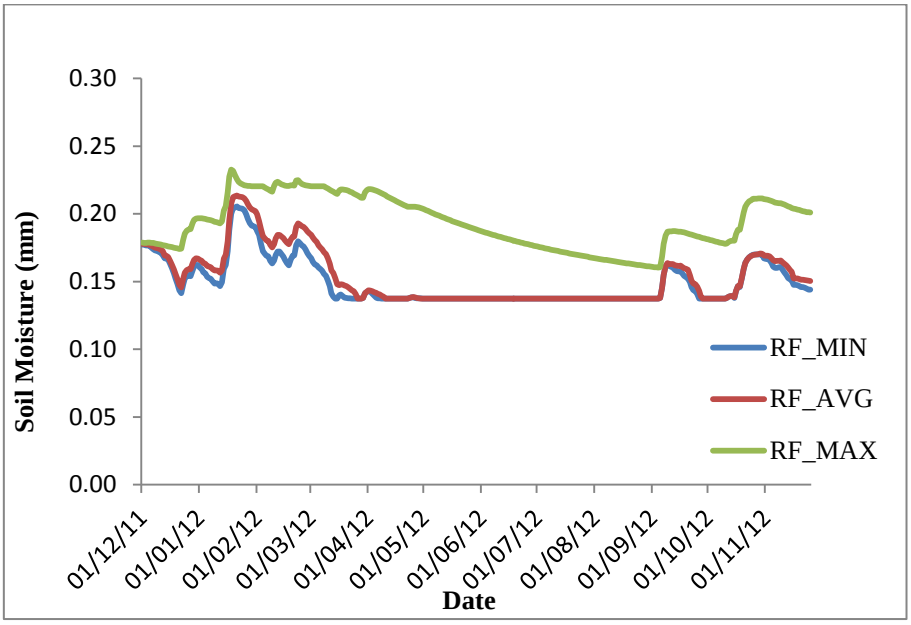

Figure 6.14 A comparison of change in B-Horizon soil moisture storage for EVTR3, using differing A-Horizon root fraction options

Table 6.18 Statistical comparison between soil water evaporation for EVTR3, using differing A-Horizon root fraction options

Soil water evaporation (mm)			
	RF-MIN	**RF-AVG**	**RF-MAX**
Total	58.83	59.55	86.19
Mean	0.16	0.16	0.24
Med	0.00	0.04	0.18

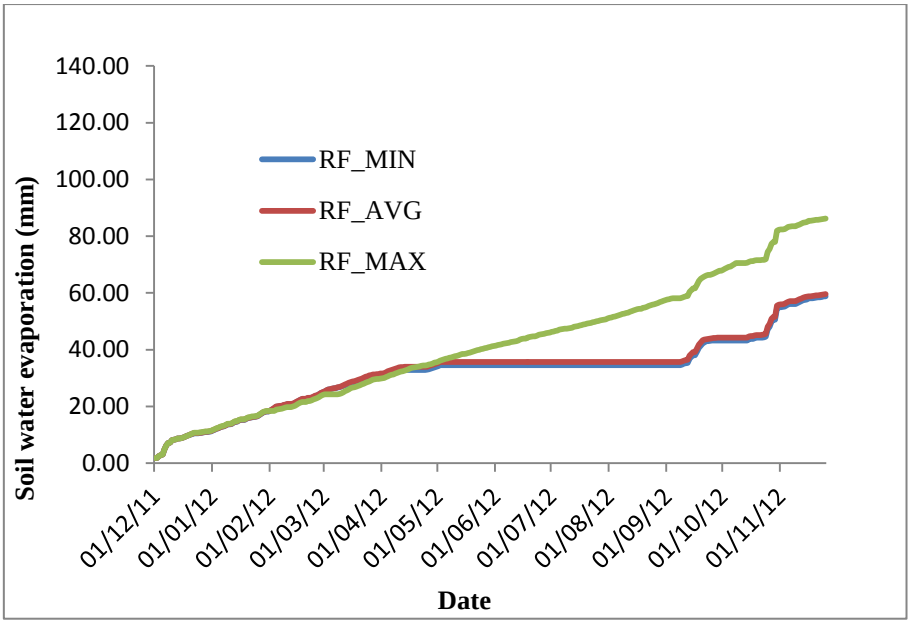

Figure 6.15 A comparison of soil water evaporation for EVTR3, using differing A-Horizon root fraction options

Table 6.19 Statistical comparison between actual transpiration for EVTR3, using differing A-Horizon root fraction options

ATRAN (mm)			
	RF_MIN	**RF_AVG**	**RF_MAX**
Total	646.44	644.87	537.84
Mean	1.79	1.79	1.49
Med	0.00	0.33	0.50

A frequency analysis test was conducted to better understand the effects which the root fraction parameter values specified in ACRU would have on the daily simulated runoff. The results of the frequency analysis, shown in Table 6.21, indicate that the runoff, which exceeded 20%, 50% and 80% of the time, is fairly similar for all months for the RF-min and RF-avg rooting fraction parameter options. The runoff, exceeded 20%, 50%, and 80% of the time for the RF-max rooting fraction parameter option, has increased for all months.

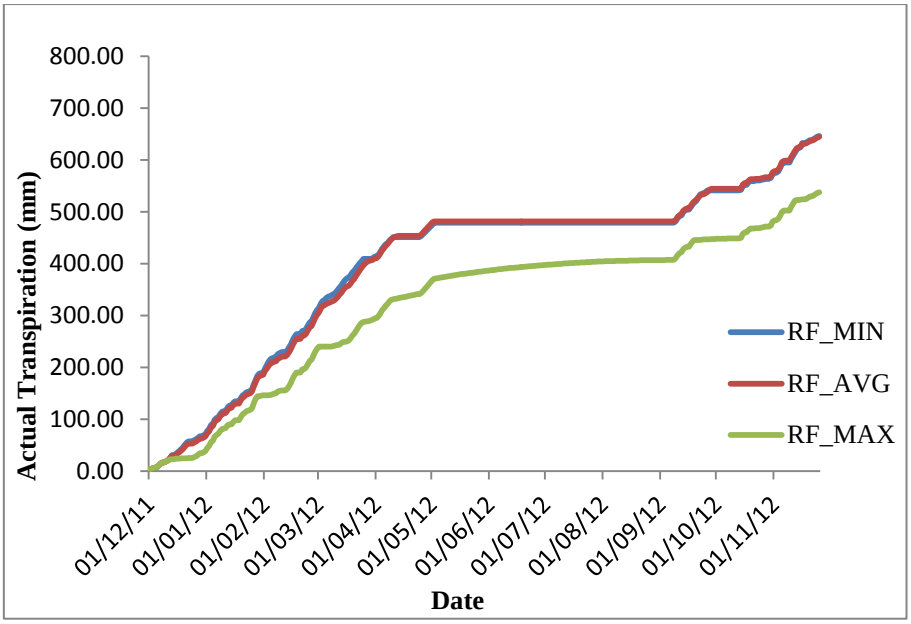

Figure 6.16 A comparison of actual transpiration for EVTR3, using differing A-Horizon root fraction options

Table 6.20 Statistical comparison between runoff for EVTR3, using differing A-Horizon root fraction options.

Runoff (mm)			
	RF_MIN	**RF_AVG**	**RF_MAX**
Total	119.34	119.34	134.05
Mean	0.33	0.33	0.37
Med	0.06	0.06	0.11

The results discussed in this section indicate that there are marginal differences in the simulated hydrological parameters between the RF-MIN and RF-AVG rooting fraction parameter options. However, significant differences are noted for the RF-MAX rooting fraction parameter options. Taking into consideration the results presented and discussed in this section, it can be concluded that it is necessary to utilize representative rooting fraction parameter values as inputs to ACRU, to ensure that the simulated output is representative of the system being modelled.

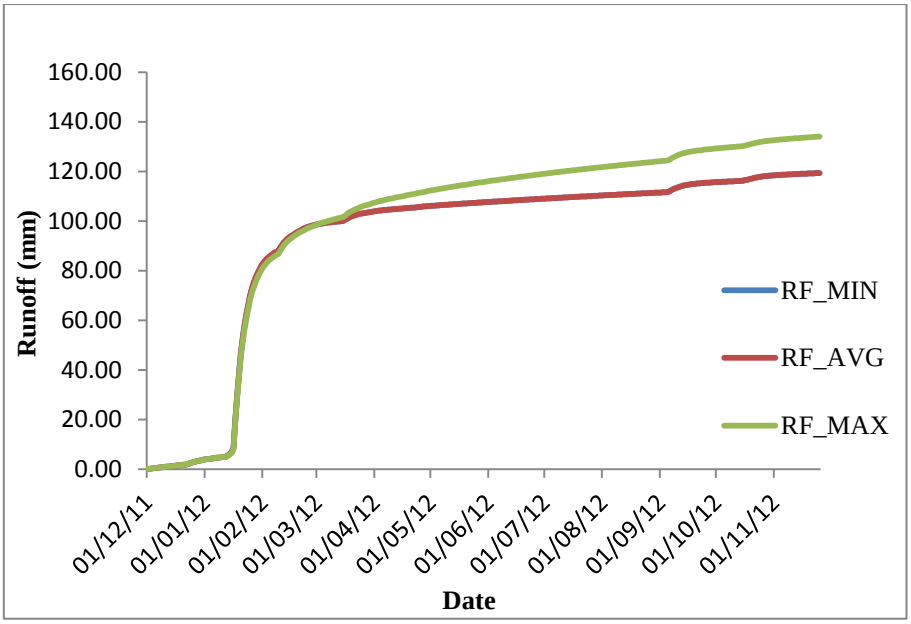

Figure 6.17 A comparison of runoff for EVTR3, using differing A-Horizon root fraction options

However it should be noted that the results which were obtained using an average root fraction value for the entire catchment and the root fraction value for eucalyptus were fairly similar. Therefore choosing eucalyptus as a dominant land use did not severely affect the EVTR3 routine.

Table 6.21 Percentage exceeded between simulated daily runoff for RF-min

% exceeded of simulated runoff for RF-MIN												
Percentile	**Oct**	**Nov**	**Dec**	**Jan**	**Feb**	**Mar**	**Apr**	**May**	**Jun**	**Jul**	**Aug**	**Sep**
20	0.16	0.05	0.17	4.70	0.84	0.23	0.09	0.06	0.05	0.04	0.04	0.22
50	0.07	0.04	0.09	1.33	0.52	0.14	0.07	0.05	0.05	0.04	0.04	0.08
80	0.04	0.03	0.09	0.10	0.36	0.09	0.06	0.05	0.04	0.04	0.04	0.05
% exceeded of simulated runoff for RF-AVG												
Percentile	**Oct**	**Nov**	**Dec**	**Jan**	**Feb**	**Mar**	**Apr**	**May**	**Jun**	**Jul**	**Aug**	**Sep**
20	0.15	0.04	0.17	4.57	0.83	0.23	0.09	0.06	0.05	0.04	0.04	0.22
50	0.06	0.04	0.09	1.30	0.47	0.13	0.07	0.05	0.05	0.04	0.04	0.08
80	0.04	0.03	0.09	0.10	0.34	0.09	0.06	0.05	0.04	0.04	0.04	0.05
% exceeded of simulated runoff for RF-MAX												
Percentile	**Oct**	**Nov**	**Dec**	**Jan**	**Feb**	**Mar**	**Apr**	**May**	**Jun**	**Jul**	**Aug**	**Sep**
20	0.16	0.07	0.17	4.51	0.87	0.34	0.18	0.13	0.11	0.09	0.08	0.26
50	0.08	0.06	0.09	1.33	0.52	0.24	0.16	0.12	0.10	0.09	0.08	0.12
80	0.07	0.05	0.09	0.10	0.39	0.21	0.15	0.11	0.10	0.08	0.07	0.08

7. CONCLUSIONS AND RECOMMENDATIONS

7.1 Conclusion

Hydrological models and tools are often used as decision support systems to inform water resources management. However, the successful application of these models and tools are largely dependent on the data which is used to drive them. Total evaporation data is regarded as one of the key factors in assisting water resources management. Conventional field-based techniques, which are used to acquire total evaporation data have long been utilized to assist water resources management; however, issues such as the spatial resolution of estimates and capacity constraints, such as, cost and time expended have limited the feasibility of applying these techniques to large-scale water resources management.

Satellite-derived total evaporation estimates provide a relatively timeous and cost-effective means of acquiring spatially representative total evaporation estimates, which are sought after by various water resources managers and planners. However, the hydrological community, both locally and internationally, has displayed an unwillingness to utilize satellite earth observation data for hydrological applications. This is largely due to the lack of appropriate technology required to handle and process satellite earth observation data, the lack of knowledge regarding the application of these techniques and the reluctance to move away from traditional and reputable methods (Schultz and Engman, 2000; Xu *et al*., 2014).

The focus of this study was to develop an approach to allow for the integration of satellite-derived total evaporation data into the ACRU hydrological model. In order to meet this overarching objective, various specific objectives were outlined, to inform the tests and analyses that were performed. The results of these investigations were divided into two separate sections focusing on the validation of the SEBS model and the integration of the satellite-derived SEBS total evaporation estimates in the ACRU hydrological model.

The SEBS model was initially applied in the Komatipoort Research site for the period 01st December 2011 to 25th November 2012. The SEBS total evaporation estimates were validated against historical observed total evaporation estimates.

The results of this comparison indicated that the SEBS model consistently oversimulated daily total evaporation when compared with total evaporation estimates obtained from the surface renewal technique. The model did perform better during the summer months as opposed to winter. However, even in the summer months the daily total evaporation was oversimulated when compared with the surface renewal technique.

The poor relationship between the SEBS estimates and the observed data was attributed to the difference in the spatial resolution at which SEBS total evaporation estimates are generated and surface renewal total evaporation estimates are captured. This was further exacerbated by the scattering and absorption of radiation by cloud coverage in a large majority of the MODIS Level1_B images, as well as the infilling of missing data in the observed record.

Although the model poorly estimated the daily total evaporation for the Komatipoort Research site, it was once again applied to estimate the daily total evaporation for the quarternary catchment X23_A. McCabe and Wood (2006) detail the restricted ability which MODIS Level1_B data has to capture the spatial variability of energy fluxes at the field level. However Gibson *et al*. (2011) states that coarse resolution satellite earth observation data may be appropriate for the partitioning of energy at the catchment scale. Therefore it was assumed that the use of MODIS Level1_B data in SEBS would provide acceptable daily total evaporation estimates for the quarternary catchment X23_A.

The SEBS Model was applied to estimate the daily total evaporation for the quarternary catchment X23_A, for the 01st December 2011 to 25th November 2012. These daily total evaporation estimates would then be used as an input to ACRU to model streamflow. Due to, complete cloud coverage for twenty-eight days in the MODIS Level1_B data, there remained missing data records in the SEBS derived total evaporation time series.

The EVTR3 option used to incorporate the SEBS total evaporation time series ACRU requires a continuous daily record. Therefore the use of an infilling technique was required to infill the missing data records within the time period 01st December 2011 to 25th November 2012. The linear interpolation and Kc_{act} techniques were applied and tested to infill the missing records in the SEBS derived total evaporation time series.

Two tests were conducted to assess the representativeness and accuracy of these techniques. The results of these tests indicated that the linear infilling technique was the most suitable technique to infill the missing records in the SEBS total evaporation time series, as it performed within acceptable limits for both of the tests that were conducted.

The linear interpolation technique was applied to infill the missing records in the SEBS derived total evaporation time series. Once the continuous SEBS derived total evaporation time series had been generated, these values were then ready to be used as an input to the ACRU Model.

As stated previously, the ACRU4 Version of the ACRU Model described in Clark *et al.* (2009) does not accommodate actual total evaporation, as an input. Therefore, in order to utilize the SEBS total evaporation estimates, as an input to ACRU, a new option was required, to be added to the model. This option was termed EVTR3

The methodology of the EVTR3 approach, which was derived and discussed in this study, and which seeks to incorporate the satellite-derived total evaporation estimates in the ACRU hydrological model, is not site or model-specific and can therefore be repeated elsewhere. The added advantage of this technique is that it is not limited to satellite-derived total evaporation data. If available, actual total evaporation estimates from conventional techniques can be used as an input to ACRU, to perform various hydrological modelling scenarios.

Total evaporation estimates obtained from the SEBS Model for the period 01st December 2011 to 25th November 2012 were used as an input to the ACRU Model, in conjunction with climate, land use, soils and topographical data, to model the streamflow for the quarternary catchment X23_A. The application of satellite-derived total evaporation estimates in ACRU resulted in poor simulations of daily streamflow, when compared to observed streamflow for the aforementioned time period. ACRU was found to generally under-simulate streamflow on a daily time step, with large over-simulations of streamflow during periods of high rainfall.

However, when comparing the accumulated simulated streamflow with the accumulated observed flow for the aforementioned time period, it was found that ACRU under-simulated streamflow by 10.32% for EVTR3. Similar results for streamflow modeling were obtained when conducting simulations using the conventional evaporation routine available in ACRU.

The application of FAO Penman-Monteith reference evaporation data in ACRU resulted in equally poor simulations of daily streamflow, when compared to observed streamflow for the aforementioned time period; however, the accumulated streamflow was only 10.68% less than the accumulated observed streamflow.

The general under-simulation of daily streamflow and the under-simulation of accumulated streamflow were largely due to the manner in which the quarternary catchment X23_A had been configured with regards to land use. A variety of land uses were identified within the quarternary catchment; however, eucalyptus plantations were selected as the sole land use in the X23_A quarternary catchment X23_A, as this was the dominant land use present in the X23_A1 and X23_A2 sub-catchments. The under-simulation of streamflow was therefore expected, as commercial afforestation is a known streamflow reduction activity in South Africa.

Eucalyptus plantations were selected as the sole land use, due to the differences in spatial resolution between the land uses identified in the catchment and the spatial resolution at which the satellite-derived total evaporation estimate was generated. A few of the land uses which were identified within the X23_A1 and X23_A2 sub-catchments were less than 1 km^2, which is the resolution at which the total evaporation estimate had been generated. Therefore, these estimates may not have been representative of the total evaporation actually taking place for these land uses.

The inability of coarse resolution satellite imagery to capture the spatial variability of energy fluxes at smaller spatial scales has been well-documented. This has also been presented in the results of the validation of the SEBS Model in the Komatipoort Research Site. The simplistic configuration which had to be adopted in ACRU as a result of, the coarse resolution of imagery used to generate the total evaporation estimates may introduce further inaccuracies in the representation of hydrological parameters.

The root fraction parameter, which is pertinent to the EVTR3 approach, affects the partitioning of water to transpiration and soil water evaporation which, in turn, influences soil moisture storage and other associated processes. The lack of observed climatic data for a relevant period of time and the limited satellite earth observation data which was processed due to time constraints, posed further limitations to the study.

In spite of, the aforementioned limitations, the results of the study indicated that the accumulated streamflow obtained for simulations, using the satellite-derived SEBS total evaporation estimates compared favourably, with the accumulated observed streamflow and even more so with the accumulated streamflow obtained, using the FAO Penman-Monteith reference evaporation data.

The good correlation between the simulated streamflow for the conventional evaporation option (EVTR2) in ACRU and the new evaporation option (EVTR3) added to ACRU, indicates that there is potentially a great deal of promise for the integration of satellite earth observation data and the ACRU Model *viz*. satellite-derived total evaporation estimates.

7.2 Recommendations for future research

The recommendations outlined below can be used to address the major limitations experienced in this study and provide assistance for future studies:

- The generation of total evaporation estimates in SEBS can be fairly time-consuming especially; if an extensive time series is required. Due to, time constraints, only 361 total evaporation estimates were generated for this study (i.e. from 01st December 2011 to 25th November 2012). Increasing the record length, of the input data sets used in ACRU, can assist in producing more representative outputs. It is therefore advisable to automate processing procedures, to assist overcoming time constraints.
- The major limitation associated with the modelling of total evaporation in SEBS was the resolution of the imagery used. MODIS Level 1_B data, which is available at a 1 km resolution, was used as an input to the model. MODIS Level 1_B data was selected for this study, due to it being freely available, easily accessible and available at a daily time step. However, the use of finer resolution imagery could allow for a better understanding of land use specific total evaporation, therefore finer resolution imagery should be used, if possible. If finer resolution imagery is not available, the downscaling of coarse resolution imagery can be used to assist in improving the representativeness of the SEBS total evaporation estimate.
- An improvement to the validation of the SEBS model can be made by determining the evaporative fraction and averaging this value at a daily time step. This would assist in directly showing if the SEBS hypothesis (evaporative fraction is constant) is valid.

In addition, using the evaporative fraction does not require calibration, while the surface renewal technique does. Furthermore differences found between SEBS and observed data can be handled in more depth. The use of different up-scaling techniques (of which one requires calibration and the other does not) could possibly contribute to differences found between the observed data and the SEBS estimates.

- The use of finer resolution imagery, in turn, will influence the hydrological modelling in ACRU for the EVTR3 option. The constraints to the total evaporation input can be limited or made obsolete through the use of finer resolution satellite imagery for the estimation of total evaporation. Furthermore finer resolution imagery can allow for a more detailed land use configuration in ACRU, thereby reducing the assumptions which have to be made *viz.* the rooting fraction of the A and B Horizons.
- If possible LAI should be validated for the study area as the MODIS15A2 LAI product can behave differently from what is expected; this is because MODIS15A2 LAI is produced as an eight day product, while the TERRA satellite has a sixteen day repeat cycle. The first eight days of observations are different from the second eight days. This may lead to errors in the final product. If possible LAI can be interpolated between MODIS15A2 LAI production days.
- Rainfall data is of critical importance to any hydrological model. The altitude of the station, the distance away from the catchment, the amount of errors in the data record, missing records and records that have been infilled, need to be known, as these factors significantly influence the representativeness of the model. The observed rainfall data used in this study were obtained from an ARC-ISCW automatic weather station (coordinates: 25.81 S and 31.01 E). This station was selected as the driver station for the quarternary. The rainfall values for this station were not corrected in ACRU, as the record length (seven years) was not adequate to generate representative rainfall correction factors. Inaccuracies may have been introduced to the simulated output due to the uncertainties associated with the station data that was used in the study.
- Global precipitation products such as TRMM, CMORPH, CHIRPS and ECMWF can be used to provide rainfall data. These products can be recalibrated using the stations rainfall stations data. This would provide a better representation of rainfall data which can be used.

8. REFERENCES

Abdelrady, RA. 2013. Evaporation over fresh and saline waters using SEBS, Unpublished Msc Thesis, Geo-Information Science and Earth Observation, University of Twente, The Netherlands.

Allen, RG, Pereira, LS, Raes, D and Smith, M.1998. Crop Evapotranspiration: Guidelines for Computing Crop Water Requirements, FAO Irrigation and Drainage Paper 56, FAO, Rome, 300.

Allen, R, Tasumi, M, Morse, A, Trezza, R, Wright, J, Bastiaanssen, W, Kramber, W, Lorite, I and Robison, C. 2007. Satellite-Based Energy Balance for Mapping Evapotranspiration with Internalized Calibration (METRIC)—Applications. *J Irrig Drain Eng* 133(4): 395–406.

Angus, GR. 1987. A distributed version of the ACRU Model. Unpublished MscEng Dissertation, University of Natal, Pietermaritzburg, Department of Agricultural Engineering: 137.

ASCE-EWRI. 2005. The ASCE standardized reference evapotranspiration equation. Environmental and water resources institute of the ASCE standardization of reference evapotranspiration task committee, *American Society of Civil Engineers*.

Badola, A. 2009. Validation of Surface Energy Balance System (SEBS) over forest land cover and sensitivity analysis of the model, Unpublished Msc Thesis, International Institute for Geo-Information Science and Earth Observation, Enschede, The Netherlands.

Basson, MS and Rossouw, JD. 2003. Inkomati Water Management Area Overview of Water Resources Availability and Utilization, National Water Resource Strategy Final Report, BKS Report No H141405, DWAF Report No PWMA 05/090/00/0203.

Bastiaansen, WGM, Menenti, M, Feddes, RA, Holtslag, AAM. 1998a. A remote sensing surface energy budget algorithm for land (SEBAL). 1. Formulation. *Journal of Hydrology* 212-213(1-4): 213.

Bastiaansen, WGM. 2000. SEBAL – based sensible and latent heat fluxes in the irrigated Gediz Basin, Turkey. *Journal of Hydrology* 229: 87-100.

Bastiaanssen, WGM and Harshadeep, NR. 2005. Managing scarce water resources in Asia: The nature of the problem and can remote sensing help? *Irrigation and Drainage Systems* 19: 269-284.

Bastiaansen, WGM, Cheema, MJM, Immerzeel, WW, Miltenberg, IJ and Pelgrum, H. 2012. Surface energy balance and actual evapotranspiration of the transboundary Indus Basin estimated from satellite measurements and the ET Look model. *Water Resources Research*, 48. Issue 11, Article first published online 21 November 2012, W11512. DOI:10.1029/2011WR010482.

Brutsaert, W. 1982. Evaporation into the atmosphere.

Bulcock, H.H and Jewitt, G.P.W. 2010. Spatial mapping of leaf area index using hyperspectral remote sensing for hydrological applications with a particular focus on canopy interception. *Hydrology Earth System Science* 14: 383–392.

Calder, IR. 1982. Forest evaporation. Associate Committee on Hydrology, National Research Council for Canada. *Canadian Hydrology Symposium* 82:173-193.

Clark, DJ, Smithers, JC, Hughes, DA, Meier, KB, Summerton, MJ and Butler, AJE. 2009. *Design and Development of a Hydrological Decision Support Framework*. WRC Report No. 1490/1/09. Water Research Commission, Pretoria, South Africa.

Clark, DJ. 2013. Case Study. In: ed. Smithers, JC and Clark, DJ. *Model integration for operational water resources planning and management*, Ch.4, 150-200.

Courault, D, Clastre, P, Guinot, JP and Seguin, B. 1994. Analyse des s´echeresses de 1988 `a 1990 en France `a partir de l'analyse combin´ee de donn´ees satellitaires NOAA-AVHRR et d'un mod`ele agrom´et´eorologique. *Agronomie* 14: 41–56.

Courault, D, Seguin, B and Olioso, A. 2005. Review on estimation of ET from remote sensing data: From empirical to numerical modelling approaches, *Irrigation and drainage sytems* 19: 223-249.

Doorenbos, J and Pruit, WO. 1977. Guidlines for predicting crop water requirements. *FAO Irrigation and Drainage Paper* 24:144

DWA. 2012a. Departmetn of Water Affairs, Hydrological Services – Surface Water (Data, Dams, Floods and Flows). (Internet). Available from http://www.dwaf.gov.za/Hydrology. (Accessed 11 May 2012).

DWAF. 2001. Proposal for the Establishment of a Catchment Management Agency for the Inkomati Basin, Prepared on behalf of the Inkomati Catchment Management Agency Reference Group by MBB Consulting Engineers, ACER (Africa) Environmental Management Consultants and the Association for Water and Rural Development (AWARD) under the auspices of the Department of Water Affairs and Forestry: Mpumalanga.

DWAF. 2009. *Inkomati Water Availability Assessment*. Report No. PWMA 05/X22/00/0808. Pretoria, R.S.A.

Elhaddad, A, and Garcia, L.A. 2008. Surface energy balance-based model for estimating evapotranspiration taking into account spatial variability in weather, *J. Irrig. Drain. Eng ASCE* 134(6): 681–689.

Elhag, M, Psilovikos, A, Manakos, Iand Perakis, K. 2011. Application of the Sebs Water Balance Model in Estimating Daily Evapotranspiration and Evaporative Fraction from Remote Sensing Data Over the Nile Delta. *Water Resources Management* 25: 2731–2742.

Engman, E and Gurney, R. 1991. *Remote Sensing in Hydrology*. Chapman & Hall, London.

Engman, E. 1995. Recent advances in remote sensing in hydrology, u.s. national report, 1991-1994. *Rev Geophys American Geophysical Union* 33 Suppl.

Ershadi, A, McCabe, MF, Evans, JP, Walker, JP and Pipunic, R. 2011. Estimation of evaporation using the surface energy balance system (SEBS) and numerical models, *3rd International Symposium on Remote Sensing of Environment, Sydney, Australia, 10-15 April.*

Ershadi, A, McCabe, MF, Evans, JP, Chaney, NW and Wood, EF. 2014. Multi-site evaluation of terrestrial evaporation models using FLUXNET data. *Agricultural and Forest Meteorology* 187: 46-61.

Fern´andez-Prieto, D, van Oevelen, P, Su, Z and Wagner, W. 2012. Advances in Earth observation for water cycle science. *Hydrol Earth Syst. Sci* 16: 543–549.

Food and Agricultural Organization of the United Nations. 1998. Crop evapotranspiration – Guidelines for computing crop water requirements, *FAO irrigation and drainage papers*, 56.

Frezghi, MS. 2012b. E-mail Communication RE: Coverages. Johannesburg, RSA.2012/05/14.

Gibson, LA, M¨unch, Z and Engelbrecht, J. 2011. Particular uncertainties encountered in using a pre-packaged SEBS model to derive evapotranspiration in a heterogeneous study area in South Africa. *Hydrol Earth Syst Sci* 15: 295–310.

Gentine, P, Entekhabi, D, Chehbouni, A, Boulet, G and Duchemin, B. 2007. Analysis of evaporative fraction diurnal behavior. *Agricultural and Forest Meteorology* 143: 13-19.

Gentine, P, Entekhabi, D and Polcher, J. 2011. The Diurnal Behavior of Evaporative Fraction in the Soil-Vegetation-Atmospheric Boundary Layer Continuum. *Journal of Hydrometeorology* 12:1530-1546.

Gowda, PH, Chavez, JL, Colaizzi, PD, Evett, SR, Howell, TA and Tolk, JA. 2007. ET mapping for agricultural water management: present status and challenges. Irrigation Science. DOI 10.1007/s00271-007-0088-6.

Hardy, S, Dugdale, G, Milford, JR and Sutcliffe, J. V. 1989. The use of satellite derived rainfall estimates as inputs to flow prediction in the River Senegal. Pp 23-29 in: New Directions for Surface Water Modeling, *Proceedings of the Baltimore Symp, IAHS Publications*, 181.

Haumann, JK. 2008. *Crocodile (East) River Development, Reconnaissance Study*. PD Naidoo and Associates (Pty) Ltd.

Jarmain, C, Bastiaansen, W, Mengistu, MG and Kongo, V. 2009. A Methodology for Near-Real TimeSpatial Estimation of Evaporation, *WRC Report No. 1751/1/09*, ISBN 978-1-77005-725-8.

Jarmain, C. 2012, WatPLAN Spatial Earth Observation Monitoring for Planning and Water Allocation in the International Incomati Basin, Uncertainty Estimations – A report on validation and uncertainty of the System.

Jarmain, C, Singels, A, Obando, E, Paraskevopoulos, A, Olivier, F, Munch, Z, van der Merwe, B, Walker, S, van der Laan, M, Fessehazion, M, Savage, M, Pretorious, C, Annandale, J and Everson, E. 2013. Water use efficiency of irrigated agricultural crops determined with satellite imagery, Deliverable 6 - Water use efficiency Report 2012/13, Report describing progress with Water use efficiency estimation and student involvement

Jewitt, GPW and Schulze, RE. 1999. Verification of the *ACRU* Model for forest hydrology applications. *Water SA* 25: 483–489.

JIBS. 2001. Joint Incomati Basin Study Report. Phase 2. 2001 Maputo/Johannesburg. Consultec Report Number: C14-99MRF BKS ACRES Report Number: P8491/08.

Jia, L, Zhongbo, S, van den Hurk, B, Menenti, M, Moene, A, De Brein, HAR, Yrisarry, JJB, Ibanez, M and Cuesta, A. 2003. Estimation of sensible heat flux using the Surface Energy Balance System (SEBS) and ATSR measurements *Physics and Chemistry of the Earth* 28: 75–88.

Jin, X, Wan, L and Su, Z, 2005. Research on evaporation of Taiyuan basin area by using remote sensing *Hydrol Earth Syst Sci* 2: 209–227.

Jovanovic, N and Israel, S. 2012. Critical Review of Methods for the Estimation of Actual Evapotranspiration in Hydrological Models, *Council for Scientific and Industrial Research, Stellenbosch, South Africa.*

Kite, GW and Pietroniro. 1996. Remote sensing applications in hydrological modeling *Hydrological Sciences-Journal-des Sciences Hydrologiques* 41 (4): 563-591.

Kite, G and Kouwen, N. 1992. Watershed modeling using land classifications. *Water Resources Research* 28(12): 3193-3200.

Kongo, VM and Jewitt, GPW. 2006. Preliminary investigation of catchment hydrology in response to agricultural water use innovations: A case study of Potshini Catchment – South Africa. *Physics and Chemistry of the Earth* 31(15-16): 976-987.

Kristensen, KJ. 1974. Actual evapotranspiration in relation to leaf area. *Nordic Hydrology* 5: 173-182.

Kuttinen, R. 1985. Report on application of remote sensing to hydrology in the Nordic countries, in Nordic Hydrological Program, 9. NHP, Helsinki, Finland. The Coordinating Committee for Hydrology in Norden KOHYNO.

Kustas, WP and Daughtry, CST. 1989. Estimation of the soil heat flux/net radiation ratio from spectral data. *Agr Forest Meteorol* 49: 205–223.

Lagouarde, JP and Brunet, Y. 1991. Suivi de l'´evapotranspiration r´eelle journali`ere `a partir des donn´ees NOAA-AVHRR lors de la campagne HAPEX-MOBILHY. 5`eme coll.int.“Mesures physiques et signatures en t´el´ed´etection”. *Courchevel* 319: 569–572.

Larson, R. and Farber, F. 2003. Elementary statistics: Picturing the world, Second edition.

Lhomme, JP and Elguero, E. 1998. Examination of evaporative fraction diurnal behaviour using a soil-vegetation model coupled with a mixed-layer model. *Hydrology and Earth System Sciences* 3(2): 259- 270.

Li ZL, Jia L, Su Z, Wan L and Zhang RH (2003). A New Approach for Retrieving Precipitable Water from ATSR-2 Split Window Channel Data over Land Area. *2* 24 5095-5117.

Li F, Kustas WP, Anderson MC, Prueger, JH and Scott, R.L. 2008. Effect of remote sensing spatial resolution on interpreting tower-based flux observations. *Remote Sens Environ* 112: 337–349.

Li, Z, Tang, R, Wan, Z, Bi, Y, Zhou, C, Tang, B, Yan, G and Zhang, X. 2009. A Review of Current Methodologies for Regional Evapotranspiration Estimation from Remotely Sensed Data. *Sensors* 9(5): 3801-3853.

Li, X, Li, XW, Roth, K, Menenti, M and Wagner, W. 2011. Observing and modeling the catchment scale water cycle. *Hydrol Earth Syst Sci* 15: 597–601.

Liang, S. 2001. Narrowband to broadband conversions of land surface albedo I: Algorithms. *Remote Sensing of Environment* 76(2): 213-238.

Liang, SJS. 2002. Narrowband to broadband conversions of land surface albedo: II. Validation. *Remote Sensing of Environment*, 84(1): 25-41.

Lin, W. 2006. Satellite based regional scale evapotranspiration in the Hebei Plain, Northeastern China, Msc Thesis, International Institute for Geo-information Science and Earth Observation, The Netherlands.

Long, D and Singh, VP. 2012. A modified surface energy balance algorithm for land (M-SEBAL) based on a trapezoidal framework *Water Resour Res* 48, W02528, doi:10.1029/2011WR010607.

Lynch, SD and Kiker, GA. 2001. *ACRU Model Development and User Support*. WRC Report No. 636/1/01. Water Research Commission, Pretoria, South Africa.

Ma, W, Ma, Y, Hu, Z, Su, Z, Wang, J and Ishikawa, H. 2011. Estimating surface fluxes over middle and upper streams of the Heihe River Basin with ASTER imagery. *Hydrol Earth Syst Sci* 15: 1403–1413.

Ma, W, Hafeez, M, Ishikawa, H and Ma, Y. 2012. Evaluation of SEBS for estimation of actual evapotranspiration using ASTER satellite data for irrigation areas of Australia. *Theor Appl Climatol*. DOI: 10.1007/s00704-012-0754-3.

Ma, W, Ma, Y and Ishikawa, H. 2014. Evaluation of the SEBS for upscaling the evapotranspiration based on in-situ observations over the Tibetan Plateau. *Atmospheric Research* 138: 91-97.

Martinez, CJ, Campbell, KL, Annable, MD and Kiker, GA. 2008. An object-oriented hydrologic model for humid, shallow water table environments. *J. Hydrol* 351(3-4): 368–381.

Matinfar, RH and Soorghali, M. 2014. Estimate evapotranspiration (ET) using SEBS Model based on Landsat 5 (TM) thermal data and GIS. *Indian Journal of Fundamental and Applied Life Sciences* 4(3): 30-34.

McCabe, MF and Wood, EF. 2006. Scale influences on the remote estimation of evapotranspiration using multiple satellite sensors. *Remote Sens Environ* 105: 271–285.

Menenti, M. 1984. Physical aspects of and determination of evaporation in deserts applying remote sensing techniques. *Report 10 (special issue)*, Institute for Land and Water Management Research (ICW), The Netherlands.

Menenti, M and Choudhury, B. 1993. Parameterization of land surface evaporation by means of location dependent potential evaporation and surface temperature range. Proceedings of IAHS conference on Land Surface Processes. *IAHS Publ* 212: 561-568.

Mengistu, MG, Everson, CS, Moyo, NC and Savage, MJ. 2014. The validation of the variables (evaporation and soil moisture) in hydrometeorological models. *WRC Report No. 2066/1/13*, ISBN 978-1-4312-0514-1

Mertz, SK. 2010. Evapotranspiration measurement: *informing water management in Australia*, Waterlines Report Series Number 35.

Mkhwanazi, MM and Chavez, JL. 2013. Mapping evapotranspiration with the remote sensing Et algorithms METRIC and SEBAL under advective and non-advective conditions: accuracy determination with weighing lysimeters. *Hydrology Days 2013.*

Monteith, JL. 1973. *Principles of environmental physics*. Edward Arnold Press. 241 pp.

Mu, Q, FA, Heinsch, Zhao, M and Running, SW. 2007. Development of a global evapotranspiration algorithm based on MODIS and global meteorology data. *Remote Sensing Environ* 11:519–536.

Muhammad, AH. 2012. Satellite based evapotranspiration estimation and runoff simulation: A top model application to the Gilgel Abay Catchment, Ethiopia, Msc Thesis, Enschede, The Netherlands, 2012.

Nile, ES. 2010. Sensible heat flux estimation under unstable conditions for sugarcane using temperature variance and surface renewal. Unpublished PhD thesis, University of KwaZulu-Natal, Pietermaritzburg, South Africa. Pp. 190.

Pardo, N, Sanchez, LM, Timmermans, J, Su, Z, Perez, IA and Garcia, MA. 2014. SEBS validation in a Spanish rotating crop. *Agricultural and Forest Meteorology* 195-196: 132-142.

Peck, E, Keefer, T and Johnson, E. 1981. Strategies for using remotely sensed data in hydrological models. NASA-CR- 66729.

Pietroniro, A and Prowse TD. 2002. Applications of remote sensing in hydrology. *Hydrologic Process* 16(8): 1537-1541.

Rahman, H and Dedieu, G. 1994. SMAC: a simplified method for the atmospheric correction of satellite measurements in the solar spectrum, *Int. J. Remote Sensing* 15(I): 123-143.

Ridell, ES and Jewitt, GPW. 2010. A Management Tool for the Inkomati Basin with focus on Improved Hydrological Understanding for Risk-based Operational Water Management, Report providing updated catchment information and identifying study focus areas, *Deliverable no. 1: Project K5/1935*.

Ridell, ES, Chetty, KT, Saraiva-Okello, A and Jewitt, GPW, with assistance from Gokool, S and Wickham, B. 2011. A Management Tool for the Inkomati Basin with focus on Improved Hydrological Understanding for Risk-based Operational Water Management, Report on new sources of catchment information, *Deliverable no. 3: Project K5/1935*.

Ritchie, JT. 1972. Model for predicting evaporation from a row crop with incomplete cover. *Water Resources Research* 8:1204-1213.

Rwasoka, DT, Gumindoga, W and Gwenzi, J. 2011. Estimation of actual evapotranspiration using the Surface Energy Balance System (SEBS) algorithm in the Upper Manyame catchment in Zimbabwe. *Physics and Chemistry of the Earth* 36(14-15): 736–746.

Rutter, AJ. 1967. An analysis of evaporation from a stand of Scots Pine. In: Sopper, WE and Lull, HW (Eds). Interantional Symposium on Forest Hydrology. Pergamon Press, Oxford, 403-417.

Sandholt, I, Andersen, J, Dybkjaer, G, Lo, M, Rasmussen, K, Refsgaard, JC and Hogh-Jensen, K. 1999. Use of remote sensing data in distributed hydrological models: applications in the Senegal River basin. *Geografisk Tidsskrift-Danish Journal of Geography* 99(1): 47-57.

Santos, C, Lorite, IJ, Tasumi, M, Allen, RG and Fereres, E. 2008. Integrating satellite-based evapotranspiration with simulation models for irrigation management at the scheme level. *Irrig Sci* 26(3): 277-288.

Savage MJ, Everson CS, Odhiambo GO, Mengistu MG and Jarmain C. 2004. Theory and practice of evaporation measurement, with a special focus on SLS as an operational tool for the estimation of spatially-averaged evaporation, Water Research Commission Report No. 1335/1/04, Pretoria, South Africa. ISBN 1-77005-247-X.

Schultz, GA.1993. Application of GIS and remote sensing in hydrology. Proceedings of HydroGIS 93: Application of Geographic Information Systems in Hydrology and Water Resources. *IAHS Publ* 211 (193): 127-140.

Schultz, GA and Engman, ET. 2000. *Remote Sensing in Hydrology and Water Management*, Springer, Heidelberg, Germany, 2000.

Schulze, RE. 1975. *Catchment evapotranspiration in the Natal Drakensberg*. Unpublished PhD thesis. University of Natal, Pietermaritzburg, Department of Geography.

Schulze, RE 1995. Hydrology and Agrohydrology: A text to accompany the ACRU 3.00 agrohydrological modeling system, Chapter 6, 2-5.

Schulze, RE 1995. Hydrology and Agrohydrology: A text to accompany the ACRU 3.00 agrohydrological modeling system, Chapter 7, 1-23.

Schulze, RE and Maharaj, M. 2004. Development of a database of gridded daily temperatures for Southern Africa. WRC Report No. 1156/2/04

Schulze, RE. 2008. Electronic version of the South African atlas of climatology and agrohydrology. South African Atlas of Climatology and Agrohydrology. RE Schulze. Water Research Commission, Pretoria, South Africa, WRC Report 1489/1/06, Section 1.1.

Senay, GB, Budde, M, Verdin, JP and Melesse, AM. 2007. A coupled remote sensing and simplified surface energy balance approach to estimate actual evapotranspiration from irrigated fields. *Sensors* 7(6): 979–1000.

Sobrino, JA and Raissouni, N. 2000. Toward Remote Sensing Methods for Land Cover Dynamic Monitoring Application to Morocco. *International Journal of Remote Sensing* 21(2) 353-366.

Sobrino, JA, El Kharraz, J and Li, ZL. 2003. Surface temperature and water vapour retrieval from MODIS data. *International Journal of Remote Sens*ing 24(24):5161–5182.

Stewart, JB. 1996. Extrapolation of evaporation at time of satellite overpass to daily totals, In: J.B. Stewart *et al.* (editors) *Scaling up in Hydrology using Remote Sensing*. Wiley, Chichester, UK.

Su, Z, Schmugge, T, Kustas, WP and Massman, WJ. 2001. An evaluation of two models for estimation of the roughness height for heat transfer between the land surface and the atmosphere. *Journal of Appl Meteorol* 40(10): 1933-1951.

Su, Z. 2002. The Surface Balance Energy System (SEBS) for estimating turbulent heat fluxes. *Hydrology and Earth System Sciences*, 6(1): 85-99.

Teixera, DCA and Bastiaansen, WGM. 2012. Five methods to interpret field measurements of energy fluxes over a micro-sprinkler irrigated mango orchard. *Irrig Sci* 30(1): 13–28.

Timmermans, WJ, van der Kwast, J, Gieske, ASM, Su, Z, Olioso, A, Jia, L and Elbers, J. 2005. Intercomparison of energy flux models using ASTER imagery at the SPARC 2004 site. *ESA proceedings WPP-250: SPARC final workshop, 2000*.

Timmermans, J. 2011. Estimation of energy balance terms using AATSR/MERIS and global meteorology data. Tutorial guidelines. International Institute of Geo-information sciences and Earth Observation (ITC), Enschede, the Netherlands.

Timmermans, J. 2012. Personal communication. International Institute of Geo-information sciences and Earth Observation (ITC), Pietermaritzburg, South Africa, 06/2012.

Timmermans, J, Su, Z, van der Tol, C, Verhoef, A and Verhoef, W. 2013. Quantifying the uncertainty in estimates of surface-atmosphere fluxes through joint evaluation of the SEBS and SCOPE models. Hydrological Earth Systems Science. 17: 1561–1573

Timmermans, J. 2014. Personal communication. International Institute of Geo-information sciences and Earth Observation (ITC), Pietermaritzburg, South Africa, 23/09/2014.

Theron, BC. 2006. Concession Creek Dam and Peripheral Development: Draft Scoping Report. BSL Mpumalanga Consulting Engineers CC. 43pp

Thornton-Dibb, SLC, Clark, DJ and Smithers, JC. 2013. Case Study. In: ed. Smithers, JC, and Clark, DJ, *Model integration for operational water resources planning and management*, Ch.7, 236-285.

Thornton-Dibb, SLC. 2014. Personal communication. UKZN, Pietermaritzburg, South Africa, 21/2/2014.

Twine. TE, Kustas, WP, Norman, JM, Cook, DR, Houser, PR, Meyers, TP, Prueger, JH, Starks, PJ and Wesley, ML. 2000. Correcting eddy-covariance flux underestimates over a grass land. *Agric For Meteorol* 103: 279–300.

Van Dijk AI and Renzullo LJ. 2011. Water resource monitoring systems and the role of satellite observations. *Hydrology and Earth System Science* 15 39–55.

Van der Kwaast, J, Timmermans, W, Gieske, A, Su, Z, Olioso, A, Jia, L, Elbers, J, Karssenberg, D and de Jong, S. 2009. Evaluation of the Surface Energy Balance System (SEBS) applied to Aster imagery with flux-measurements at the SPARC 2004 site (Barrax, Spain). *Hydrology and Earth System Sciences* 13(7): 1337-1347.

Von Hoyningen-Huene, J, 1983. Die Interzeption des Niederschlages in landwirtschaftlichen Pflanzenbeständen. *Deutscher Verband für Wasserwirtschaft und Kulturbau*, Verlag Paul Parey-Hamburg, *Schriften*, 57, 1-66.

Wagner, W, Verhoest, NEC, Ludwig, R and Tedesco, M. 2009. *Remote sensing in hydrological sciences*. *Hydrol Earth Syst Sci* 13(6): 813–817.

Wagener, T, Sivapalan, M, Troch, PA, McGlynn, BL, Harman, CJ, Gupta, HV, Kumar, P, Rao, CS, Basu, NB and Wilson, JS. 2010. The future of hydrology: An evolving science for a changing world. *Water Resources Research* 46, W05301, doi:10.1029/2009WR008906.

Wang, L. 2010. Practical Session Instructions WATER RESOURCES (SEBS). International Institute of Geo-information sciences and Earth Observation (ITC), Enschede, the Netherlands.

Warburton, ML, Schulze, RE and Jewitt, GPW. 2010. Confirmation of *ACRU* model results for applications in land use and climate change studies. *Hydrol Earth Syst Sci* 14: 2399–2414, doi:10.5194/hess-14-2399-2010, 2010.

Whitmore, JS. 1971. South Africa's water budget. *South African Journal of Science* 67(3): 166-176.

Wu, B, Yan, N, Xiong, J, Bastiaansen, WGM, Zhu, W and Stein, A. 2012. Validation of ET Watch using field measurements at diverse landscapes: A case study in Hai Basin of China. *J Hydrol* 436–437, 67–80,doi:10.1016/j.jhydrol.2012.1002.1043.

Xu, X, Li, J and Tolson, BA. 2014. Progress in integrating remote sensing data and hydrologic modelling. *Progress in Physical Geography* DOI: 10.1177/0309133314536583

Yang, D, Chen, H and Lei, H. 2010. Estimation of evapotranspiration using a remote sensing model over agricultural land in the North China Plain. *International Journal of Remote Sensing* 31(14): 3783–3798.